High-pressure Raman scattering studies on the vibrational properties of dilute nitrides

A thesis submitted to The University of Manchester for the degree of
Doctor of Philosophy
in the Faculty of Engineering and Physical Sciences

2008

Mark P Jackson

School of Electrical and Electronic Engineering

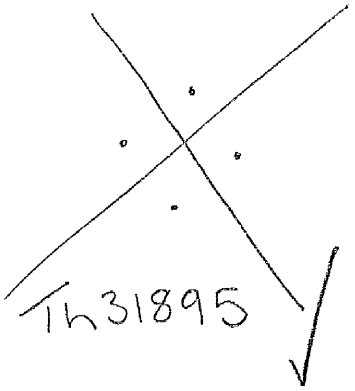

Contents

Word count: 32,715

List of tables

List of figures

List of abbreviations

AlN	Aluminium Nitride
Ar	Argon
As	Arsenide
B_0	Bulk modulus
BCC	Body Centred Cubic
CCD	Charged Coupled Device
DAC	Diamond Anvil Cell
DOS	Density of States
FCC	Face-centred Cubic
FPA	Focal Plane Arrays
Ga	Gallium
GaN	Gallium Nitride
He-Cd	Helium-Cadium
HVPE	Hydride Vapour Phase Epitaxy
In	Indium
InN	Indium Nitride
K	Kelvin
LA	Longitudinal Acoustic
LED	Light Emitting Diode
LO	Longitudinal Optical
LVM	Local Vibrational Mode
LW	Long Wavelength
MBE	Molecular Beam Epitaxy
MOVPE	Metal Organic Vapour Phase Epitaxy
MSL	Material Science Laboratory
N	Nitrogen
NaCl	Sodium Chloride
ND	Neutral Density
P	Phosphide (Phosphorus)

P-DOS	Phonon Density of States
PL	Photoluminescence
Sb	Antimonide (Antimony)
SIMS	Secondary Ion Mass Spectrometry
STFC	Science and Technology Facilities Council
TA	Transverse Acoustic
TO	Transverse Optical
UV	Ultra Violet

Abstract

This thesis has been presented by Mark P Jackson and submitted (April 2008) to The University of Manchester for the degree of Doctor of Philosophy and is entitled "High-pressure Raman scattering studies on the vibrational properties of dilute nitrides".

The thesis presents results and calculations on the vibrational properties of three different dilute nitrides and a III-V semiconductor under hydrostatic pressures using Raman scattering measurements up to their phase transitions. The samples of interest are $InSb_{0.9932}N_{0.0068}$, $GaSb_{0.985}N_{0.015}$, $GaP_{0.979}N_{0.021}$ and the semiconductor of bulk GaP.

With the aid of a diamond anvil cell, the pressure induced shifts of these dilute nitrides were measured by an in-house system that contained either a Renishaw or a 1 metre Spex spectrometer. Three different light sources were available allowing the possibility of using four different excitation wavelengths to study the samples. The emitted wavelengths were 325nm and 442nm from a Helium-Cadmium laser, 514nm from an Argon laser and finally a 623nm emission from a Helium-Neon laser.

Raman scattering measurements form each sample are presented in their own chapter, allowing an in depth discussion to be achieved. The first of the result chapters is that of the group III-V semiconductor GaP. It was discovered during a literature review on Raman studies of $GaP_{1-x}N_x$ samples that the phase transition (I-II) of GaP has not been observed using Raman scattering. This presented an excellent opportunity allowing pressure induced shifts of the TO and LO phonons of GaP to be measured and the determination of the Grüneisen parameters. The phase transition (I-II) was observed near to 24.5GPa while the Grüneisen parameters were calculated to be 1.12 and 0.98.

The next chapter presents the study of the dependence of the vibrational spectrum of $GaP_{0.979}N_{0.021}$ up to 20GPa. The zincblende optical phonons of the ternary alloy show great similarities to those found in the binary GaP. Results show no significant changes to the phase transition, the linear fit parameter or to the Grüneisen parameters for the GaP-like modes. Further studies were performed on the local nitrogen mode frequency in $GaP_{0.979}N_{0.021}$ up to 10GPa. The pressure induced shift was found to be considerably larger than the phonon modes in GaN which indicates that the local mode does not show a GaN-like behaviour under pressure.

A similar study to $GaP_{0.979}N_{0.021}$ was performed on the GaSb dilute nitride sample of $GaSb_{0.985}N_{0.015}$. The optical phonons of the GaSb-like modes were studied under pressure up to 7.5GPa providing calculations on the linear fit and Grüneisen parameter showing that within the experimental accuracy, there is no significant change in the pressure behaviour of the GaSb-like phonons due to nitrogen incorporation. The local vibrational mode of the nitrogen atoms was also studied and again the parameters were calculated to be larger than those for GaN, indicating that the GaN-like mode does not show a GaN-like behaviour under pressure.

Finally, the last chapter presents Raman measurements on the dilute nitride of InSb. This sample had the least nitrogen content so detecting the local mode would be more difficult. As it proved, measurements were found to be inconclusive due to the signal being too weak when being observed in the diamond anvil cell. However, the InSb-like phonon modes were observed under hydrostatic pressures and showed that nitrogen has little influence on the pressure behaviour of the host phonon modes of InSb.

DECLARATION

No portion of the work referred to in the thesis has been submitted in support of an application for another degree or qualification of this or any other university or other institute of learning.

COPYRIGHT

i. The author of this thesis (including any appendices and/or schedules to this thesis) owns any copyright in it (the "Copyright") and s/he has given The University of Manchester the right to use such Copyright for any administrative, promotional, educational and/or teaching purposes.

ii. Copies of this thesis, either in full or in extracts, may be made only in accordance with the regulations of the John Rylands University Library of Manchester. Details of these regulations may be obtained from the Librarian. The page must form part of any such copies made.

iii. The ownership of any patents, designs, trade marks and any and all other intellectual property rights except for the Copyright (the "Intellectual Property Rights") and any reproduction of copyright works, for example graphs and tables ("Reproductions"), which may be describe in this thesis, may not be owned by the author and may be owned by third parties. Such Intellectual Property Rights and Reproduction cannot and must not be made available for use without the prior written permission of the owner(s) of the relevant Intellectual Property Rights and/or Reproductions.

Further information on the conditions under which disclosure, publication and exploitation of this thesis, the Copyright and any Intellectual Property Rights and/or Reproductions described in it may take place is available from the Head of School of Electrical and Electronic Engineering.

Acknowledgements

There are a huge number of people who I would like to thank for their help and support over the last four years during my research for my PhD. It has taken a while and I must admit that the work seemed never ending, but here I am with my thesis. People's patience must have been close to breaking point but thanks you for sticking by me.

The biggest thank you and the deepest gratitude goes to my supervisor Dr Matthew Halsall for his time, patience and excellent guidance throughout my research.

I would also like to thank my collaborators Prof. Peter Klar and Martin Güngerich at the Philipps-University Marburg for supplying the dilute nitride samples and in assisting me with any questions and problems that I had. My thanks also go to Dr John Geisz at the National Renewable Energy Laboratory in Colorado and Dr Louise Buckle and her co workers at the QinetiQ Malvern site for growing the samples.

I wish to thank the Engineering and Physical Research Council (EPSRC) for their financial support and the Electrical and Electronic Engineering Department at the University of Manchester for taking over the administration side of my PhD after the merger of UMIST and Manchester University.

A thank you goes to Ray Jones and Chris Corrigan at the Material Science Laboratory at STFC Daresbury for providing the use of their spark eroder and any assistance in gasket indenting.

Many thanks go to the staff at the University of Manchester for their help, especially Eric for his technical knowledge and construction skills in the laboratory.

Many thanks to my colleagues (Ben, John, Sam, Iain, Paul, Darren, Nikos and Greg) in the research group who have assisted me in the laboratory, providing friendship and support.

A special thank you must go to my mum who has always supported me through my physics degree at Sheffield Hallam University and my PhD. She has believed in everything I have done and I'm sure my dad is doing the same from above. My thanks go to the rest of my family for their support too.

Finally, I would like to give a special thank you to my fiancée Jo for her love, patience, support and encouragement. It has been very hard being so far way but now being able to live with you in Finland makes completing this PhD even more special. I can't wait for the 24th October 2008.

Publications

1. *Vibrational properties of GaP and $GaP_{1-x}N_x$ under hydrostatic pressures up to 30GPa,*
   M. P. Jackson, M. P. Halsall, M. Güngerich, P. J. Klar, W. Heimbrodt and J. F. Geisz. Physica Status Solidi (b) **244** (1) 336 (2006)

Chapter 1: Introduction

1.1 Introduction

Silicon is the classical semiconductor material that has been developed and extensively used for more than 50 years. Even today, it is the base material that still dominates the microelectronic industry and the semiconductor market. In the past twenty years a new market has developed in the form of optoelectronic devices and more recently, more energy efficient devices. These devices started initially with semiconductor group III-V compounds in the form of GaAs, AlAs, InP and GaP [1-4] however they are limited to infrared and green wavelengths. For example phosphorous based semiconductors are ideal for red and green light emission while arsenic based semiconductors are used in infrared detectors.

One of the great technological challenges in recent years has been the extension of this range into the blue and ultra violet (UV) regions of the visible spectrum allowing semiconductors to emit and detect the three primary colours. This would have a major impact on the fabrication of graphic and imaging applications with the development of solid state lighting and displays. One solution is the group III-V nitrides of GaN, AlN and InN [5-7] which have been for many years considered as a promising material and are now being used in commercial blue LEDs and lasers [8-9]. As a result, in the past fifteen years there has been a phenomenal increase in the research of III-nitride semiconductors, due to their technological importance and far superior material properties.

Unlike their group III-V cousins these nitrides have wide direct bandgaps covering the energy range from 0.7eV for InN to 3.4eV for GaN and upto 6.2eV for AlN [10-12]. These wide bandgaps are ideal for high temperature transistors and other specific applications such as high frequency and high photon energy optical devices.

Over the past 10 years, a new type of semiconductor has been developed in the form of dilute nitrides. These dilute nitrides involve the incorporation of small amounts of nitrogen into a group V lattice structure resulting in a decrease in the bandgap [13]. By varying the amount of nitrogen being added, it will be possible to grow narrow bandgap epilayers which would lead to optical devices emitting in the 1.3 to 1.55μm emission range [14].

These materials include ternary and quaternary alloys in the form of $Ga_{1-y}In_yN_xAs_{1-x}$ to produce semiconductors such as $GaN_{1-x}As_x$, $InN_{1-x}As_x$ and $InN_{1-x}Sb_x$. Figure 1.1 shows bandgaps for several dilute nitrides in relation to pure nitrides and semiconductors. Bandgap bowing, as it is known, is indicated by the dashed line on the graph below and highlights how the bandgap varies with nitrogen incorporation. Devices fabricated from these new nitrides have the potential for thermal imaging and photovoltaic devices [15] while a number of solar cells have used dilute nitrides in their fabrication [16].

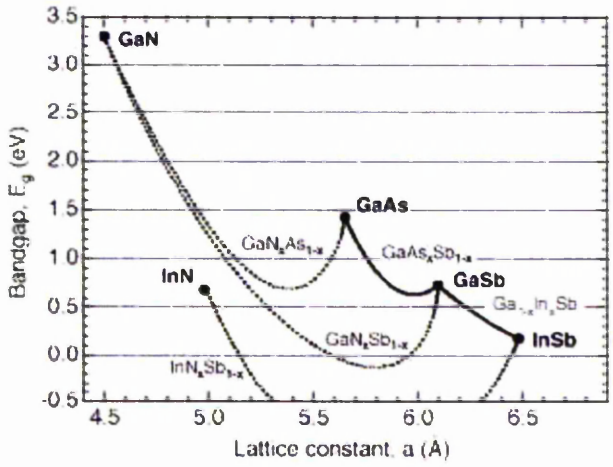

Figure 1.1: Bandgap vs lattice constant for a number of III-V semiconductors and their nitrides. The dotted line highlights the change in bandgap size when the amount of nitrogen is varied.

1.2 Historical development of group III-V dilute nitrides

Developments in dilute nitrides have only recently started to gather pace within in the past 10 to 15 years due to improvements in growth techniques and through research in pure nitrides such as GaN, AlN and InN. The first initial interest in nitrides was when GaN was first synthesised in powder form in 1938 by Juza and Hahn [17].

However it was not until 1969 when the idea of using semiconductors as part of device applications was taking off when Maruska and Tietjen [18] were able to deposit large areas of GaN film layers onto a sapphire substrate. This involved a chemical vapour deposition technique called hydride vapour phase epitaxy (HVPE) to produce GaN in epitaxial form. These early forms of GaN films had a number of undesirable features including a large concentration of electrons due to background doping. This resulted in a conducting n-type material even though they were not deliberately doped. However, this prevented the growth of p-type materials and, due to no suitable substrates being available, interest soon diminished.

High quality epitaxial group III nitrides were achieved with the introduction of various growth methods, the most successful being molecular beam epitaxy (MBE) and metal organic vapour phase epitaxy (MOVPE). Yoshida et at in 1983 [19] were able to grow a buffer layer of AlN in between the sapphire substrate and the GaN film while in 1988 Amano et al [20] were the first to succeed in fabricating p-type conductivity in GaN.

Once these breakthroughs were achieved, there was a rapid increase in developments throughout the 1990's from the first p-n junction GaN LED in 1989 [21] to the first layered structures of $InGa_{1-x}N_x$\GaN in 1993 [22]. 1996 saw the first demonstrations by Nakamura et al [23] of the first InGaN LED and laser diodes emitting blue and green emissions. Nakamura's work truly reignited interests in dilute nitrides as the problems with substrate mismatch and p-type doping were over.

The first step towards dilute nitrides was in 1992 when Weyers et al [14] made an unexpected discovery. They found that by incorporating small amounts of nitrogen to GaAs, there was a rapid reduction in the bandgap energy resulting in a red shift

emission. They also discovered that the reduction in energy per atomic percentage of nitrogen was more than ten times greater than the typical increase in other semiconductor alloys.

Kondow et al [24] were the first to publish results on a new quaternary alloy in the form of $Ga_{1-y}In_yN_xAs_{1-x}$ which allowed independent control over the Ga:In and N:As ratios. It was shown that by increasing the Ga:In ratio, the bandgap would decrease while the lattice parameter would be increased. For the N:As ratio, if this was increased, a decrease in the bandgap would occur too but the lattice parameter would also decrease. This meant that the quaternary alloy allowed the flexibility of tailoring the bandgap and lattice parameter, opening up a wide range of applications.

A 1.3μm laser emission was achieved by Nakamura in 1998 [25] and in 2000 the emission wavelength was raised to 1.515μm by Fischer et al [26]. The problem with early dilute nitride lasers was their high thresholds and low scope efficiencies compared to nitrogen free lasers.

Alloying nitrogen to ternary and quaternary alloys is not restricted to arsenide but can also be incorporated with antimonies. Research in $InSb_{1-x}N_x$ nitrides has lead to the cut-off point wavelength being achieved from 7μm at 300k to 8-12μm at the atmospheric transition band [28].

To date, despite their promising applications and encouraging experimental results [29] very little is known about the physical properties of these dilute nitrides. One main factor is the difficulty of incorporating nitrogen into the structure while maintaining good quality optical samples. Therefore much research has yet to be undertaken to understand growth, composition and annealing conditions.

A full understanding of the band structure of such dilute nitrides is still not known while fundamental electronic interactions, the effects on localised nitrogen states and the mechanism for light emission in these materials are yet to be fully understood.

1.3 Historical development of Raman spectroscopy

Raman spectroscopy is a powerful tool for the investigation of molecular vibrations and rotations. The Raman effect was first discovered by the Indian physicist Chandrasekhara Venkata Raman on the 28th February 1928 simultaneously with two Russian physicists G.S Landsberg and L.I Mandelstam. Raman with his assistant K.S Krishnan made their discovery in Calcutta, India while searching for an optical analogue of the Compton Effect. This investigation was based on Raman's previous work in 1922 when he observed the depolarisation of water as a function of wavelength and from his interest of light scattering in liquids. During a trip to Europe in 1921 onboard a steam liner, Raman became fascinated by the colour of the Mediterranean Sea. Back in India he started his light scattering experiments with liquids as the phenomenon was already predicted theoretically by Smekal, Kramers and Heisenberg.

In the experiment that resulted in the discovery of the Raman Effect, Raman used the most powerful light source available at the time, the sun. He focused the sunlight using a telescope to produce an intense beam that passed through a green filter creating a beam of green light. By passing the green light through a yellow filter, Raman observed the light as it interacted with a solution of liquid benzene. He could see that a weak yellow light was being emitted from the solution and instantly knew that this was the light phenomenon he was seeking. The new phenomenon was the inelastic scattering of light due to the interaction of green light with the benzene molecules causing the energy of the emitted photons to be shifted into the yellow part of the light spectrum [27]. This was viewed as frequency shifted lines upon a spectrum and due to the relative high intensity of the polarised scattered light, Raman could rule out the possibility of fluorescent radiation.

Raman published his work in the journal Nature on the 31st March and 21st April 1928 [28] while Landsberg and Mandelstam article appeared in the Die Naturwissenschaften on the 6th May 1928. Their work involved the use of pure quartz to study Einstein's and Debye's theories of the specific heats of solids. They concluded that when the frequency of light is scattered by a crystal, it would not only be scattered

by the Debye elastic waves acting as a grating but would also experience a frequency shift caused by the elastic waves propagating at the velocity of sound. At the same time as Raman first noticed the Raman Effect in his studies, Landsberg and Mandelstam noticed that the frequency shift in quartz was different to what they expected but were unconvinced by their findings. It was not until Raman published his first article in Nature that the Russian scientists realised they had observed the same new phenomenon. In their article they wrote

"At this moment, it is not possible for us to judge if, and to what extent, there exists a relation between the phenomenon observed by us and that for the first time shortly discussed by Raman, because of the brevity of his description"

This short remark by Landsberg and Mandelstam [29] was an acknowledgement of Raman's work which was one of the main reasons why the Noble prize for physics was awarded to Raman in 1930 and, consequently, the phenomenon being named after him. The Noble prize committee didn't believe that they obtained their work independently while Raman had more nominations; the committee felt that Raman's studies involving solids, liquids and gases established the universality of the effect. Even though some people were sceptical with his results, a number of other physicists accepted Raman discovery such as Sommerfeld while Pringsheim repeated Raman experiments successfully.

Today, Raman spectroscopy is much more sophisticated and simpler to measure due to a number of technological advances. In the pre-laser era, the main drawback was an insufficient intense radiation source however with the development of lasers this has changed. From using sunlight to lamps made from cadmium, helium, thallium, bismuth, lead, mercury and zinc, lasers provide an intense monochromatic chromatic beam. This beam can be concentrated on to a small area with a small energy spread and being so powerful, it is over one million times more intense than sunlight.

The second major technological advancement was the development of detectors to record the scattered light. Initially, photographic plates was used to record the Raman

spectrum however this was time consuming and very unreliable. Each spectrum would require huge amounts of time to record the scattered light, ranging from a few hours to half a day. However the technique was unreliable as the plates would have to be developed first (not a quick process) to discover if the optics were aligned correctly.

The next step was the development of the photomultiplier tube which was a sensitive optical transducer that converted photons into electrons. The device was so sensitive that it could count individual photons and thus allowed the number of photons at a particular frequency to be counted. The problem of using photomultipliers is that a whole spectrum could not be taken within a single integration. The increases in frequency energy were taken in very small steps and so a spectrum could take over an hour to be completed. These disadvantages reverted people back to the old concept of using photographic plates but in the form of digital cameras. Cameras known as charged coupled devices (CCD) were introduced allowing integrated chips that are sensitive to light and can produce a spectrum in seconds.

Not only has the introduction of lasers increased the sensitivity of Raman spectroscopy but has allowed the development of new techniques. These include surface enhanced Raman spectroscopy, Hyper Raman, resonance Raman scattering, stimulated Raman spectroscopy and coherent anti-Stokes Raman scattering.

1.4 Historical developments of the diamond anvil cell

High pressure studies today are mainly conducted using the diamond anvil cell (DAC) which has revolutionised high pressure research. However before the introduction of the DAC into the high pressure research community other techniques and materials were available to obtain the high pressure required to study the high pressure behaviour of solids. The generation of high pressure is related to the strength of the material used to contain the pressure and the technique involved in achieving this. The pressure limit is set by the compressive strength of the material.

Designing a piece of equipment to contain the high pressure is one of the main problems of high pressure research and it was not until the Bridgman era (1910 to 1950) that this issue was solved. This saw a phenomenal expansion in the knowledge of matter under high pressures due to P.W Bridgman inventing and developing both the Bridgman anvil and piston cylinder device [30]. During this time investigations were mainly conducted for electrical resistance and compressibility measurements up to 10GPa. A major development by Bridgman was the change in materials in constructing the pressure vessel from hardened steel to sintered tungsten carbide.

During the post Bridgman era in the late fifties and early sixties the piston cylinder device was further developed allowing the study of high pressures and high temperatures simultaneously. High pressure research took another step forward with a number of innovations with the development of the belt apparatus [31] featuring a combination of both the geometry of the anvil cell and the piston cylinder.

At the same time a new breed of pressure cells were being developed in the form of multi anvil cells [32]. These cells, or presses as they were known, had an increasing popularity due to the ability to study phase transitions and material synthesis but also the ability to hold a relatively large sample. These multi anvil cells could hold half a cubic centimetre of sample. A number of different types of presses were developed such as the tetrahedral press designed by Hall, the cubic and octahedral press [33-35].

The popularity of multi anvil cells did not last due to the size and complexity of the system but also due to the emerging diamond anvil cell. As the name suggests, the cell contains diamonds as the material to produce the pressure. It has long been known even during the Bridgman era that diamond was the hardest material know to man but no-one is quite sure why Bridgman never used it himself within his pressure cells. Diamond also has the benefits of being transparent to a large range of wavelengths, ideal for Raman, x-ray and infrared spectroscopy.

It was not until 1950 when Lawson and Tang [36] were the first to employ diamond as the containment of pressure in a piston cylinder setup. This was forgotten until 1959 when two independent and different versions of the DAC came out. Jamieson et al [37] at the University of Chicago developed a clamp type cell that used a 90 degree

configuration (light beam normal to the stress direction) while Weir et al [38] (at the National Bureau of Standards) adopted the 180 degree geometry (light beam coincident with the stress axis). This was due to both groups' initial intentions with Jamieson's interest in high pressure x-ray diffraction while Weir's was in infrared transmission measurements. The Weir setup also used a spring loaded lever arm system for applying the pressure and, with the cell, these have become essential features of the DAC.

Since 1959, the DAC has evolved from the original Weir setup into a fine quantitative tool for high pressure research. Since that day, a number of developments and innovations have enhanced the reputations of the DAC. These are the introduction of the metal gasket technique [39] for the generation of hydrostatic pressures, the discovery of the ruby fluorescence technique for pressure calibration [40-42], the development of the pressure scale based on the ruby line shift and the introduction of a new pressure transmitting medium [43]. All these developments were pioneered by the group at the National Bureau of Standards (NBS) while the DAC used in these studies was first developed in 1978 by Mao and Bell [44] at the Geophysical Laboratory in Washington. The Mao and Bell cell is based on the NBS cell by Piermarini and Block [45] (1975) and can exceed pressures of 100GPa.

1.5 Thesis outline

Over the past few years dilute III-V antimonide and phosphide nitrides, due to their potential for reduced cost and increased performance in LW (long wavelength) and FPA (focal plane arrays) applications, have become a new area of research. This interest is due to developments, primarily in the experimental and theoretical side of the work. These ternary Ga-N-V and In-N-V alloys have received attention from a number of theoretical and experimental studies on the bandgap borrowing and structural properties including strain and lattice perfection [46].

The introduction of a small percentage of nitrogen in these studies has seen an alteration in the bandgap so that it is smaller than the associated binary materials [47].

Similar studies in dilute arsenide nitrides, which have received much more attention, show that the substitution of nitrogen into arsenic sites reduces not only the bandgap but the lattice constant as well. These alloys have an optical fibre wavelength range of 1.3 to 1.55μm while the lattice matches that of GaAs [48].

It is also predicted that for InSb and GaSb the response wavelength moves towards the infrared regions of longer wavelengths when a small percentage of nitrogen is added [49]. A possible reason for this is due to the electronegative mismatch between antimony and nitrogen. Compared to other combinations of group V elements the bandgap reduction is expected to be greater in antimonide nitrides.

A recent review by Vurgaftman and Meyer [50] highlights the very little attention that has been given to Ga-N-V and In-N-V alloys and the lack of experimental results. Efforts to correct this have come from the collaboration between the research groups at QinetiQ Ltd and the University of Surrey which has closely looked at the theoretical bandgap bowing model, band anticrossing, and growth techniques [51] to increase nitrogen content and improve material quality of dilute III-V nitrides. Similar research has been conducted by Klar and Güngerich [52] from the Philipps University in Marburg, Germany into the study of vibrational properties of $GaAs_{1-x}N_x$ under hydrostatic pressures. Working in collaboration with these physicists, I have been able to work in this area for my PhD thesis.

I have tried to highlight in the above statements that the incorporation of nitrogen into group III-V alloys not only strongly modifies the band structures of these semiconductors but also changes their optical properties. Kent and Zunger [48] proposed that the nitrogen forms isoelectronic electron traps which persist at localised states up to a few percentage of nitrogen. These localised states on the global electronic properties of the alloy have been found to depend sensitively on the local environments of the Nitrogen atom.

One method to observe these impurities in ternary alloys is the study of their vibrational properties using known optical characterisation techniques such as Raman spectroscopy. Raman spectroscopy is a versatile standard optical characterisation technique which is non-destructive, contact-less and requires little or no special sample

preparation such as thinning or polishing. Raman scattering is ideal for studying the phonon properties of crystalline materials and other aspects such as lattice, electronic and magnetic properties.

Previous work by Buyanova et al [53] highlights the observation of a local vibrational mode (LVM) of nitrogen at room pressure. By studying the LVM of nitrogen over a range of high pressures with the aid of a diamond anvil cell, it will provide a powerful tool for obtaining information about the influence of nitrogen incorporation on the crystalline structure and about the local nitrogen environment. This will be the basis of my thesis.

Chapter 2 introduces the basic concepts of group III-V dilute nitrides, high pressure and Raman scattering. This covers the basic crystal structure, space groups and quantum structure. The chapter then discusses the effect of nitrogen incorporated into dilute nitrides and how it can be studied by observing the local vibrational mode due to lattice vibrations. The diatomic model, phonon dispersion curves, overtones and phonon density of states are discussed before going on to explain the different optical processes (Raman) that are used in this thesis while quickly covering other optical processes in semiconductors. The effect of applying pressure to sample is discussed and how by measuring the vibrational properties leads to the determination of the mode Grüneisen parameter and anharmonicity of a bond between atoms.

Chapter 3 talks about the experimental details employed in this thesis, especially the use of Raman spectroscopy and the diamond anvil cell. The chapter also discusses sample characteristics and how they were prepared for studying.

The next chapters (4 to 7) are the results section of the thesis, starting with bulk GaP. In chapter 4, the Raman scattering measurements of GaP under hydrostatic pressures up to 30GPa are presented. The measurements allow the phonon modes of GaP to be observed under pressure using Raman scattering for the first time. From these pressure induced Raman shifts, the mode Grüneisen parameter and anharmonicity of Ga-P bonds are calculated and compared to existing data for GaN and GaAs.

Chapter 5 is the first of three chapters that studies dilute nitrides. For this chapter, the sample is $GaP_{1-x}N_x$ where a small percentage of nitrogen (N) atoms have

been substituted into the GaP lattice. The effect of nitrogen incorporation in the crystal structure is measured by its vibrational properties which are studied under hydrostatic pressures using Raman scattering. The pressure induced phonon modes and the local vibrational mode of nitrogen are measured and compared to those measured in chapter 1 to assess if the incorporation of nitrogen behaves in a Ga-N-like way. Overall the mode Grüneisen parameter and anharmonicity are calculated.

Chapter 6 is the dilute nitride of $GaSb_{1-x}N_x$ and similar measurements are taken of the vibrational properties as in chapter 3 and 4. Previous Raman measurements under pressure have been taken for its group III-V semiconductor which allows a perfect opportunity to study the $GaSb_{1-x}N_x$ local vibrational mode and assesses the impact of nitrogen substitution.

Finally chapter 7 is the dilute nitride of $InSb_{1-x}N_x$. Very little experimental work has been carried out on this type of dilute nitride due to the lower percentages of nitrogen that can be incorporated into the crystal structure. Due to this difficulty in present day growth techniques, the use of Raman scattering to measure the optical phonon modes presents an excellent opportunity. The results from this study including the mode Grüneisen parameter and the shift in phonon modes of $InSb_{1-x}N_x$ are presented here.

1.6 References

[1] S. Minomura and H. G. Drickamer. J. Phys. Chem. Sol. **23** 451 (1962)

[2] S. Froyen and M. L Cohen. Phys. Rev. B. **28** 3258 (1983)

[3] Y. G. Vohra, S. T. Weir and A. L. Ruoff. Phys. Rev. B. **31** 7344 (1985)

[4] A. Onodera, N. Kawi, K. Ishizaki and I. L. Spain. Sol. Stat. Commun. **14** 803 (1974)

[5] J. I. Pakove. J. Luminescence. **7** 114 (1973)

[6] J. Lang, Y. Laurent, M. Maunaye and R. Marchand. Prog. Cryst. Growth Charact. **2** 207 (1979)

[7] R. Juza and H. Hahn. Zeitschr. Anorgan. Allgen. Chem. **239** 282 (1938)

[8] S. Nakamura, Physics World (February 1998)

[9] S. Nakamura, Electronics and Communications in Japan Part II-Electronics **81**, 1-8 (1998)

[10] A. G. Bhuiyan, A. Hashimoto, and A. Yamamoto, J. Appl. Phys. **94** 2779 (2003).

[11] L. H. Qin, Y. D. Zheng, D. Feng, Z. C. Huang, and J. C. Chen, J. Appl. Phys. **78** 7424 (1995)

[12] P. B. Perry and R. F. Rutz, Appl. Phys. Lett. **33** 319 (1978)

[13] I. A Buyanova, W. M Chen and B. Monemar. MRS Internet J. Nitride Semicond. Res. **2** 2 (2001)

[14] M. Weyers, M. Sato and H. Ando. Jpn. J. Appl. Phys. **31** 835 (1992)

[15] J. Geisz, D. J. Fridman, J. M. Olson and S. R. Kurtz. J. Cryst Growth. **195** 401 (1998)

[16] M. Settings. III-V's Review. **16** (6) 53 (2003)

[17] R. Juza and H. Hahn. Z. Anorg. Allg. Chem. **234** 282 (1938)

[18] H. P. Maruska and J. J. Tietjen. Appl. Phys. Lett. **15** 327 (1969)

[19] S. Yoshida, S. Misawa, and S. Gonda. Appl. Phys. Lett. **42** 427 (1983)

[20] H. Amano, I. Akasaki, T. Kozawa, K. Hiramatsu, N. Sawak, K. Ikeda , and Y. Ishi.. J. of Lumin. **40** 121 (1988)

[21] H. Amano, M. Kito, K. Hiramatsu, and I. Akasaki. Jpn. J. Appl. Phys. Part 2 Lett. **28** 2112 (1989)

[22] S. Nakamura, T. Mukai, and M. Senoh. Appl. Phys. Lett. **64** 1687 (1994)

[23] S. Nakamura, M. Senoh, S. Nagahama, N. Iwasa, T. Yamada, T. Matsushita, H. Kiyoku, and Y. Sugimoto, Jpn. J. Appl. Phys. Part 2 Lett. **35** 74 (1996)

[24] M. Kondow, K. Uomi, K. Hosomi and T. Mozume. Jpn. J. Appl. Phys **33** 1056 (1994)

[25] K. Nakahara, M. Kondow and T. Kitatani. IEEE Photonics Tech. Lett. **10** 487 (1998).

[26] M. Fischer, M. Reinhardt and A. Forchel. Electron. Lett. **36** 1208 (2000)

[27] C. V. Raman and K. S. Krishnan. Nature. **121** 501 (1928)

[28] http://www.deltanu.com/dn06/tutorials.htm 28/12/07

[29] R. Singh. Phys. Perspect. **4** 399 (2002)

[30] P. W. Bridgman. *The Physics of High Pressure.* Bell (1952)

[31] H. T. Hall. Rev. Sci. Instrum. **31** 125 (1960)

[32] F. P. Bundy. *Modern High Pressure research. Vol 1.* Butterworths (1962)

[33] E. C. Lloyd, V. O. Hutton and D. P. Johnson. J. Res. **63C** 59 (1959)

[34] J. Osugi, K. Shimizu, K. Inoue and K. Yasunami. Rev. Phys. Chem. Jpn. **34** 1 (1964)

[35] A. Ohtani, A. Onodera and N. Kawi. Rev. Sci. Instrum. **50** 308 (1979)

[36] A. W. Lawson and T. Y. Tang. Rev. Sci. Instrum. **21** 815 (1950)

[37] J. C. Jamieson, A. W. Lawson and N. D Nachtrieb. Rev. Sci. Instrum. **30** 1016 (1959)

[38] C. E. Weir, E. R. Lippincott, A. Van alkenburg and E. N Bunting. J. Res. **63A** 55 (1959)

[39] A. Van Valkenburg. Conference Internationale Sur-les-Hautes Pressions, Le Creusot, (1965)

[40] R. A. Forman, G. J. Piermarini, J. D. Barnett and S. Block. Science. **176** 284 (1972)

[41] J. D. Barnett, S. Block and G. J. Piermarini. Rev. Sci. Instrum. **44** 1 (1973)

[42] G. J. Piermarini, S. Block, J. D. Barnett and R. A. Forman. J. Appl. Phys. **46** 2774 (1975)

[43] G. J. Piermarini, S. Block and J. D. Barnett. J. Appl. Phys. **44** 5377 (1973)

[44] G. J. Piermarini and S. Block. Rev. Sci. Instrum. **46** 973 (1975)

[45] H. K. Mao and P. M. Bell. Carnegie Inst. Washington Yearb. **77** 904 (1978)

[46] P. J. Klar. Prog. Sol. Stat. Chem. **31** 301 (2003)

[47] J. D. Perkins. A. Mascarenhas, Y. Zhang. J. F. Geisz and J, Friedman. Phys. Rev. Lett. **82** 3312 (1999)

[48] P. R. C. Kent and A. Zunger. Phys. Rev. B. **64** 115208 (2001)

[49] T. Makimoto, T. Saito, T. Nishida and N. Kobayashi. Appl. Phys. Lett. **70** 2984 (1997)

[50] I. Vurgaftman, J. R. Meyer and L. R. Ram-Mohan. J. Appl. Phys. **89** 5815 (2001)

[51] J. P. Itie, A. Polian and C. Jauberthie-Carillon. Phys. Rev. 40 9709 (1989)

[52] M. Güngerich, P. J. Klar, W. Heimbrodt, J. Koch, M. P. Halsall and P. Harmer. Phys. Rev. B. **71** 075201 (2005)

[53] I. A. Buyanova, W. M. Chen, E. M. Golddys, P. Xin and C. W. Tu. Appl. Phys. Lett. **78** 3959 (2001)

Chapter 2: Theory of dilute nitrides under hydrostatic pressure and Raman scattering

2.1 Crystal structures

A crystal is a finite regular arrangement of atoms in space which have an infinite number of unit cells which can be repeated to make up a highly ordered structure. This structure consists of a number of lattices that have an infinite array of points in space, arranged so that every point has an identical surrounding. Therefore crystals are categorised by their crystal structure and the underlying lattice. This is known as Bravais classification.

Name	Number of Bravais lattices	Conditions	Primitive	Base-centred	Body-centred	Face-centred
Triclinic	1	$a_1 \neq a_2 \neq a_3, \alpha \neq \beta \neq \gamma$	•			
Monoclinic	2	$a_1 \neq a_2 \neq a_3, \alpha = \beta = 90^o \neq \gamma$	•	•		
Orthorhombic	4	$a_1 \neq a_2 \neq a_3, \alpha = \beta = \gamma = 90^o$	•	•	•	•
Tetragonal	2	$a_1 = a_2 \neq a_3, \alpha = \beta = \gamma = 90^o$	•		•	
Cubic	3	$a_1 = a_2 = a_3, \alpha = \beta = \gamma = 90^o$	•		•	•
Trigonal	1	$a_1 = a_2 = a_3, \alpha = \beta = \gamma < 120^o \neq 90^o$	•			
Hexagonal	1	$a_1 = a_2 \neq a_3, \alpha = \beta = 90^o, \gamma = 120$	•			

Table 2.1: Bravais lattices for three dimensional crystals.

In three dimensional structures, Bravais lattices consist of fourteen lattices in seven different types of cell. These cell groups are given in the table 2.1 which also shows the conditions required for each lattice to occur.

Of these lattices, a large number of semiconductor materials have cubic structures in the form of body centred cubic (bcc) and the face-centred cubic (fcc). Figure 2.1 shows these cubic lattices as well as the simple cubic structure.

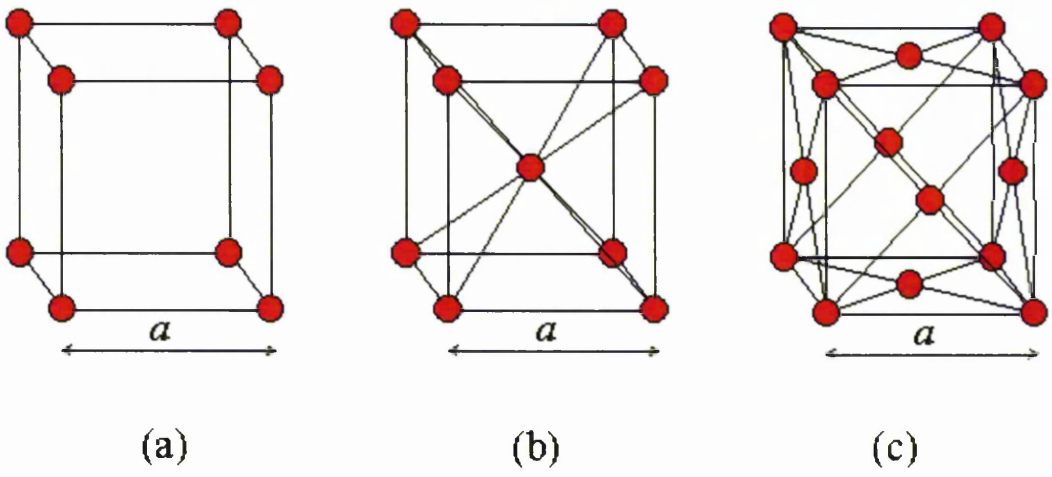

Figure 2.1: The simple cubic (a), the body-centred cubic (b) and the face-centred cubic (c) lattice.

For the case of Gallium Nitride (GaN), this is a wurtzite structure, constructed from two interpenetrating hexagonal closed packed structures shown in figure 2.2. It shows that the Ga atom is tetrahedrally surrounded by four nitrogen atoms which forms covalent tetrahedral bonding.

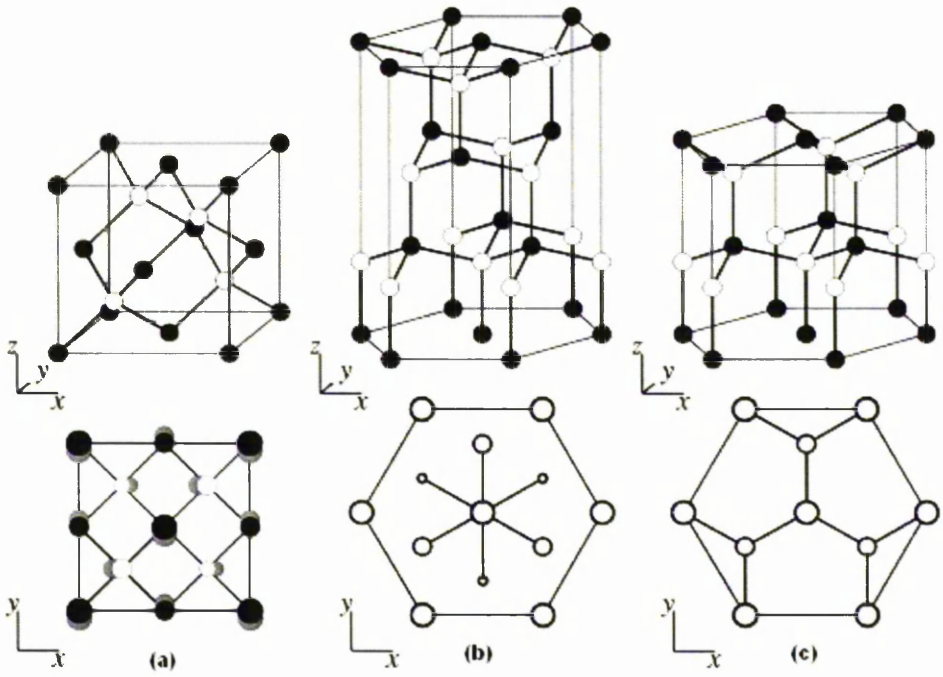

Figure 2.2: Zinc-blende crystal structures represented as a cubic cell (a) and hexagonal cell (b) while (c) is the wurtzite crystal structure [1].

Dilute nitrides materials are of great interest in this study. When pressure is applied to the samples, their structures will change by going through phase transitions. This results in a new structure being formed where the transitions are either termed "reconstructive" in cases where the bonds are broken and reformed to create new structures or "displacive". Examples of reconstructive transitions are the fourfold coordinated insulating phases which are stable at normal room pressure but change to a sixfold coordinated metallic phases under pressure [2]. Displacive transitions are those by which the position of the atoms changes by fairly small amounts.

All III-V compounds (including dilute nitrides) have been the subject of pressure studies using high-pressure devices over recent years and so information about their phase transitions is well known. Table 2.2 highlights the crystal structure of these group III nitrides before pressure is applied and the structure once it has been through their first phase transition. A combination of these semiconductors (where the amount

of nitrogen is only a few percent) with other III-V materials produces ternary Ga-N-V alloys ($GaP_{1-x}N_x$, $GaSb_{1-x}N_x$, and $InSb_{1-x}N_x$). Studies in this thesis have been carried out to see how this small percentage of nitrogen has an affect on the pressure dependence of lattice dynamic properties and how this relates to their underlying crystal structure such as bond strength.

Semiconductor material	Structure before first phase transition	Structure after first phase transition
GaN	Wurtzite	Cmcm
GaP	Zinc-blende	Cmcm
GaSb	Zinc-blende	β-tin
InSb	Zinc-blende	s-Cmcm

Table 2.2: Crystal structures for different group III-V semiconductors before and after phase transition. The space group Cmcm is an orthorhombic crystal structure [1].

2.2 Space groups

There are 230 unique space groups which are a result of combining 7 crystal systems with 14 Bravais lattices, 32 point groups, screw axes and glide planes. A space group is a group of symmetry operations that are combined to describe the symmetry of a region of 3 dimensional space. In space groups, symmetry elements do not have to intersect at a single point unlike in point groups where all symmetry elements pass through one point in the object.

A space group is designated by a capital letter which identifies the lattice type followed by a point group symmetry symbol. Further symbols represent the rotation and reflection elements in the screw axes and glide planes. The Cmcm structure is one of these space groups whose crystal system is a based-centred orthorhombic. The space group is also centrosymmetric and can be understood as a distortion of the NaCl

structure. These distortions consist of (a) a shearing of alternating (001) planes in the [010] direction, (b) a puckering of the [100] atomic rows of NaCl in the [010] direction and (c) an orthorhombic adjustment of the cell [1].

The Cmcm structure can be seen in figure 2.3 along side the NaCl structure so that comparisons due to distortions mentioned above can be made. A closely related structure to Cmcm is that of s-Cmcm (super-Cmcm). This structure is observed at high pressures in InSb and the difference between the two is the number of shearing planes involved in the distortion. In Cmcm, two planes are involved while for s-Cmcm there are six resulting in the s-Cmcm structure being three times as long in the z direction as Cmcm.

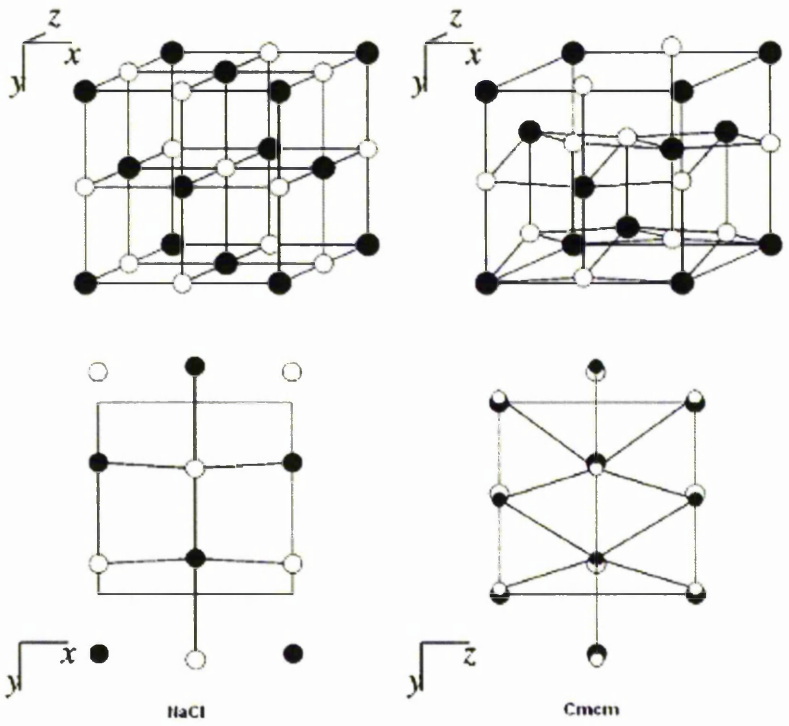

Figure 2.3: NaCl (left) and Cmcm (right) crystal structures.

2.3 Quantum structures

Modern crystal growth techniques have made it possible to grow narrow layers of semiconductor material that are able to contain the motion of carriers (electrons and holes) in a one dimensional (1-D) confinement. These are known as heterostructures that involve layers of different semiconductor material being grown upon each other during epitaxial growth. As properties of semiconductor depends on growth material, by altering the design of the structure such as layer thickness, composition and carrier confinement, we are able to grow quantum well structures.

Esaki and Tsu in 1970 first proposed that using growth methods such as molecular beam epitaxy, heterostructures could be fabricated and if the layers were thin enough, quantum confinement effects would arise [3]. The simplest semiconductor structure that can be grown is in the form of a single crystal such as an epitaxial layer of GaN while in heterostructures, at least two different bandgaps are used.

As carriers (electrons and holes) propagate in a narrow bandgap semiconductor, their motion is perpendicular to the heterointerfaces and so is quantised. This leads to a number of discrete energy levels being allowed in the conduction and valence bands, thus modifying the band structure. These energy levels and device characteristics can be altered by varying the thickness and composition of the materials during growth leading to new devices.

2.4 Nitrogen incorporation in dilute nitrides

When a fraction of the host anions is replaced isoelectronically by nitrogen anions, the substituting anions act as strong local perturbations of the host material [4]. This is due to large differences in the size and electronegativity between the nitrogen atoms anions and the host anions. This behaviour is described by the term isoelectronic impurity.

The incorporation of nitrogen into III-V semiconductors has only become feasible in recent years due to improvements in growth techniques. By increasing the

concentration of nitrogen from doping levels by a few percent, this results in a dramatic change in the band structure. With increasing nitrogen content, strong perturbed host states and localised clusters states of the nitrogen impurity coexist in the conduction band. The strong local perturbation due to nitrogen disturbs the translational symmetry of the crystal structure giving rise to a large degree of disorder.

In $GaAs_{1-x}N_x$ studies by Klar et al [5] it was shown that these nitrogen cluster states are formed with energies below a single nitrogen level. The phonon replicas of the nitrogen modes extend into the bandgap and can be clearly seen with Raman or PL spectroscopy. These optical techniques also show no change in the bandgap of the host atoms indicating that nitrogen has no effect on the host atoms.

To help us understand and observe changes in the local nitrogen environment, Raman spectroscopy is a useful tool that can be used to study the local vibrational mode of the nitrogen atom. In conjunction with this, the use of pressure induced experiments allow us to observe changes in the band structure of these dilute nitrides. This will help to answer the question of whether band structure concepts such as the definition of band effective masses (which rely on translational symmetry and crystal periodicity) are applicable to dilute nitrides. If not, do we consider these nitrides to have an amorphous character and thus is a new unified description required?

2.5 Lattice vibrations in semiconductors

As a semiconductor lattice vibrates, atoms which are not fixed in space vibrate collectively as modes that propagate throughout the material. Such propagating modes can be considered as a wave where interactions between atoms produce lattice vibrations that have quantised energy levels. These quanta of vibration are known as phonons and can interact with photons, electrons and neutrons when momentum is involved (see optical processes). Phonons do not have any momentum as the centre of mass in a crystal does not change its position under vibrations.

If atoms of the same type interact with each other, the vibrations are called acoustic phonons and can be either transverse (TA) or longitudinal (LA) waves. When different types of atoms interact, these vibrations are called optical phonons and again are in the form of transverse (TO) or longitudinal (LO) waves. Acoustic phonons correspond to sound waves in the lattice whose frequency becomes small when their wavelength is large. Where as optical phonons have a minimum frequency of vibration even when their wavelength is large.

Optical phonons are so called because they easily interact with light due to positive and negative ions at adjacent lattice sites vibrating against each other creating a time-varying electric dipole moment. Optical phonons interacting in this way are called infrared active while phonons that are Raman active interact indirectly with light (see section on Raman scattering).

Optical phonon modes in ternary semiconductors will exhibit one of three different behaviours, either a "one-mode", "two-mode" or a "one-two-mode". A one-mode system (Figure 2.4a) is so called because the appearance of a Raman spectrum will exhibit one set of vibrational optical phonon modes. This mainly occurs in the majority of I-VII alloys while for the majority of III-V alloys, a two-mode behaviour (Figure 2.4b) is present. These exhibit two distinct sets of optical phonons whose frequencies are characteristic to each binary material and whose intensity is roughly proportional to the respective concentration.

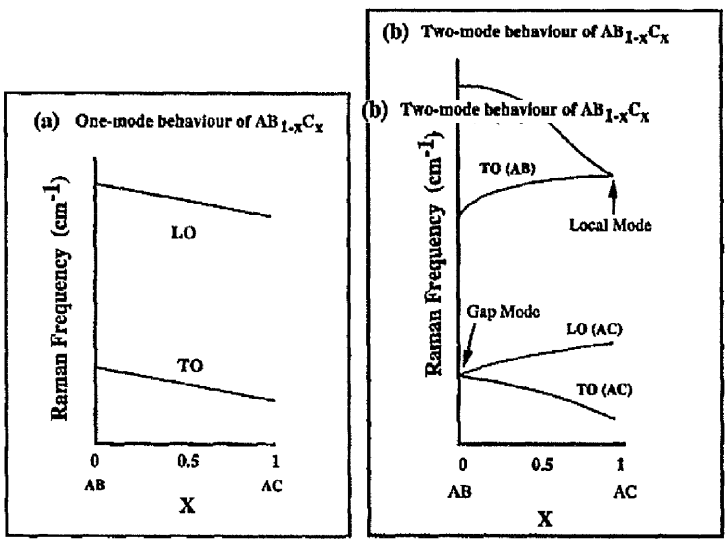

Figure 2.4: These two diagrams illustrate a one-mode (a) and two-mode behaviour (b) of an $AB_{1-x}C_x$ crystal structure over various x concentration values [6].

Finally a one-two-mode is when a system exhibits a single mode for part of the concentration range with two modes appearing over the rest.

In figure 2.4b the term "local mode" is of great importance to work in this thesis as it arises when considering interactions on the lattice vibrations that is localised in real and frequency space. This results in a vibrational frequency that will lie above the lattice phonon frequency range. An example of this is when a host atom is replaced by an impurity atom and is discussed in greater depth in section 2.9.

An example of a two-mode behaviour in a mixed III-V semiconductor material has been presented by Cherng et al [7] who has used Raman scattering to observe the behaviour of long-wavelength optical phonons in GaP and GaSb. These real binary materials are of interest to this thesis and their optical phonons (LO and TO) are shown for various values of x in figure 2.5a.

For a dilute nitride such as $GaP_{x-1}N_x$ (Figure 2.5b) it has been reported by Buyanova et al [8] that this ternary semiconductor also exhibits a two-mode behaviour (for nitrogen concentration less than 3%), observing a GaP-like and GaN-like optical phonon modes. All data points in figure 2.5 represent experimental data collected by the authors while solid curves show theoretical results.

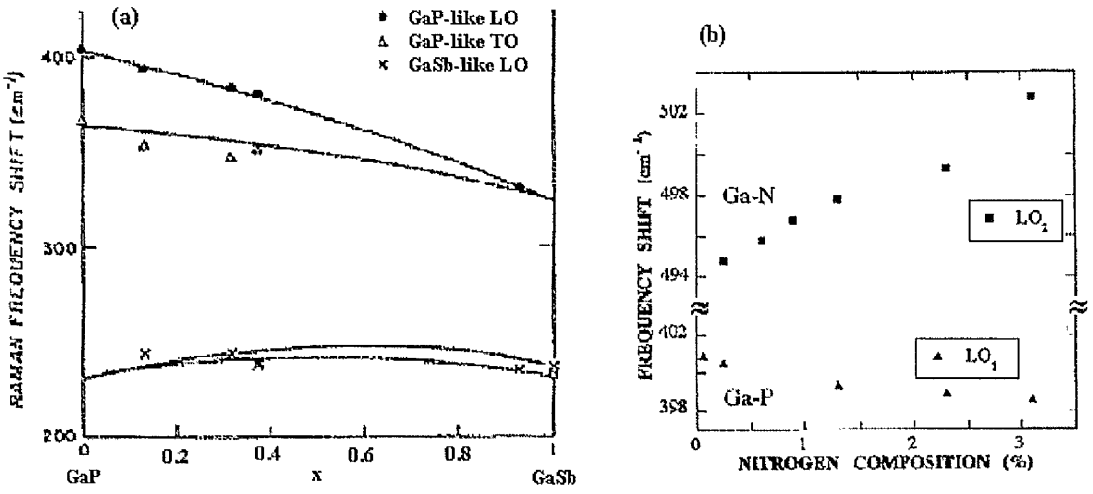

Figure 2.5: Long-wavelength behaviour of LO and TO mode frequencies in GaP\GaSb mixed crystal (a) and $GaP_{x-1}N_x$ (b).

2.6 Diatomic atom model

The diatomic model is used to quantitatively describe the phonon frequencies and frequency shifts of various local vibrational modes. In this model, an impurity such as nitrogen has a mass (m) which is attached by a spring k to a host atom of mass M. Thus the vibrational frequency of the diatomic molecule is given by

$$\omega = \sqrt{k\left(\frac{1}{\chi M} + \frac{1}{m}\right)} = \sqrt{\frac{k}{\mu}} \qquad \text{Equation 2.1}$$

Where the mass of the atom is multiplied by an empirical constant χ to account for the vibrations of other host atoms and μ is the reduced mass. A diatomic molecule is a molecule that is made up of two atoms of the same or different elements. The diatomic atom model can be summarised by a diatomic chain diagram (Figure 2.6) where the same type of atoms are equally spaced "a" and each diatomic basis is represented by an integer n. The displacement of the heavier atom from its equilibrium position is denoted as $U_n(t)$ while for the lighter atom, the displacement is denoted as $V_n(t)$. For both atoms, it is assumed that they oscillate in the same direction in the lattice along the longitudinal vibration.

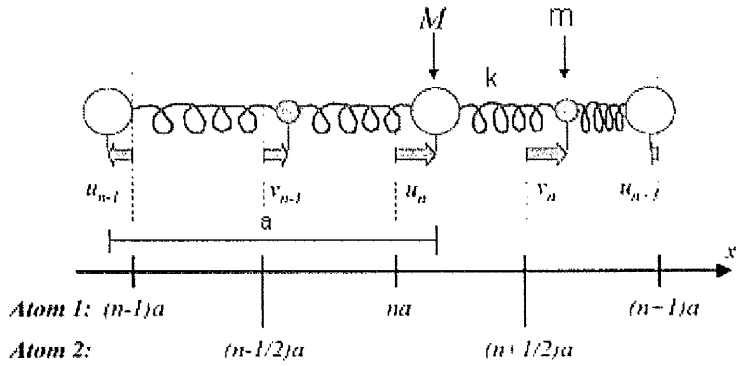

Figure 2.6: Interactions of atoms in a diatomic harmonic crystal structure [9].

Equation 2.1 allows the possibility of two dispersion relations denoted $\omega_+(K)$ and $\omega_-(K)$ which relates the angular frequency to wavenumber. These can be plotted in the first Brillouin zone (Figure 2.7) representing the phonon spectrum of a one dimensional diatomic harmonic crystal.

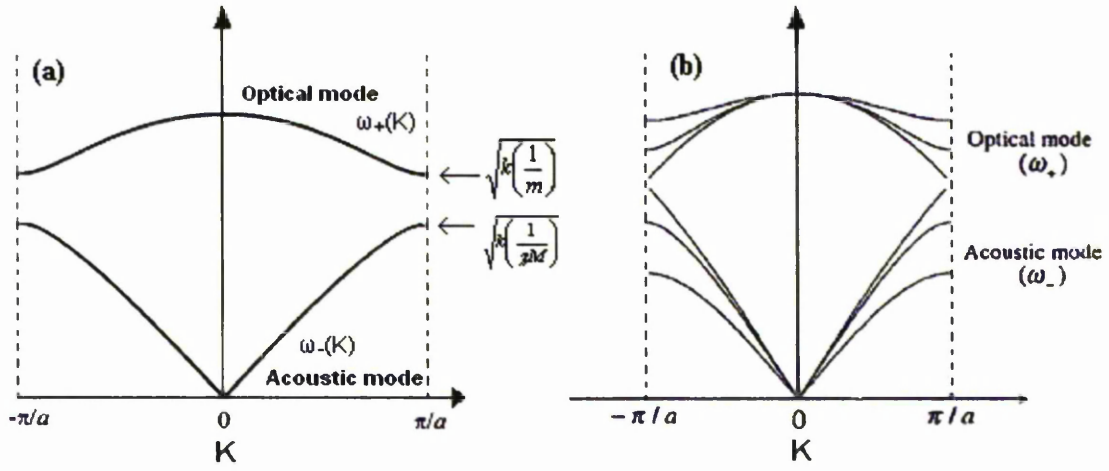

Figure 2.7: The first Brillouin zone highlighting the dispersion relations of a simple model (found in most text books) involving a single curve (a) and a more advance \ realistic model which is represented by a number of curves due to LO-TO splitting (b)

The above diagrams arise due to the displacement in which the vibrating modes move such that both the motion of the LO and TO modes are along symmetrically equivalent directions. When the wavevector is equal to zero (K = 0) the types of motion become exactly equivalent. In this case one would expect that the LO and TO frequencies would be equal as seen in figure 2.7a but this is a simplified outlook on the dispersion relation which in the majority of situations does not happen. A more realistic diagram is given in figure 2.7b which illustrates what happens when the wavevector is not zero.

For wavevectors that are close to but not exactly at K = 0, optical phonon modes generate electrical fields that are either parallel or perpendicular to the modes direction of propagation. This results in having a significant effect on the frequency on these modes as $\omega = 0 > \omega = \infty$ causing a split in the LO and TO frequencies. This

phenomenon is known as LO-TO splitting (as shown in figure 2.7b) where $\omega_{LO} > \omega_{TO}$ highlighting the fact that when the wavevector is exactly equal to zero it is the only time when the frequencies are the same.

In addition, figure 2.7 highlights the optical and acoustic branches of equation 2.1. The top curves represents the optical phonon mode for $\omega_+(K)$ while the lower curves represents the acoustic phonon mode for $\omega_-(K)$. The maximum wave-vector permitted by the cyclic nature of the chain is when the $K = \pi\backslash a$ and thus the frequency of each phonon mode at this point is given by $\sqrt{k\left(\frac{1}{\chi M}\right)}$ and $\sqrt{k\left(\frac{1}{m}\right)}$.

The diatomic model was first put forward by Jusserland et al [10] in which it was suggested that due to quantisation, the frequency of the highest optical branch in superlattices decreases. This model can also be used for dilute nitrides due to the different forces between atoms which have different mass densities. There are two important assumptions for the diatomic model [11]. The first being that only interactions within 2a of each atom are considered and secondly $|K| = K \propto \frac{1}{a}$ where K is the wavevector and a is the thickness of the layer.

2.7 Phonon dispersion curves and density of states

A phonon dispersion curve is a plot of frequency verses wavevector for lattice vibrations in crystals used along high-symmetry directions such as [100] or [111] of the Brillouin zone. Phonons can be classed as transverse or longitudinal according to whether their displacement are perpendicular or parallel to the direction of the wavevector K.

Phonon dispersion curves are calculated in two ways, experimentally and theoretically and are plotted together to see how both calculations compare. For example the theoretical approach allows one to develop their own unique model by incorporating known crystal force constants which are obtained by modelling

interactions between ions in terms of various parameters. These include bulk modulus, sound velocity and zone-centred phonon frequencies which are adjusted and fitted using a number of models. Force constant, shell, bond and bond charge are a few examples of models used to calculate the theoretical curves.

On the other hand experimental data can be used to determine phonon dispersion curves by measuring phonon frequencies along the Delta, Sigma, Lambda and Z-lines of the Brillouin zone using Raman scattering. In the case of GaP (Figure 2.8) its phonon dispersion curves were calculated from experimental data points [12-13] and theoretical curves from ab initio calculations [14]. Ozolins et al [15] have also been able to calculate the phonon dispersion curves for GaP using first-principles density-functional linear-response theory.

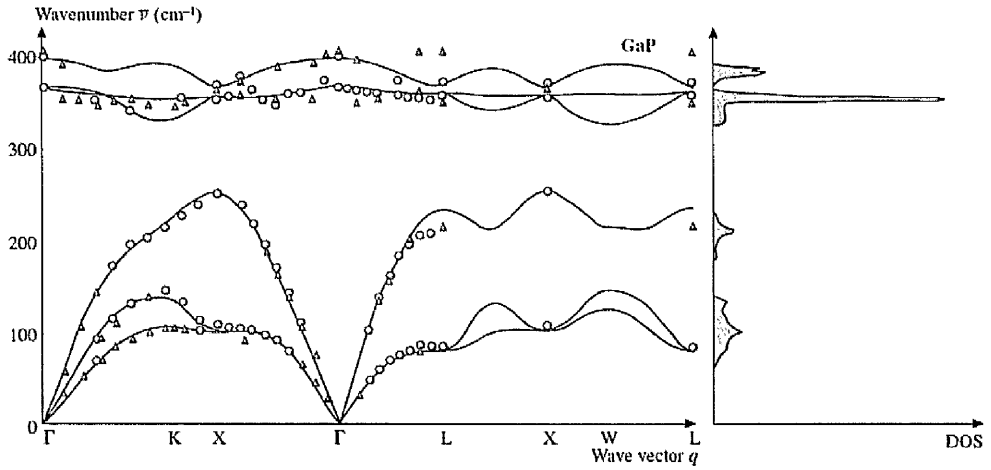

Figure 2.8: Phonon dispersion curves (left) and phonon density of states (right) for bulk GaP taken from [16]. Experimental data points are the open [12] and closed [13] symbols while the theoretical curves are obtained from ab initio calculations [14].

The phonon dispersion curve for a binary material such as GaP (Figure 2.8) is similar for other zinc-blende crystals such as GaSb (Figure 2.9a) and InSb (Figure 2.9b) in that the LO phonon frequency is higher than the TO phonon. The differences in frequencies are due to the partially ionic nature of bonding in zinc-blende crystals. Taking GaP as

an example, the P atom contributes more electrons to the bond than the Ga atom resulting in the covalent bond spending on average more time nearer to the P atoms than the Ga atoms. This means that the P atoms are slightly more negatively charged than the Ga atoms which are slightly positive. In addition to this, there is a restoring force (Coulomb's) which is present in LO phonons and not in TO phonons that affects the difference in frequencies.

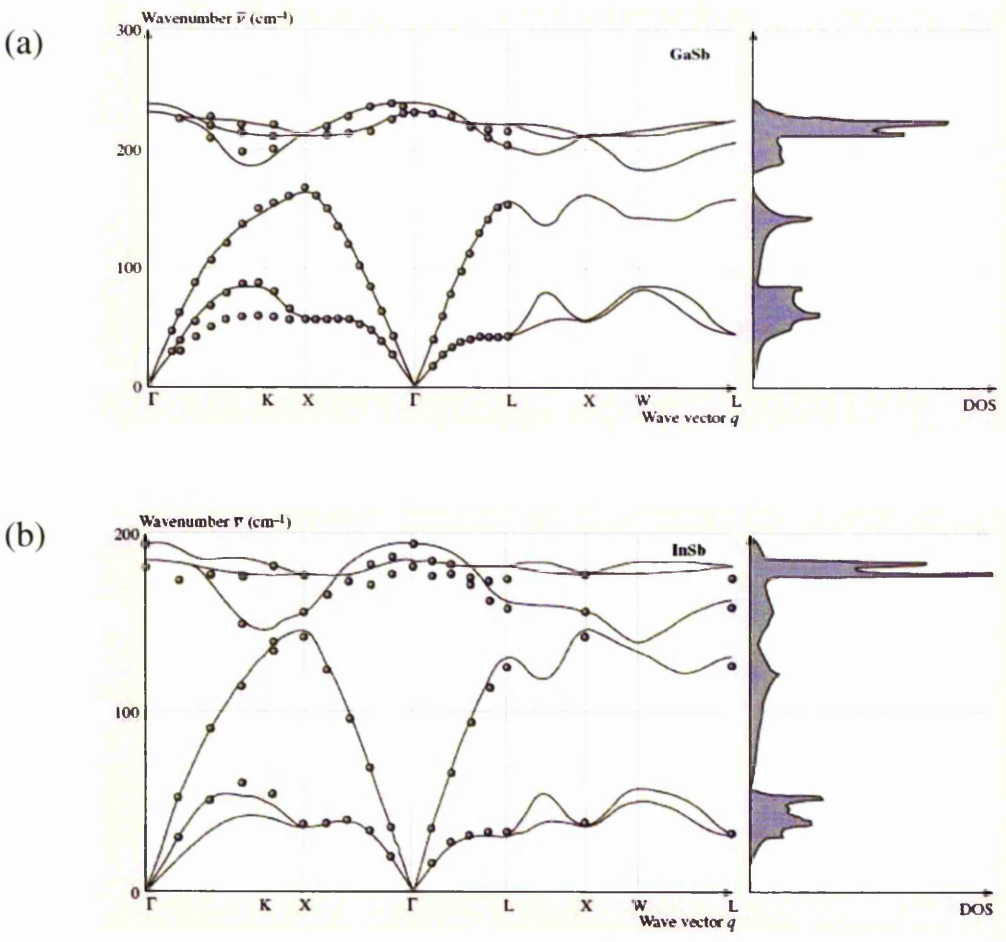

Figure 2.9: Phonon dispersion curves (left) and phonon density of states (right) for bulk GaSb (a) and bulk InSb (b) taken from [16]. GaSb: Experimental data points are presented [17] while the theoretical curve is obtained from ab initio calculations [18]. InSb: Experimental data points are presented [19] while the theoretical curve is obtained from ab initio pseudopotential calculations [20].

The phonon density of states as seen in the right-hand panels of figure 2.8 and 2.9 for GaP, GaSb and InSb gives the number of states that phonons can occupy per unit volume of crystal per unit energy. The phonon density of states (P-DOS) helps to determine the number of phonons with a given wavelength and energy and thus allows calculations for the specific heat of a crystal and properties of electron scattering and trapping to be determined. P-DOS can be calculated using equation 2.2 where the summation is taken from all over the wavevector K and phonon branches n.

$$g(\omega) = \sum_{K,n} \delta\lfloor \omega_n(K) - \omega \rfloor \qquad \text{Equation 2.2}$$

Firstly, we need to consider the Debye model which was developed to describe the observed heat capacity of solids. It relies upon equation 2.1 where the phonon branches in figure 2.7 are replaced with a longitudinal and two transverse acoustic branches. The phonon frequencies are given by

$$\omega_n(K) = v_n|K| = v_n k \qquad \text{Equation 2.3}$$

Where k is the normal \ length of the wavevector K, n is a index (e.g l or t) while v_l and v_t are the longitudinal and transverse sound velocities respectively. Equation 2.3 gives a linear line (Figure 2.10) producing a simplification in the phonon dispersion spectrum.

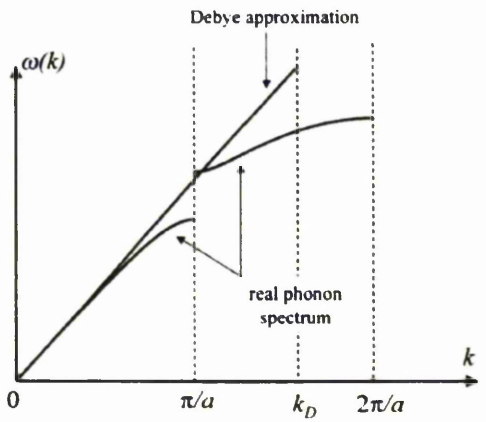

Figure 2.10: An illustration of the Debye model in the phonon dispersion curve.

The linearisation in figure 2.10 implies that the frequency depends solely on the length of the wavevector and so some boundary conditions must be changed in this model. In a real phonon dispersion relation the wavevector range is limited to the first Brillouin zone. So for the model to be accurate, a Debye wavenumber needs to be introduced so that the volume of the first Brillouin zone is equal to

$$k_D^3 = \frac{6\pi^2 N}{V} \qquad \text{Equation 2.4}$$

where k_D is the Debye wavenumber and thus corresponds to the Debye frequency ω_D.

$$\hbar\omega_D = \hbar v_0 k_D \qquad \text{Equation 2.5}$$

Referring back to equation 2.2, the discrete wavevector K can be considered as quasi-continuous where the volume is taken into account. A summation is preformed over the entire values of K in the first Brillouin zone and the P-DOS becomes

$$g(\omega) = \frac{4\pi V}{(2\pi)^3} \sum_n \int_0^{k_D} \delta[\omega_n(K) - \omega] k^2 dk \qquad \text{Equation 2.6}$$

We can now integrate from 0 to the Debye wavenumber to keep in agreement with the Debye model. Substituting equation 2.3 into equation 2.6 we get two terms

$$g(\omega) = \frac{V}{2\pi^2} \sum_n \int_0^{k_D} \delta[v_n k - \omega] k^2 dk \qquad \text{Equation 2.7}$$

$$g(\omega) = \frac{V}{2\pi^2} \sum_n \int_0^{k_D} \delta[x - \omega] \frac{x^2}{v_n^3} dk \qquad \text{Equation 2.8}$$

Letting the variable $V_nK = x$, there is a non-zero solution only if a wavenumber k between 0 and K_D such that $x = v_n$ and $k = \omega$.

$$g(\omega)=\frac{V}{2\pi^2}\sum_n \frac{\omega^2}{v_n^3} \qquad for \quad 0 \le \omega \le \omega_D$$

Equation 2.9

$$g(\omega)=0 \qquad for \quad \omega_D \le \omega$$

Remembering that in the Debye model, there are three acoustic modes, we get a value for the P-DOS.

$$g(\omega)=\frac{3V\omega^2}{2\pi^2 v_0^3} \qquad for \quad 0 \le \omega \le \omega_D$$

Equation 2.10

$$g(\omega)=0 \qquad for \quad \omega_D \le \omega$$

Where Equation 2.11 is the inverse average sound velocity.

$$\frac{1}{v_0^3}=\frac{1}{3}\left(\frac{1}{v_l^3}+\frac{2}{v_t^3}\right)$$

Equation 2.11

The phonon density of states in relation to the Debye model using equation 2.10 can be illustrated in figure 2.11.

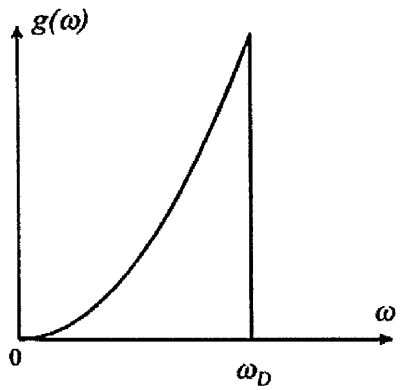

Figure 2.11: This diagram illustrates the change in P-DOS with increasing frequency until it reaches the Debye frequency when it drops to zero.

Figure 2.11 shows that the P-DOS follows a parabolic curve which suddenly drops when the Debye frequency is reached. After this point the P-DOS is equal to zero. Although the Debye model is a simple approximation, the choice of Debye wavenumber ensures that the area under the curve is the same for the real curve of the P-DOS.

A P-DOS clearly applies to a one-mode behaviour but as stated in section 2.5 group III-V semiconductors exhibit a two-mode behaviour. In this case, a two-phonon density of states is applicable and is obtained from a P-DOS curve based on the phonon dispersion curves but twice the phonon frequency. The two-P-DOS can then be compared with the linear combination (Γ_1+4Γ_{12}) part of a two-phonon Raman spectrum which has been divided by the factor $[N(\omega) + 1]^2$ where $N(\omega)$ is the Bose-Einstein occupation number of the phonon modes with frequency ω. This eliminates the effect of the phonon occupational number resulting in a comparable comparison between the two spectra. A two-phonon density of states can be defined as

$$D_2(k_1) = \sum_{k_2 k_3} \delta_{k_1 k_2 - k_3} \delta(\omega_1 - \omega_2 - \omega_3) \qquad \text{Equation 2.12}$$

Summing over the combinations of k_2 and k_3 (Figure 2.12) that satisfy momentum and energy conservation with k_1 (where k is the wavenumber)

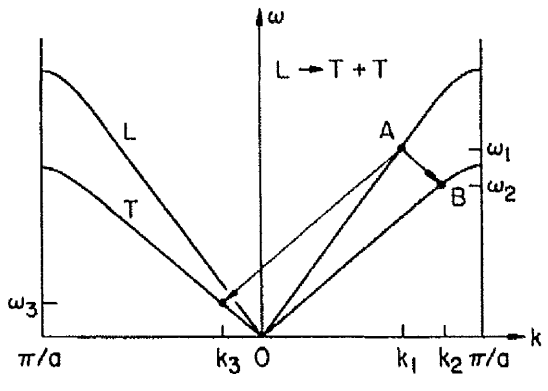

Figure 2.12: A schematic picture to illustrate the spontaneous decay of a longitudinal phonon at point A into two transverse phonons considering momentum and energy.

2.8 Overtones

Often in spectra there are features that can not be assigned or be identified as first order Raman peaks. These peaks are approximately twice the frequency of a phonon mode or close to the sum of two modes. These are known as overtones or combination bands and their presence in the Raman spectra can be explained by the Morse curve.

A molecule consists of a series of electronic states each of which contain a large number of vibrational and rotational states. To illustrate a molecule's typical ground electronic state a simple sketch known as a Morse curve can be drawn (Figure 2.13).

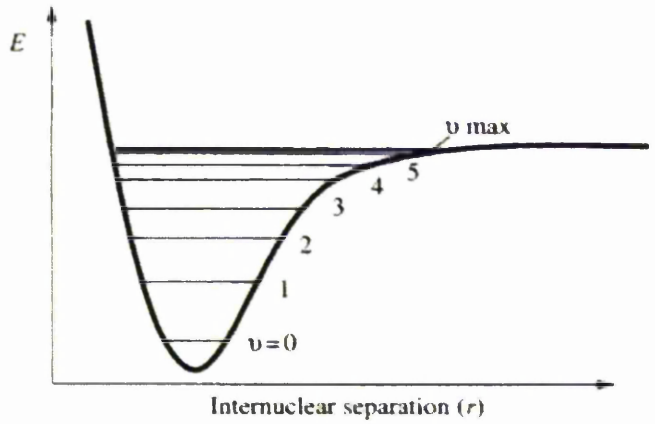

Figure 2.13: A typical Morse curve for an electronic state showing the vibrational states as horizontal lines.

The curved line represents an electronic state of a molecule comparing the energy (E) of a system with increasing internuclear separation (r). At large separations the atoms are essentially free and are attracted to each other to form a bond. If they approach too closely, the nuclear repulsion force causes the atoms to be repelled from each other resulting in a rapid rise of the molecule's energy (as shown). The lowest energy is thus the length of the bond but not every energy is possible since the molecules will be

vibrating. In addition the vibrational energies which are quantised also have to be taken into account and these vibrational states are represented as horizontal lines.

The Morse curve in figure 2.13 refers to just one vibration where $v = 0$ is the ground state and $v = 1$ is the first vibrational state. Above this ($v = 2, 3, 4, 5$) are states which required energy that is approximately but not quite exactly two times, three times, four times etc the energy required by the molecule to jump from its ground state to the first vibrational level. When the energy change is greater than one quantum the peak obtained in a Raman spectrum is known as a overtone (Figure 2.14).

In addition to overtones, combination bands can also be present where the energy of one vibrational level combines with another (e.g involving one optical phonon with an acoustic phonon). In both cases, overtones and combination bands are very weak and only appear in certain circumstances. If all this information was added onto the Morse curve, it would become very crowded and complex. So it is simpler to show all the levels for one vibration or one vibration level for each vibration.

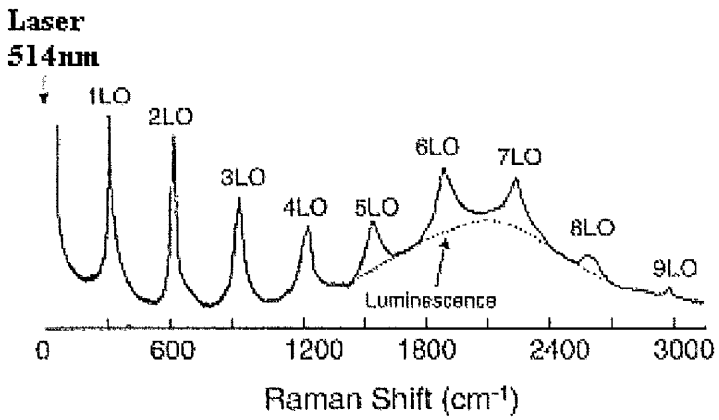

Figure 2.14: A sketch to highlight multiple LO phonon excitations (overtones) that could be present in a Raman spectrum.

2.9 Local vibrational mode

The substitution of impurities into a host crystal, whose masses are significantly less than the masses of the host atoms, not only affects the electrical properties of a crystal but also causes a modification in their vibrational characteristics. The addition of these impurities introduces new energy levels into the bandgaps while the translational symmetry of the host lattice is destroyed. This gives rise to new vibrational modes that have a higher \ greater frequency than the vibrational modes of the host crystal.

Vibrational spectroscopy of these high frequencies has become an important probe into the detection of defects in solids, often providing information about the defect structure and properties that can not be obtained by other methods. The phenomenon is only restricted to impurities that are significantly lighter than the host atoms but nevertheless it is an important limitation.

In terms of dilute nitrides, properties of an III-V semiconductor can be improved by adding impurities to the structure, such as adding nitrogen to GaP or GaSb to create $GaP_{1-x}N_x$ or $GaSb_{1-x}N_x$. The effects of substituting nitrogen into the crystal lattice can be observed through their local vibrational mode (LVM). The LVM occurs due to the nitrogen atom being lighter than the host lattice atom resulting in an atomic oscillation. This oscillation may be induced in a limited range around the nitrogen impurities and so the vibration becomes highly localised around the nitrogen site.

LVM are so called because of their spatial localisation of vibrational energies while the number of LVM seen in a spectrum depends on whether the impurity forms a complex with a second impurity or with an intrinsic defect. The local masses and force constants are modified resulting in the formation of two of three new LVM lines depending on the reduction in the local tetrahedral symmetry.

Local vibrational modes can not propagate through the lattice and so only the impurity and its nearest neighbours will have significant vibrational displacements. Such vibrational modes will have a frequency greater than the maximum lattice frequency ω_{max} provided that the local force constants are similar or greater than those of the host. As force constants depends on the local bonding, a nitrogen donor atom in

GaP occupying a Ga-lattice and bonded to a P-neighbour will have a different vibrational frequency from that of a N donor atom occupying a P-lattice site bonded to a Ga-neighbouring atom.

A bonded substitutional impurity in a compound semiconductor such as GaP is shown in figure 2.15 highlighting a simple two-parameter Keating cluster model [21] used to study the LVM of a light impurity. The model involves host lattice bond stretching force constants (α) represented as lines and angle bending constants (β) between adjacent bonds. Each gives a reasonable fit to the phonon dispersion and the density of phonon modes. Bonds which are centred on the impurity are given as α' and β' due to these constants being modified and can be determined by LVM frequencies.

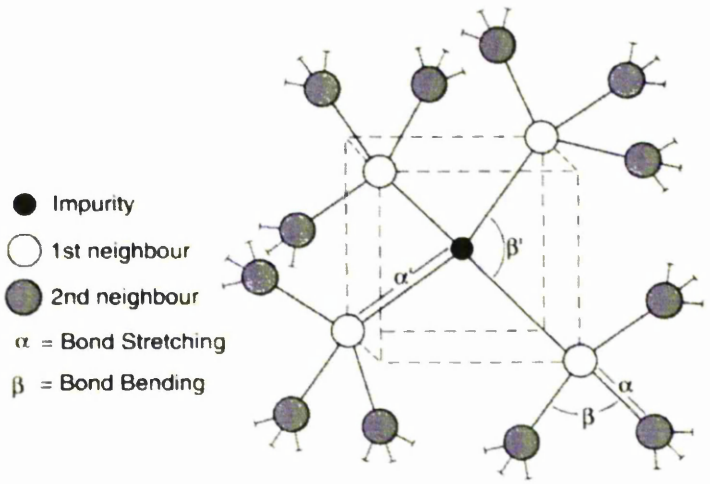

Figure 2.15: A two-parameter Keating cluster model representing bond stretching (α) and bond bending (β) force constants for a substitutional impurity in a compound semiconductor.

If the impurity is displaced to the right, the neighbouring atoms must clearly move in the opposite direction so that there is no movement of the centre of mass. As displacement in second tier neighbours has been found to be negligible then the LVM angular frequency ω_{LVM} is the same as equation 2.1 seen in section 2.6.

As the LVM is sensitive to the nitrogen local environment due to the formation of complexes, by observing sharp, narrow but weak vibrational lines by Raman spectroscopy the shift in peak frequency from nitrogen (isotopic substitution) or additional perturbations can be resolved. This will provide useful information about the incorporation of nitrogen on the crystalline structure.

2.10 Optical processes in semiconductors

There are a number of characterisation techniques that can be used to study the physical properties of materials, each with its own advantages and disadvantages. For semiconductor characterisation, optical techniques stand out the most due to their non-destructive process that requires almost no or very little sample preparation time. These optical techniques include Raman spectroscopy, photoluminescence spectroscopy (PL) and optical absorption measurements.

2.10.1 Optical absorption

By measuring the optical absorption spectrum, it is the simplest optical technique available to study the band structure of a semiconductor. In this process, an electron in a lower energy state absorbs a photon and is promoted up to a higher energy state. There are a number of absorption processes that can occur but the most common one will be discussed in this section.

In terms of a semiconductor which consists of bands, an electron in the valence band absorbs a photon that has an energy which is either equal or greater than that of the energy gap E_g. This process involved the electron being promoted to the conduction band and thus is called band to band absorption. This transition is shown in figure 2.16 and can occur when the absorbed photon has an energy of $h\nu \geq E_g$

As phonons carry negligible momentum p and to conserve momentum, transitions can only occur when the wavefactor k is conserved. As $p = \hbar k$ for a direct bandgap only vertical transitions are allowed while for an indirect bandgap the phonon requires additional interaction. This is either an absorption or emission of a phonon of energy E_p. For example $E_g + E_p$ or $E_g - E_p$

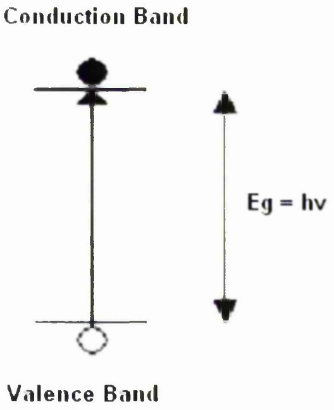

Figure 2.16: Band to band absorption.

2.10.2 Optical Emission

When a material is in an excited state, the excess carriers due to optical absorption recombine to produce an emission of light. This process is known as optical emission and is the opposite process to absorption. In semiconductor materials, the most common process is band to band recombination known as photoluminescence. However there are a number of other optical emission processes which do not occur in this work. These are excitonic, phonon assisted, free to band and bond to bond recombination that are not covered in this thesis but can be easily found in other scientific literature. Most optical processes are by Raman scattering while photoluminescence is used in pressure measurements using ruby emission peaks.

2.10.2.1 Band to band recombination

When a semiconductor material is in an excited state, an electron-hole pair exists within the conduction and valence bands. When the excess electron in the conduction band relaxes, it recombines with an excess hole in the valence band and thus the excess energy is given up as a photon. This process is called band to band recombination (Figure 2.17) and is the most common of all the emission processes occurring in direct bandgap semiconductors.

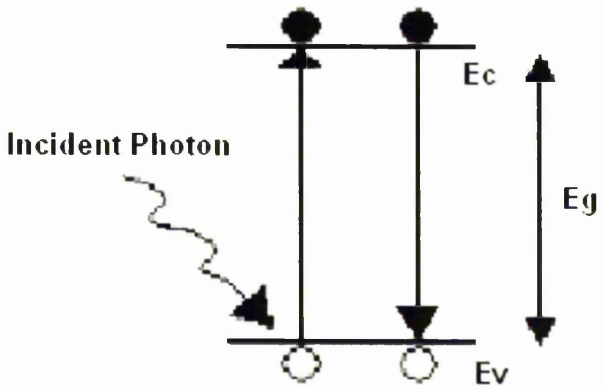

Figure 2.17: Band to band recombination.

After the creation of an electron-hole pair by the absorption of a photon and before the band to band recombination, the electron and hole can experience non-radiatively phonon emission. This is due to the electron relaxing to a lower energy state in the conduction band if available and the hole relaxing to the highest available energy state in the valence band. This will occur before the recombination of the electron and hole by a vertical transition. As in the absorption process, vertical transitions occur in direct bandgaps (same value of k) and the emitted photon relates to the size of the energy gap of the material. This process is known as photoluminescence (PL).

The emitted spectra peaks are narrow due to the emission process occurring at or very close to the band edge. If the temperature rises the carrier density also increases

and so recombination occurs from higher energy states. This results in a broadening of the emission peaks and the creation of a temperature dependant tail towards higher energies. This is due to a thermal distribution of energies where the carriers relax and so occupy high energies states, emitting phonons with higher energies than E_g.

2.10.3 Raman scattering

The scattering phenomenon known as the Raman effect is observed when incident photons are scattered inelastically resulting in a change in the scattered photon frequency. When light encounters the surface of a sample such as a semiconductor, most of the light is reflected, absorbed or transmitted. However, a small percentage of this light is scattered, either as elastically or inelastically interactions. The majority of scattered light is known as Rayleigh scattering where the elastically scattered light has the same energy or frequency as the incident photon. An even smaller probability than Rayleigh scattering is where the incident photons interact inelastically with phonon modes resulting in an outgoing photon whose energy or frequency has been shifted from the incoming values.

This Raman scattering as it is known, is induced by an excitation in the sample. The process involves the Raman scattered photon to gain energy by absorbing a phonon (anti-Stokes shift) or losing energy by emitting a phonon (Stokes shift). Figure 2.18 schematically shows the differences between the incident and scattered photon energies for elastic and inelastic processes.

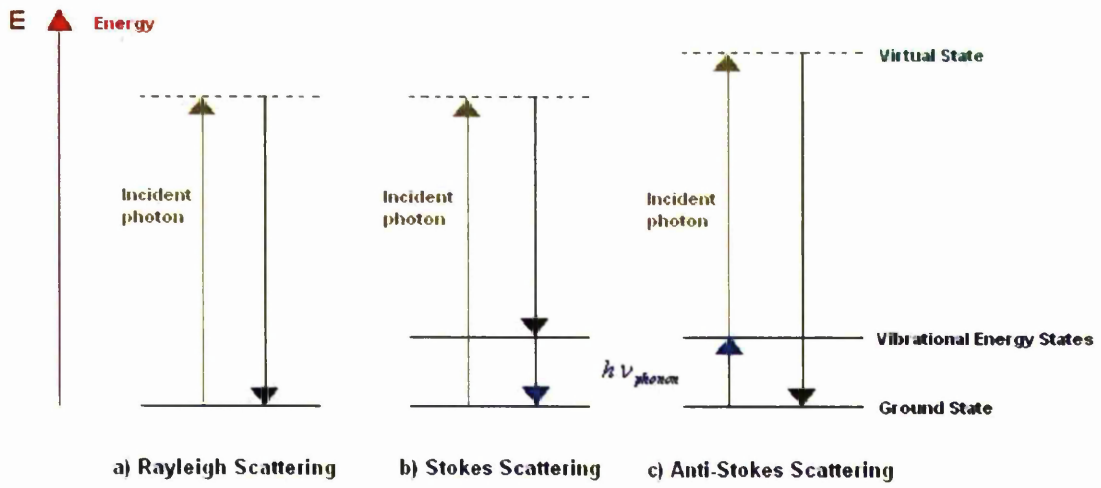

Figure 2.18: Energy level diagrams for Rayleigh (a) and Raman scattering giving either Stokes (b) or anti-Stokes (c) scattering.

According to energy and momentum conservation rules, Stokes and anti-Stokes scattering (Figure 2.19) occurs in first order Raman scattering for the following selection rules:

$$\omega = \omega' \pm \Omega \qquad \text{Equation 2.13}$$

$$k = k' \pm K \qquad \text{Equation 2.14}$$

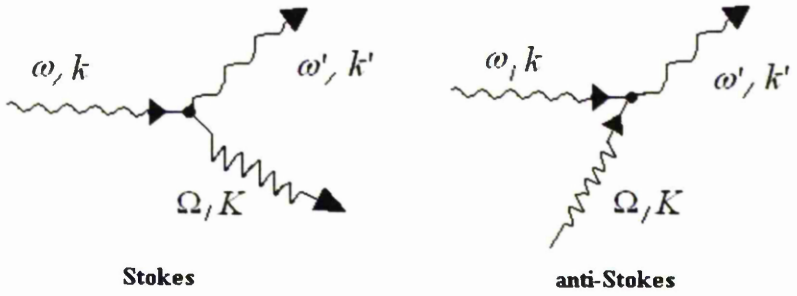

Figure 2.19: Conservation of momentum in Stokes and anti-Stokes scattering.

where ω and k are the frequency and wavevector of the incident photon respectively, ω' and k' are the frequency and wavevector of the scattered photon while Ω and K are the frequency and wavevector of the created or destroyed phonon.

This shows that the difference between the incident photon and the Raman scattered photon corresponds to the vibrational frequencies of the phonons. Due to the sample already being in an excited stated, the line intensity of an anti-Stokes shift is weaker than a Stokes line. This is primarily due to Boltzmann distribution between the lowest vibrational states (See Equation 2.15). Figure 2.20 schematically shows this difference including the locations of each shift in relation to the Rayleigh emission line.

$$\frac{I_{stokes}}{I_{anti-stokes}} = \frac{(\omega-\omega')^4}{(\omega+\omega')^4}\exp\left(\frac{hc\omega}{kT}\right) \qquad \text{Equation 2.15}$$

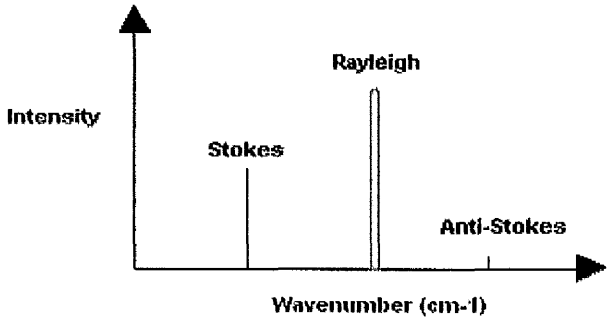

Figure 2.20: A schematic view of the peak intensities of Stokes and anti-Stokes scattering.

Raman shift is usually expressed as wavenumbers (cm^{-1}) which describes the number of units the Raman peak is from the Rayleigh line in figure 2.20 or laser line. Wavenumber is the measure of how many wavelengths fit into one centimetre and is proportional to frequency thus energy.

As the full theory of Raman scattering is complex, the best way to explain the effect is by a classical view which considers the change in the lattice electric

susceptibility due to an excitation of the crystal. This is known as lattice polarisability when an electric field (E) is applied, an electric dipole moment (P) is induced. The polarisability of the matter ε(ω) determines the size of the induced dipole moment.

$$P = \varepsilon(\omega)E \qquad \text{Equation 2.16}$$

If u is the coordinate describing the phonon normal modes, the polarisability of the matter can be written in terms of a Taylor series expansion [22]:

$$\varepsilon(\omega,u) = \varepsilon(\omega) + \left(\frac{d\varepsilon}{du}\right)u + \frac{1}{2}\left(\frac{d^2\varepsilon}{du^2}\right)u^2 + ... \qquad \text{Equation 2.17}$$

So combining equation 2.16 and 2.17 we get an expression for the dipole moment induced by the radiation electric field given as,

$$P = \varepsilon(\omega)E + \left(\frac{d\varepsilon}{du}\right)uE + \frac{1}{2}\left(\frac{d^2\varepsilon}{du^2}\right)u^2E + ... \qquad \text{Equation 2.18}$$

So that the small nonlinear terms of uE and u^2E are the ones that generate the Raman side bands at the phonon frequency. A mode that has a frequency Ω has a phonon coordinate of $u = u_0\cos(\Omega t)$ while an incoming electric field has the form $E = E_0\cos(\omega t)$. Combining these two terms into equation 2.18 then the induced dipole moment contains the term

$$[\cos\Omega t]^n \cos\omega t \qquad \text{Equation 2.19}$$

Where n = 1, 2, 3. Using standard trigonometric identities, these terms can be expressed in the form

$$\cos(\omega \pm n\Omega)t \qquad \text{Equation 2.20}$$

This means that the light re-radiated by the oscillating polarisation vector has components at the frequencies $\omega \pm n\Omega$ and thus are the Stokes and anti-Stokes shifts.

For a wurzite structure which is found in some semiconductor materials, it is predicted that there are eight phonon modes at the zone centre (Γ) of the Brillouin zone. These are $2*A_1$, $2*E_1$, $2*B_1$ and $2*E_2$ which both B_1 modes are not seen by Raman scattering while the rest are Raman active. Figure 2.21 shows the movement of these atoms to produce the phonon modes seen in a Raman spectrum.

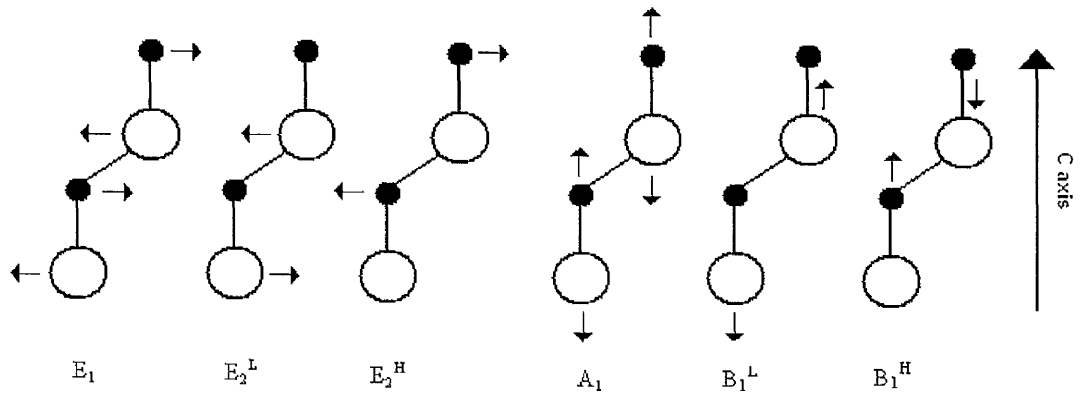

Figure 2.21: Optical phonon modes in a wurzite crystal structure.

It should also be noted that as Raman scattering comes from the interaction of the electric field vector and the polarisation vector, the direction of the electric field relative to the crystal geometry defines the strength of the Raman signal.

$$I \propto \left| \hat{e}_i \cdot R \cdot \hat{e}_s \right|^2 \qquad \text{Equation 2.21}$$

Where $\hat{e}_i$ and $\hat{e}_s$ are unit vectors giving the direction of the incident and scattered electric field respectively.

The Raman tensor (R) determines which phonon modes are allowed and which are forbidden for different sample orientations. Work in this study was carried out using backscattering geometry which means that on a (100) plane only LO phonons are seen. TO phonons are only allowed in a (110) plane while a (111) plane allows both modes to appear.

2.10.3.1 Resonance Raman

Resonance Raman is the same inelastic light scattering process as seen in Raman scattering except in this case the energy of the laser is adjusted so that the excitation frequency is close to that of an electronic transition. This corresponds to the energy difference between the ground vibrational state and the first or second vibrational state of the excited state. It is a sensitive technique allowing us to look at relatively few vibrational modes at a time. Resonance Raman reduces the complexity of the structure allowing easier identification.

Using a tuneable laser, it is possible to tune the laser into near resonance with an optical bandgap associated with a semiconductor structure of interest. It is then possible to enhance the Raman signal by many orders of magnitude, usually in the orders of 10^3 to 10^4 while up to 10^6 has also been reported. This is particularly useful that is allows samples with lower concentrations to be observed.

The resulting spectrum is simpler than traditional Raman as there are fewer peaks. This is due to the intensity of totally symmetric vibrations associated with that particular transition being enhanced usually overwhelming the Raman signal from other transitions. Different peaks can also be targeted by tuning the excitation frequency to match other specific electronic transitions so it is useful in not only obtaining vibrational information but electronic too.

However, there are some risks that need to be taken into consideration. There is an increase in the probability of fluorescence occurring and a higher chance of photodegradation (heating). Photodegradation will occur due to increase levels of energy from the laser. Another consideration is the phenomenon that occurs when the excitation frequency is exactly the same as the electronic transition energy. When it reaches this point, absorption occurs in the sample resulting in a loss of the Raman spectrum. Therefore only frequencies that are very close to the transitional energy of interest are used for Resonance Raman.

A sample of interest, GaP was one of the first bulk semiconductors to be examined using resonance Raman. Weinstein and Cardona [23] measured the first and

second order Raman scattering in GaP without the use of a variable laser. It is well known that temperature affects the bandgap of a material so by varying the temperature (78, 300, 356 and 625K) and with the use of different lasers (514, 458 and 442nm) they could observe the intensity of selective phonon modes.

It was not until 1986 [24] when variable lasers were developed that GaP could be measure using a single laser at room temperature (Figure 2.22). In terms of dilute nitrides, resonance Raman could be exploited especially in measuring the LVM of the nitrogen content. As previously stated, the LVM is very weak and any method to increase the intensity would be widely welcome.

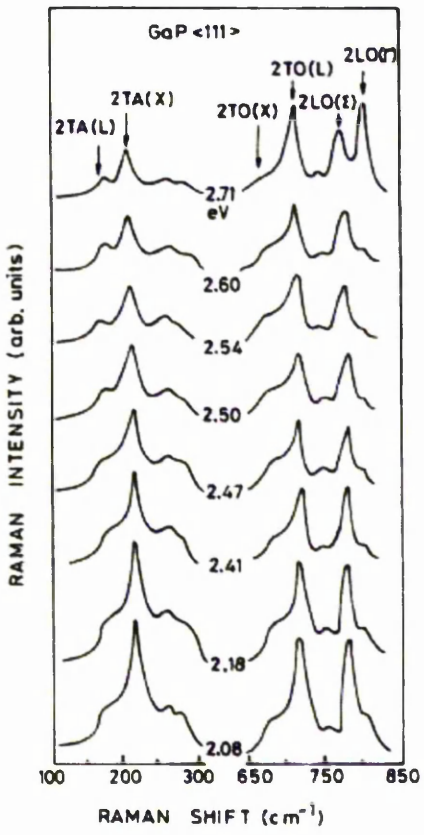

Figure 2.22: The evolution of phonon mode intensities of GaP with varying excitation frequency [24]

2.11 Pressure

Pressure can be considered as a thermodynamic variable that provides a mean of changing the inter-atomic distances in materials in a controlled manner. When pressure is applied the atoms themselves are not being compressed but the number of neighbouring atoms each atom has increases due to the decreasing distances between them. The impact of pressure is so dramatic that the physical and chemical properties of the material are significantly changed. By applying pressure to a material, the volume can decrease by nearly 50 percent compared to that of only a few percent when the temperature is increased towards the material melting point. Experiments using high pressure devices have led to the discovery of a number of phenomena including solid-solid critical point, molecular dissociation and structural phase transitions.

The thermodynamic factor that determines the phase stability of a crystal structure in a high pressure system is known as the Gibbs free energy [2].

$$G = U + PV - TS \qquad \text{Equation 2.22}$$

Where U is the total internal energy, P is the pressure, T is the temperature, S is the entropy and V is the volume. In experimental applications such as the use of a diamond anvil cell, the pressure and temperature can be applied externally. This allows the energy, volume and entropy to freely adjust to these external factors to minimise the Gibb free energy to provide a stable phase.

Equation 2.22 also shows that as the pressure is increased, structures with the lowest specific volume become favourable even if they have a higher internal energy. It also shows why temperature is less effective in producing solid-solid phase transitions due to the entropy being constant as the atomic alignment in the crystal remains the same. The enthalpy should also be considered due to how the experiments are conducted. In these experiments, the temperature remains constant as well as the entropy of the crystal and so there is a trade off between the system gaining energy and a reduction in the volume.

The following diagram (Figure 2.23) shows the variation of the Gibbs free energy as a function of the thermodynamic pressure variable. The diagram consists of two lines 1 and 2 which depict the variation of the Gibbs free energy with pressure for two phases A and B. The point of intersection between the two lines represents the pressure (P_o) where the energy of phase A is the same as phase B. This P_o value is known as the thermodynamic equilibrium pressure and shows that below this point, phase A is stable while above this point phase B is stable. So at P_o a phase transition occurs between the two phases

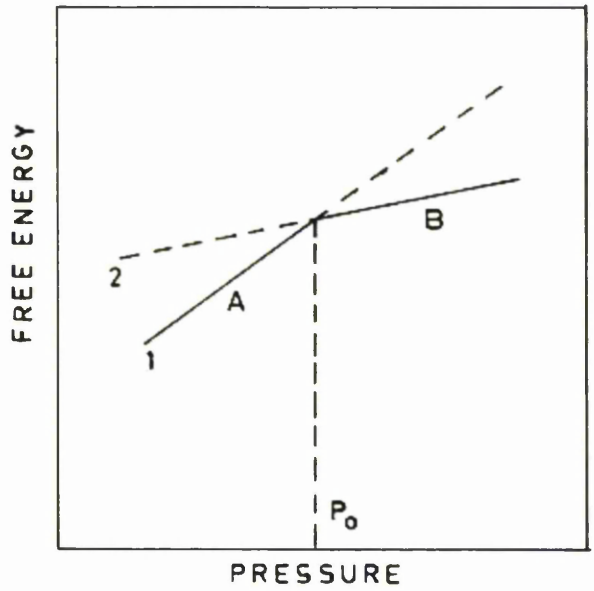

Figure 2.23: Variation of the Gibbs free energy with pressure for phases A and B in the vicinity of P_o. Above P_o phase A undergoes a first order phase transition [25].

Phase transitions are of great importance due to the sudden change in the arrangement of the atoms causing a change in the structure properties of the material. These transitions are said to occur if the change is discontinuous or continuous but with a change in the crystal symmetry. These pressure induced phase transitions are thought to be diffusionless, meaning that they are observed at higher pressures than originally predicted. This is due to the large repulsive force between the atoms which sharply increases when a pressure is applied, raising the height of the potential barrier for

diffusion to occur. So the continuous increase in pressure gradually distorts the structure, it orientation and prepares the structure to undergo phase transition with little displacement of the atoms.

Pressure can be generated by applying a force which is uniaxially if applied in one direction. This uniaxially applied pressure will produced biaxial strain that has the same magnitude in each axis. However, compressive strain (ignoring shear strain) can also be achieved hydrostatically where an equal force is applied in all directions. For hydrostatic pressure, a stress tensor is required which is a further constraint that the structure must satisfy. The stress tensor σ_{ij} must have the form

$$\sigma_{ij} = \frac{d^2U}{d\varepsilon_i d\varepsilon_j} = \begin{pmatrix} P & 0 & 0 \\ 0 & P & 0 \\ 0 & 0 & P \end{pmatrix} \qquad \text{Equation 2.23}$$

Where ε_i is the strain in the *i* direction, ε_j is the strain in the *j* direction, U is the total internal energy and P is the applied pressure.

An example of the difference between biaxial and hydrostatic compression can be seen in quantum wells and quantum dots structures. Biaxial compression occurs in quantum wells due to lattice mismatch where the c-axis remains unchanged. The remaining two axes are compressed due to being parallel with the substrate where as in quantum dots systems the structure is being compressed on all three sides. This occurs due to the lattice of the material surrounding the dot being different which results in the quantum dot being compressed hydrostatically.

Stress is the measure of force per unit area while the strain is the ratio between the change in length and the original length. However when dealing with volumes, we should consider the bulk modulus of a material which is a ratio of the stress and the strain. The bulk modulus B_0 can be defined by equation 2.24.

$$B_0 = -V\frac{dp}{dV} \qquad \text{Equation 2.24}$$

Where dp is the change in pressure, dV is the change in volume and V is the original volume. We know that pressure is defined as force (F) per unit area (A) and thus gives us the relation.

$$\frac{dV}{V} = \frac{1}{B}\frac{F}{A} \qquad \text{Equation 2.25}$$

This equation now shows that the strain is related to the stress by the constant of proportionality known as the bulk modulus or isothermal volume compressibility. In terms of a sample under compression, the following diagram (Figure 2.24) helps to illustrate the bulk modulus.

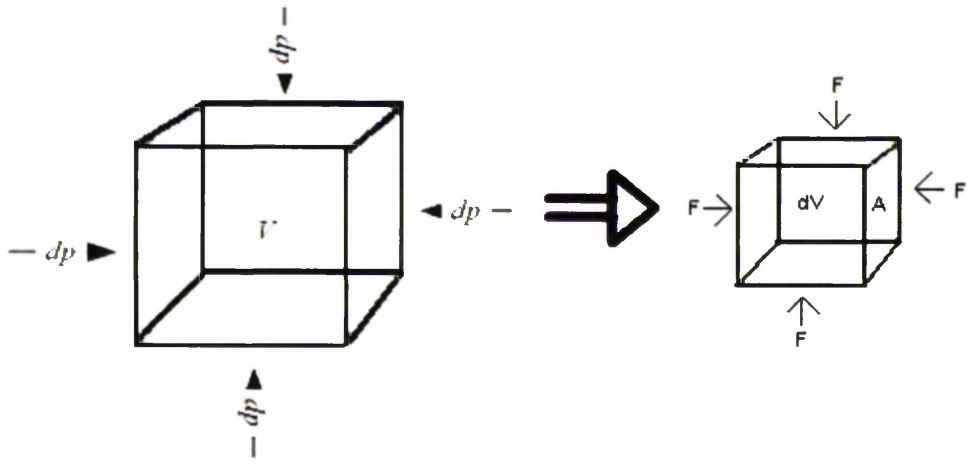

Figure 2.24: A schematic diagram showing when a cube with volume V is compressed with a force F (dp) in the all directions on its surface area, the resulting volume of the cube will have a bulk modulus B_0.

2.12 Mode Grüneisen Parameter

The mode Grüneisen parameter is a significant thermodynamic parameter that shows the relationship between thermodynamics and statistical physics. The parameter describes the alternation in a crystal lattice vibrational frequency shown by the phonon mode frequency shift based on the lattice volume increasing or decreasing. Equation (2.26) characterises the change of lattice vibrational frequency σ of the *i* th vibrational mode in a solid with volume V.

$$\gamma_i = \frac{\partial \ln \sigma}{\partial \ln V} \qquad \text{Equation 2.26}$$

The Grüneisen parameter can also be written in terms of the bulk modulus (isothermal volume compressibility) as the benefits of doing this allows the parameter to be determined experimentally.

$$\gamma_i = \frac{B_0 \partial \sigma}{\sigma \partial P} \qquad \text{Equation 2.27}$$

This derivative is evaluated at P = 0.

By plotting a graph of the pressure (P) dependence versus phonon frequency, the data points can be fitted with a quadratic equation in the form shown below.

$$\sigma(P) = \sigma_0 + \alpha P + \beta P^2 \qquad \text{Equation 2.28}$$

This form of the quadratic equation contains three fit parameters including a constant (σ_0), linear (α) and a quadratic (β) parameter. By differentiating this quadratic equation with respect to P we get the following.

$$\frac{\partial \sigma}{\partial P} = \alpha + 2\beta P \qquad \text{Equation 2.29}$$

Putting this back into the Grüneisen parameter we get

$$\gamma_i = \frac{B_0\alpha + 2B_0\beta P}{\sigma_0 + \alpha P + \beta P^2} \qquad \text{Equation 2.30}$$

Now evaluating when P = 0

$$\gamma_i = \frac{B_0\alpha}{\sigma_0} \qquad \text{Equation 2.31}$$

When studying semiconductor materials especially group III-V semiconductors and their dilute nitrides, the value used for the bulk modulus is an important factor that has to be taken into consideration. Due to the differences in bulk modulus, this could lead to some discrepancies in the Grüneisen parameter results. For example the bulk modulus is unknown for $GaP_{1-x}N_x$ where N is 2.1% so we assume that the bulk modulus is the same as bulk GaP.

2.13 Anharmonicity

Anharmonicity is the deviation of a system from being a harmonic oscillator. It is used to describe a nonlinear oscillator whose behaviour can be defined as the partial derivative of the spring constant with respect to the atomic distance. In real crystal structures, the lattice vibrations are not purely harmonic and so anharmonicity leads to coupling between the phonons and harmonic crystal. The energy difference between vibrational levels is not uniform and would continuously decrease to form a continuum

at sufficiently large vibrational frequencies. Anharmonicity becomes more important as the temperature of the crystal increases and can be calculated in the following way.

Neglecting interactions between an atom and the rest of the lattice, you can regard an atom as a simple harmonic oscillator. It spring constant (D) can then be calculated from the atom mass (m) and the frequency (ω) using

$$D = \omega^2 m \qquad \text{Equation 2.32}$$

A partial derivative $\frac{dD}{db}$ of the spring constant with respect to interatomic distance b gives the anharmonicity of an atom. In the case when a structure is compressed hydrostatically, the interatomic distances decrease while the spring constant increases. Due to the anharmonicity of the bond potential, this results in an increase of the vibrational frequency of the phonon modes.

It has been shown in previous sections that the use of high pressure devices and Raman scattering allows the pressure-induced shift of a phonon mode to be measured. This knowledge allows the anharmonicity of a bond potential to be calculated indirectly by measuring the change in the Spring constant over pressure. The anharmonicity is then given by [26]:

$$\frac{dD}{db} = \frac{dD}{dP} \cdot \left(\frac{db}{dP}\right)^{-1} \qquad \text{Equation 2.33}$$

The derivative $\frac{dD}{dP}$ of the spring constant with respect to pressure can be obtained by measuring the Raman shift of the phonon mode with pressure $\left(\frac{d(\lambda^{-1})}{dP}\right)$. This gives equation 2.34.

$$\frac{dD}{dP} = \frac{dD}{d(\lambda^{-1})} \cdot \frac{d(\lambda^{-1})}{dP} = 8\pi^2 c^2 m \left(\frac{1}{\lambda}\right)_0 \cdot \frac{d(\lambda^{-1})}{dP} \qquad \text{Equation 2.34}$$

Where c is the speed of light and $\left(\frac{1}{\lambda}\right)_0$ is the phonon Raman shift at ambient (zero) pressure.

The derivative of the interatomic distances with respect to pressure $\frac{db}{dP}$ can be calculated from the elastic compliance constants (S_{11} and S_{12}) and the value of the lattice constant a_0 at zero pressure by equation 2.35. Elastic compliance is the strain produced in a material per unit of stress applied while in some directions the compliances are the reciprocal of the Young's modulus.

$$\frac{db}{dP} = \frac{\sqrt{3}}{4} a_0 (S_{11} + 2S_{22}) \qquad \text{Equation 2.35}$$

For simplification, it can be assumed that a_0 and $S_{11}+2S_{12}$ for a semiconductor ternary nitride such as $GaP_{1-x}N_x$ can be given by Vegard's law as a linear interpolation between the values of the corresponding binary compounds GaP and zincblende GaN. Vegard's law states that there is a linear relationship between the substitutional impurity concentration and the lattice parameter where the solute and the solvent have similar bonding properties [27].

Thus by combining equations 2.34 and 2.35 we are able to calculate the anharmonicity of a bond potential from combining literature values and the pressure dependence of the phonon mode frequency.

$$\frac{dD}{db} = \frac{32\pi^2 c^2 m \left(1/\lambda\right)_0}{\sqrt{3} a_0 (S_{11} + 2S_{12})} \cdot \frac{d(\lambda^{-1})}{dP} \qquad \text{Equation 2.36}$$

2.14 References

[1] A. Mujica, A. Rubio, A. Munoz and R. J. Needs. Rev. Mod. Phys. **75** (3) 863 (2003)

[2] G. J. Ackland. Rep. Prog. Phys. **64** 483 (2001)

[3] L. Esaki and R. Tsu. J. Res. Development. **14** 61 (1970).

[4] J. D. Perkins, A. Mascarenhas, Y. Zhang, J. F. Geisz, D. J. Friedman, J. M. Olson and S. R. Kurtz. Phys. Rev. Lett. **82** 3312 (1999)

[5] P. J. Klar. Prog. Sol. Stat. Chem. **31** 301 (2003)

[6] W. H. Weber and R. Merlin. *Raman Scattering in Material Science,* Springer (2000)

[7] Y. T. Cherng, D. H. Jaw, M. J. Jou and G. B. Stringfellow. J. Appl. Phys. **65** 3285 (1989)

[8] I. A. Buyanova, W. M. Chen, E. M. Goldys, H. P. Xin and C. W. Tu. Appl. Phys. Lett. **78** 3959 (2001)

[9] M. Razeghi. *Fundamentals of Solid State Engineering,* Springer (2002)

[10] H. Ibach and H. Luth *Solid State Physics,* Springer (1991)

[11] R. L. Bjork. Phys. Rev. **105** (2) 456 (1957)

[12] P. J. Dean, D. D. Manchon Jr and J. J. Hopfield. Phys. Rev. Lett. **25** (15) 1027 (1970)

[13] P. H. Borcherds, R. L. Halls, K. Kunc and G. F. Alfrey. J. Phys. C: Solid State Phys. **12** 4699 (1979)

[14] C. Eckl, P. Pavone, J. Fritsch and U. Schröder. *The Physics of Semiconductors, Proceedings of the 23rd International Conference, Berlin, 1996*, edited by M. Scheffler and R. Zimmermann. World Scientific (1996).

[15] V. Ozolins and A. Zunger. Phys. Rev. B. **57** (16) 57 (1998)

[16] W. Martienssen and H. Warlimont. *Springer Handbook of Condensed Matter and Materials Data* Springer (2005)

[17] M. K. Farr, J. G. Traylor and S. K. Sinha. Phys. Rev. B. **11** 1587 (1975)

[18] P. Giannozzi, S. de Gironcoli, P. Pavone and S. Baroni. Phys. Rev. B. **43** 7231 (1991)

[19] D. L. Price, J. M. Rowe and R. M. Nicklow. Phys. Rev. B. **3** 1268 (1971)

[20] T. Pletl, P. Pavone, U. Engel and D. Strauch. Phys. B **263** 392 (1999)

[21] P. N. Keating. Phys. Rev. **145** 637 (1966)

[22] J. A. Koningstein *Introduction to the theory of the Raman Effect,* D. Reidel Publishing Company (1972)

[23] B. A. Weinstein and M. Cardona. Phys. Rev. **8** 2795 (1973)

[24] R. K. Soni, R. Gupta and K. P. Jain. Phys. Rev. B. **33** 5560 (1986)

[25] H. V. C. Shekar and H. G. Rajan. Bull. Matter. Sci. **24** (1) 1 (2001)

[26] M. Gungerich, P. J. Klar, W. Heimbrodt, J. Koch, W. Stolz. M. P. Halsall and P. Harmer. Phys. Rev. B. **71** 075201 (2005)

[27] M. D. McClusKey. J. Appl. Phys. **87** (8) 3593 (2000)

Chapter 3: Experimental details

3.1 Raman Spectroscopy

3.1.1 Renishaw System

Raman spectroscopy is a versatile and standard optical characterisation technique which is non-destructive, contact-less and requires little or no special sample preparation such as thinning or polishing. Vibrational Raman scattering studies the phonon properties of crystalline materials and other aspects such as coupling between the lattice and electronic or magnetic properties. To study these effects a specialised piece of equipment known as a Raman spectrometer is required.

There are a number of commercial Raman spectroscopy systems that can be used to study the vibrational properties of semiconductors. In the Manchester laboratory one such system is available, the RM1000 spectrometer manufactured by Renishaw plc. The advantage of using this spectrometer over others is the versatile nature of the system and coupling of the spectrometer to a microscope which gives it the ability to use in conjunction with other equipment available in the group such as a diamond anvil cell (DAC) or a liquid helium cryostat.

The Renishaw system is composed of a series of individual components. These are various lasers, a commercial metallurgical microscope, a mapping stage, the spectrometer itself, and a charged coupled device (CCD) camera for detecting the spectrum. To excite the III-nitride materials with photons, a light source is required. As these semiconductors have small bandgaps in principle a near infrared laser would be best as resonant excitation would be possible. However, the Renishaw system was acquired for work on large gap nitrides and is optimised for visible light excitation. Thus the light sources available are two air cooled lasers that allow one of three

different excitation wavelengths to be used. The first is a Helium-Cadmium (He-Cd) which emits either 325nm (UV) or 442nm wavelengths (blue light) and the second is an Argon (Ar+) laser emitting 514nm (green).

At the rear of the system the laser light enters the Renishaw either directly (for the argon laser system) or by a mirror (for the He-Cd) before passing through one of a number of possible neutral density (ND) filters. These internal filters allow 100%, 50%, 25%, 10% and 1% transmission and are controlled by the system software making changes simple and quick. Once through the ND filters, (Figure 3.1) the next optical component is a beam expander before passing through a laser plasma line rejection filter. The beam is then steered using a number of mirrors onto the sample and is focused through an objective lens of either 5x, 15x, 40x (long working distance) or 50x in the visible range and 15x or 40x in the UV. The mode of operation is confocal in that the same lens (the microscope objective) is used to focus and collect the light. The use of a beam expander produces a diffraction limited laser spot size of about 0.5μm in diameter.

The use of a confocal and backscattering geometry means that scattered light (elastic and inelastic) and laser light passes back through the objective lens and along the same path until it reaches a pair of holographic notch filters. At this point, as the Raman light has been shifted in wavelength, instead of being reflected back down the system towards the beam expanders, the Raman component is transmitted through the holographic notch filter and on to the spectrometer. It is the use of these filters that cuts out the laser line and the photons due to Rayleigh scattering.

The Raman component then passes through an optical slit that can be adjusted to control the system resolution and to form an aperture to restrict the light collection area along the vertical axis before being reflected by a prism onto a diffraction grating. The diffraction grating disperses the radiation spatially into different frequency components before being dispersed and focused on to a CCD camera. The CCD can detect the relative intensities of the different wavelengths before being analysed and displayed on a computer using a software program called Grams. This is an integrated spectroscopic program by Thermo Scientific which controls the Renishaw, translating the data into a

spectrograph of intensity verses wavelength or wavenumbers (cm^{-1}). The Grams software also allows basic analysis of the data acquired.

To reduce any read-out noise on the spectra and to remove any form of artificial aperture in the horizontal direction, the width of the CCD that collects the spectra can be adjusted in the vertical axis. This effectively forms an artificial slit which combined with the real slit forms an artificial aperture increasing the spatial resolution of the Raman microscope. The CCD is made up of an array of photosensitive pixels (385 ^{x} 578) which produce a photoelectron when a photon falls upon them. This gives the pixel a charge that is proportional to the intensity of the frequency and so by cutting down the area of pixels used, an artificial slit is formed. The CCD is also cooled by a Peltier cooler to reduce thermal noise.

The Renishaw system is designed so that either a static or a continuous (long range) scan can be taken of the sample. A problem for other Raman spectrometers when taking a continuous scan, a number of individual scans are required and are matched together to form a spectrum. This is because it is impossible to get the whole scan without moving the grating. The Renishaw overcomes this problem by moving the diffraction grating at the same time as it collects the data. As the grating is coupled to the charge bins of the CCD, the speed of the grating is controlled and so there is no need to match up the scans to form a spectrum as with other systems.

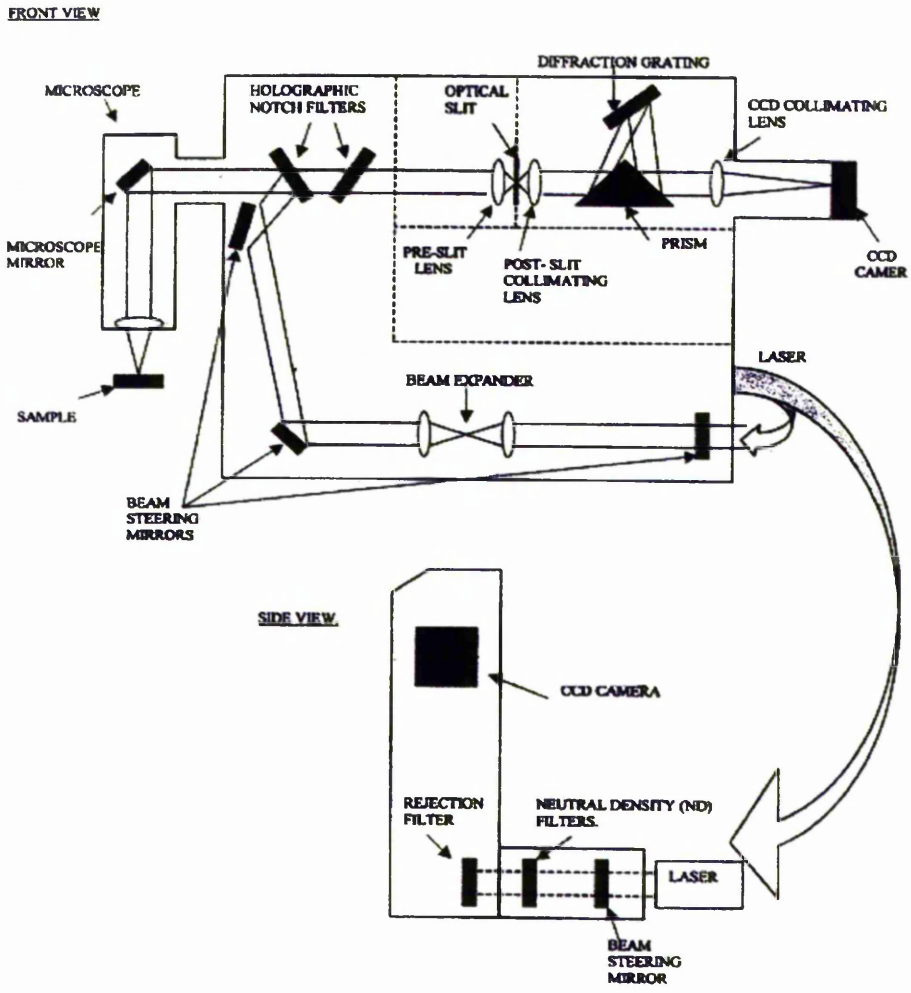

Figure 3.1: A systematic view of Renishaw RM1000 system.

3.1.2 New Raman System

This system (Figure 3.2) is a bespoke system which employs a 1 metre Spex spectrometer to disperse light and is designed as a Raman or PL system depending on the optical arrangement. The setup involves a simple optical layout that was design within the research group. The system contains a 632nm Helium-Neon laser positioned at 90^{o} to the sample \ spectrometer optical path and is injected into this optical path

using a dielectric edge filter which reflects the laser light with high efficiency. This light is then steered into a microscope objective using backscattering geometry as in the Renishaw. The light is reflected back along the incident path where it reaches the same edge filter. Here the Raman shifted light is transmitted onto a focusing lens and into the spectrometer where the Raman shift is measured.

The main difference between this system and the Renishaw is that the diffraction grating does not move when collecting the data. Therefore when the computer software produces spectra, for long continuous scans a number of spectra need to be joined together. Fortunately in the research described here, a static scan was sufficient to capture the relevant region of the Raman spectrum and so no further adjustment is required to the spectrum. This setup was used for $GaSb_{1-x}N_x$ and $InSb_{1-x}N_x$ nitride samples as the 632nm laser was found to be more suitable in detecting the vibrational phonons and the local vibrational mode of the nitrogen content. This was probably due to the use of lower energy photons which have a deeper penetration depth on the antimonides.

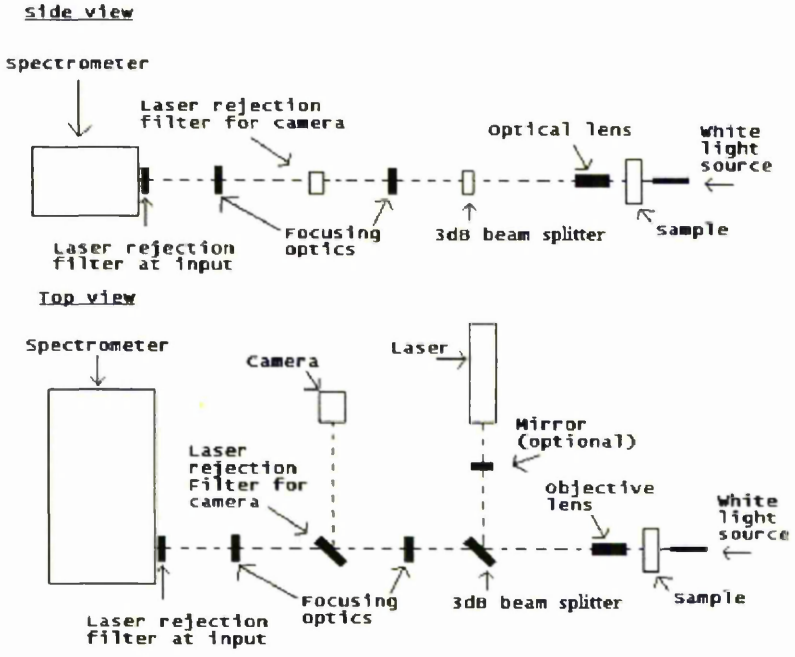

Figure 3.2: Schematic view of the new Raman system.

3.2 Diamond anvil cell

3.2.1 The cell

The diamond anvil cell (DAC) used in these studies was a Mao-Bell type cell which was developed from and has a similar design to that of the Piermarini-Block cell (Figure 3.3). The main difference between the two cells is that the Mao-Bell cell employs a longer piston and cylinder assembly ensuring the alignment of the diamonds is even more accurate [1]. Importantly, this ensures that at high pressures, the diamonds are accurately aligned which the Piermarini-Block cell is not successful at. Due to having a longer piston and cylinder assembly, the main body and lever arm has to be proportionally larger to compensate for this.

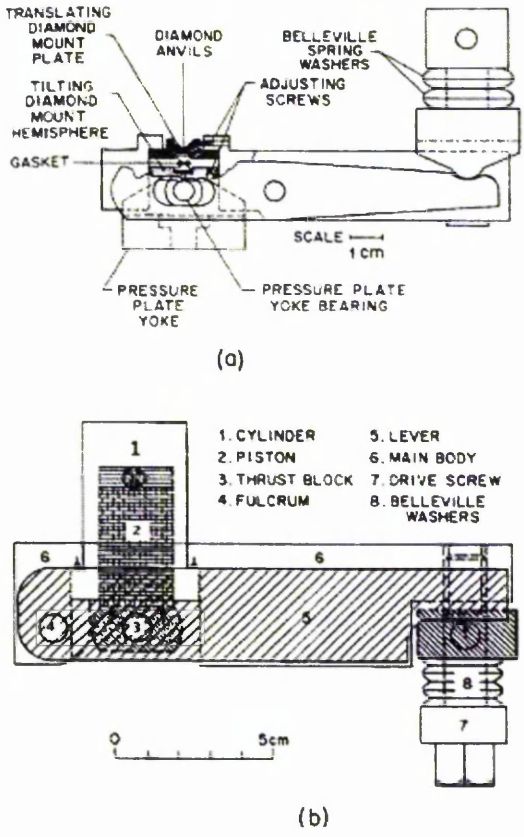

Figure 3.3: The Piermarini-Block cell (a) and the Mao-Bell cell (b).

The force application principle behind the design of this cell is similar to that of a nutcracker where the sample is placed near to the pivot of the system. Pressure is applied to the piston holding one of the diamonds by turning the screw at the opposite end causing high stress to be easily applied with very little effort. To ensure the stress is hydrostatic a pressure transmitting medium is used to fill a hole in a stainless steel gasket. The gasket is then mounted between the two diamonds and pressure is applied.

The basic principle of the DAC thus involves the sample being placed between the faces of two directly opposite mechanically flawless diamonds that either have a brilliant or a Drukker Dubbledee cut. The reason for using diamonds as a material to obtain high pressures and stress is due to their optical properties and crystalline structure. Diamonds are the hardest, least compressible and most inflexible material known to man due to their very rigid and stable structure. They are also transparent at optical wavelengths making them an ideal tool for high pressure optical research.

In between the two diamonds lies a stainless steel gasket for the containment of pressure (Figure 3.4). This is the key to generating hydrostatic pressure in the DAC as not only it provides containment for the pressure medium but also acts as a supporting ring for the diamond faces. Even though diamonds are the hardest material known, if they are forced against each other, rather than a more pliant material such as steel, they will crack so care must be taken.

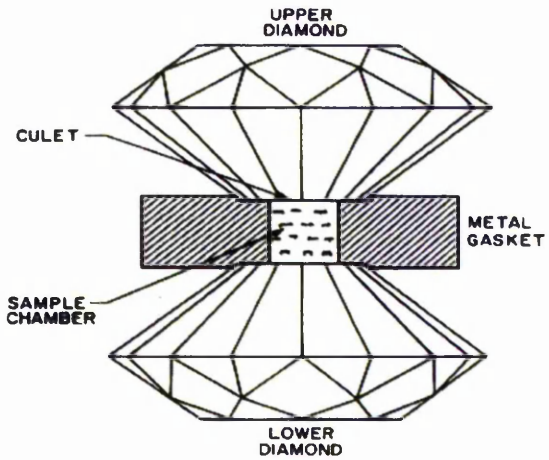

Figure 3.4: Basic principles of a diamond anvil cell.

Before loading the sample, the gasket was indented by the diamonds inside the DAC to a required thickness. This indent can range from 50 to 100μm depending on the size of the sample being studied. Once this has been done, a hole can be drilled at the centre of the indent by various methods, either by using a drill or by a method called spark erosion. This involves using a piece of apparatus called a spark eroder (Section 3.3).

The gasket hole allows containment of the pressure medium for hydrostatic forces to be applied on the sample. The choice of a good hydrostatic medium has been the subject of considerable research. However, for the materials and pressures studied here the commonly used mixture of four parts methanol and one part ethanol [2] is an excellent pressure medium and was used in all experiments. The reason for care taken over the choice of medium used is due to the ratio of the elastic modulus of the medium to the sample. If the medium has a elastic modulus comparable to that of the sample we expect the sample to be subject to substantial non-hydrostatic (uniaxial) forces. As the semiconductor samples here are considered to be relatively hard with a large bulk modules, the methanol and ethanol mixture or silicon oil are ideal and easy to load. It has also been demonstrated in a number of papers that noble gases such as Argon and other gases such as Helium and Hydrogen (H_2) are excellent pressure transmitters reaching the range of 100GPa [3-5].

Another factor of choice is the size of the top flat surface of the diamonds (the culets). In this study brilliant cut diamonds with 150μm culets were used with stainless steel gaskets (B-05) from Diacell products. These had an indent thickness of approximately 60μm with a hole of 100μm at the centre made by a spark eroder. The majority of the investigation was conducted using the methanol-ethanol mixture while experiments that concentrated collecting spectra at pressures above 20GPa to 30GPa (mainly filling gaps in the results) involved using silicon oil (silicon oil has Raman modes at low pressure which can be troublesome [6]).

Methanol-ethanol mixture is good for hydrostatic pressure measurements up to 10GPa and is still useable up to 20GPa but investigations have shown that this mixture becomes a glass and nonhydrostatic [7]. The introduction of non-hydrostatic forces in the cell can be monitored qualitatively by the increase in linewidth of the ruby spectrum

[8]. Most results were collected using the methanol-ethanol mixture which was judged to perform well using ruby fluorescence measurements.

3.2.2 Ruby pressure calibration

Another important technique involved with the use of the DAC is the ability to determine the pressure being applied on the sample at the centre of the cell. This pressure calibration involves the ruby fluorescence technique [9] and is widely used for high pressure studies. This is because the measurement of the ruby fluorescence is quick and easy to measure as ruby produces two very strong fluorescence lines in the visible range. Even inside a DAC where the majority of light is lost due to the diamonds, the signal is so strong that the laser power is reduced to 1% and a spectrum of 0.1 second is taken. Small chips of ruby are required (between 5 and 20μm) as larger pieces can swamp the Raman signal of the sample.

The ruby is excited by the laser producing two sharp and strong ruby lines known as R_1 and R_2. These fluoresce at 692.7nm and 694.2nm (1401.74cm^{-1} and 1372.39cm^{-1}) and either line can be used but generally, R_1 is taken as it is the stronger of the two. When pressure is increased up to 30GPa, the shift of the ruby line is almost linear [10] at the rate of 0.365nmGPa^{-1} or 7.53cm^{-1}GPa^{-1}. Above this pressure, the shift appears to be sublinear and two studies examining the shift of the ruby lines up to the region of 100GPa has suggested two different equations (Figure 3.5) [5,11]. Equation 3.2 is a modification of 3.1 differing slightly but should be used for actual results.

$$P(Mbar) = 3.808\left\{\left[1+\left(\frac{\Delta\lambda}{\lambda}\right)\right]^5 - 1\right\} \qquad \text{Equation 3.1}$$

$$P(Mbar) = \frac{A}{B}\left[\left(1+\frac{\Delta\lambda}{\lambda_0}\right)^B - 1\right] \qquad \text{Equation 3.2}$$

P(Mbar) is the pressure in megabars where 1Mbar equals 100GPa, $\Delta\lambda$ is the shift in wavelength and λ is the initial wavelength of the ruby line in nanometres. For the second equation A is 19.04Mbar and B is 7.665.

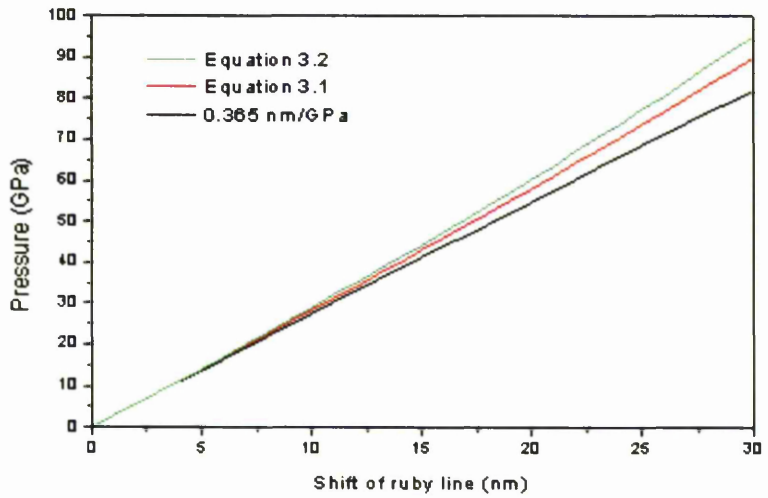

Figure 3.5: Variations between different ruby pressure equations.

Studies have also shown that ruby as a pressure calibration is usable up to a few hundred GPa but as the pressure reaches this value, the error measurement increase to between 15% and 20% [12]. Recent experiments have investigated the shift of the first order Raman peak of the anvil cell diamond with pressure. Theoretically, the shift of the phonon has been calculated up to 600GPa and results have shown reasonable agreement to the theoretical curve [13-15]. It may turn out that the use of diamond is another possible method of pressure calibration although the disadvantages are that the accuracy is not as good as that of ruby.

3.3 Spark eroder

A semi automatic Besta MH20M spark eroder (Figure 3.6) located at the Science and Technology Facilities Council (STFC) Daresbury Laboratory in the Material Science Laboratory (MSL) was used to drill gasket holes. This piece of equipment allows various diameter holes to be drilled ranging from 20μm to 500μm but most importantly ensures that before eroding, the drill needle is lined up at the centre of the gasket indent.

The MH20M spark eroder has a centring accuracy of less than 5μm. With the ability to drill through any conducting material, it has a fast drilling speed (40μm per minute for a 200μm hole in stainless steel) and a motorised drill, all of which are advantageous factors in gasket drilling [16].

Before drilling, the gaskets were indented with the diamond faces within the DAC to a thickness of approximately 60μm. This ensured that the gasket was thick enough for the sample to be studied without being crushed and that all indent thicknesses were consistent. The hole was drilled using a 100μm needle as this was the smallest size needle available / used in the MSL. This had its problems as the flat face of the diamond culets were 150μm which left no room for error.

From experimenting, it was found that this diameter hole was acceptable but if required, the gasket hole can be closed slightly by applying pressure to the gasket if placed into the DAC on its own. The results were not affected in any way as the ruby calibration ensured the spectrum obtained was collected at a known pressure.

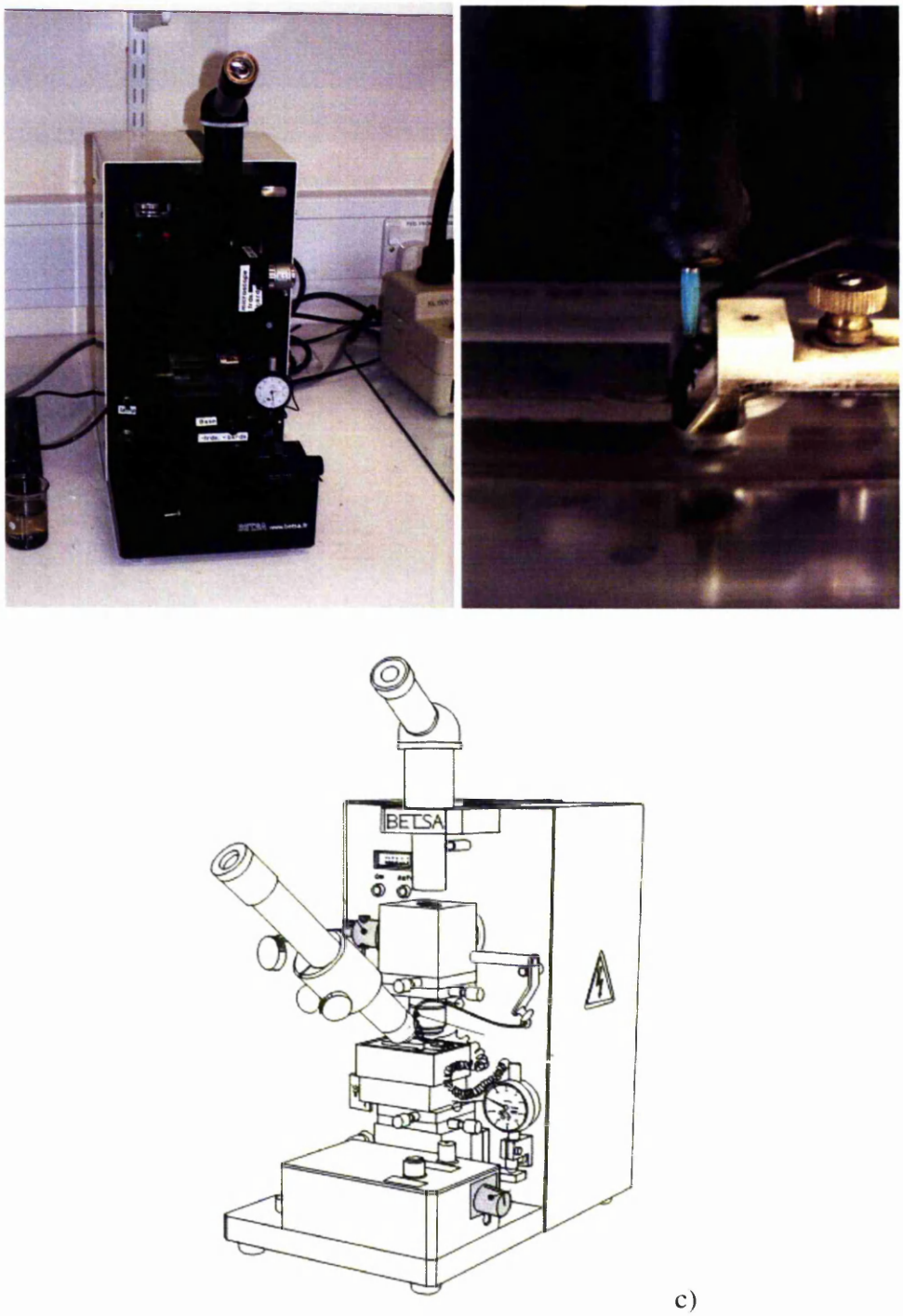

Figure 3.6: The Besta MH20M spark eroder (a), drill needle (b) and schematic view (c)

3.4 Sample characteristics and preparation

Once the gasket and diamonds have been cleaned, the cell is ready to be loaded with the sample. There are four different types of samples being investigated in these studies. The first being a sample of bulk GaP taken from an undoped single crystal, while the remaining three are all dilute nitride samples. The phosphide samples contain a small percentage of nitrogen incorporated during growth of the parent binary on a (100) undoped substrate by metal-organic vapour phase epitaxy (MOVPE) at a high temperature to form an epitaxial layer that was grown at the renewable energy laboratory in Colorado. The antimonide samples were grown by molecular beam epitaxy (MBE). The antimonide dilute nitride samples were grown at the QinetiQ Malvern site by Louise Buckle and co-workers.

The nitrides had a thickness of 1μm for $GaP_{1-x}N_x$ and 0.25μm for $GaSb_{1-x}N_x$ and $InSb_{1-x}N_x$. The nitrogen content was derived from x–ray diffraction data to form the following nitride samples $GaP_{0.979}N_{0.021}$, $GaN_{0.015}Sb_{0.985}$ and $InN_{0.0068}Sb_{0.9932}$. Material growth parameters for the three nitride samples can be seen in the table below.

Epilayer Material	Substrate Material	Epilayer Thickness \ μm	Growth Temperature \ °C	Nitrogen Percentage Content
$GaP_{1-x}N_x$	GaP	1	700	2.1 %
$GaSb_{1-x}N_x$	GaSb	0.25	-	1.5 %
$InSb_{1-x}N_x$	InSb	0.25	-	0.68 %

Table 3.1: Sample characteristics of dilute nitrides studied in thesis

The next stage is the sample preparation as a little bit of time and effort was required at this point. Due to the sample being grown on a substrate, the sample was too thick to be placed into the stainless steel gasket. Before any piece could be cleaved off, the sample had to be thinned to a thickness of 30μm by polishing most of the substrate away. This

was achieved by using a combination of silicon carbide waterproof abrasive discs with fine diamond polishing paper and paste.

The sample was attached to a glass slide using a strong wax which held the epilayer face towards the surface of the glass [Figure 3.7]. This meant the substrate faced upwards and before any polishing was done, a scan was taken of the sample to determine if the substrate did indeed faced upwards. It was also important to ensure that the sample was lying flat against the glass slide and that it was entirely covered in wax underneath the sample. At the opposite end to the sample, the glass slide had two smaller pieces of glass glued together using superglue to create an incline. This allowed the edge of the sample to be thinned protecting the remaining sample for another day.

The polishing was either done by hand onto the abrasive disks or holding it against a disk attached to a polishing machine. By letting the wheel rotations to do the polishing, the sample can be simply held against the pad. The sample was then cleaned from the wax using a number of chemical liquids including trichloroethylene, acetone and methanol. The next step was to cleave the sample into 50μm pieces or less for loading into the DAC using a hypodermic needle. The polishing of the sample greatly helped determining when loading which way the sample was facing. By looking through the microscope onto the surface of the diamond, one can observe the smoothness of the face helping to decide if the epilayer of substrate was facing upwards.

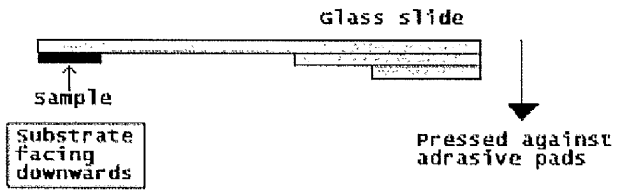

Figure 3.7: Glass slide setup used in polishing of sample

3.5 References

[1] A. Jayaraman. Rev. Sci. Instrum. **57** (6) 1013 (1986)

[2] G. J Piermarini, S. Block and J. D. Barnett. J. Appl. Phys. **44** 5377 (1973)

[3] P. M. Bell and H. K. Mao. Carnegie Inst. Washington Yearb. **80** 404 (1981)

[4] H. K. Mao and P. M. Bell. Carnegie Inst. Washington Yearb. **78** 663 (1979)

[5] H. K. Mao, J. Xu and P. M. Bell. J. Geophys. Res. Jamieson Volume. (1985)

[6] D. D. Ragan, D. R. Clarke and D. Schiferl. Rev. Sci. Instrum. **67** 494 (1996)

[7] A. Jayaraman. Rev. Sci. Instrum. **57** (6) 1013 (1986)

[8] A. Mujica, A. Munoz and R. J. Needs. Rev. Mod. Phys. **75** (3) 863 (2003)

[9] R. A. Forman, G. J. Piermarini, J. D Barnett and S. Block. Sciences. **176** 284 (1972)

[10] G. J. Piermarini and S. Block. Rev. Sci. Instrum. **46** 973 1975)

[11] H. K. Mao, P. M. Bell, J. W. Shaner and D. J. Steinberg. J, Appl. Phys. **49** 3276 (1978)

[12] K. A. Goettel, H. K. Mao and P. M. Bell. Rev. Sci. Instrum. **56** 1420 (1985)

[13] M. Hanfland, K. Syassen, S. Faby, S. G. Louie and M. L Cohen. Phys. Rev. B. **31** 6896 (1985)

[14] H. Boppart, J van Straaten and I. F. Silvera. Phys. Rev. B. **32** 1423 (1985)

[15] A. F. Goncharov, I. N. Makarenko and S. M. Sitshov. JETP Lett. **41** 184 (1985)

[16] http://www.betsa.fr/edm.html 9/11/07

Chapter 4: Raman study of bulk GaP up to pressures of 30 GPa

4.1 Introduction

While searching through literature on dilute nitrides and the incorporation of nitrogen atoms onto the crystal lattice for various semiconductor materials, a very important discovery was made. It was discovered that there are no reports of Raman measurements of bulk GaP near to its phase transition at approximately 22GPa. Through high pressure x-ray spectroscopy, studies by Baublitz et al, Itie et al and Hu et al [1-3] have all presented results that the GaP structure changes to a β-tin crystal structure; it was Nelmes et al [4] who showed that GaP changed from the cubic zincblende to the Cmcm structure which is now considered to be the correct assumption. Raman measurements have only been taken up to pressures in the region of 13GPa [5-7] and with the ability of the Mao-Bell DAC to reach pressures beyond this, a perfect opportunity was presented.

Other deciding factors which convinced me that Raman studies should be conducted on GaP up to its phase transition was the need to compare dilute GaP nitrides to its group III-V semiconductor. Studying the vibrational properties of these semiconductor materials up to and beyond its first phase transition yields a better understanding of the mechanical properties of the Ga-P bonds in Ga-V alloys. Raman studies also allow us to observe the effect of epitaxial strain and alloying on the lattice vibration due to the incorporation of nitrogen.

By studying GaP or a basic group III-V semiconductor, a comparison can be made between similar binary compounds and Ga-N-V alloys. Collecting Raman shift measurements will allow the Grüneisen parameters and the anharmonicity for GaP to be

determined. This will then give the opportunity to see how the incorporation of nitrogen affects the pressure behaviour of the host phonon modes of GaP.

For other semiconductor materials such as GaN and GaAs [8-10] there is a considerable amount of literature on Raman studies on the phase transition under hydrostatic pressure. As this literature is sufficient, no further Raman studies on these materials are required for this thesis.

Before talking about the results obtained from the Raman studies on GaP, it should be noted that the bulk modulus for this material is given as the literature value of 87.4GPa taken from reference [11]. The spectrum for GaP is dominated by two peaks, the TO and LO phonon modes [6]. These are expected to be seen at approximately 365cm^{-1} and 402cm^{-1} [12] respectively.

4.2 Experimental procedure

The sample studied was a bulk GaP, taken from an undoped single crystal. This sample initially had a thickness of 1mm but had to be polished and thinned to a thickness of 30μm. The sample was then cleaved into small pieces of about 50μm allowing the sample to be loaded inside a 100μm diameter hole through the centre of a stainless steel gasket which had a thickness of 60μm. The sample and a small speck of ruby dust was position on the surface at the centre of 150μm diamond culets.

The pressure medium used for these pressure measurements was a mixture of methanol and ethanol using a ratio of 4:1 for the majority of pressure measurements. At higher pressures, around 20GPa and upwards, silicon oil was used due to its own limited Raman signals and its weak photoluminescence in the investigated spectral range. Silicon was used at these pressures instead of the methanol \ ethanol mixture because it was found to contain the pressure more efficiently and resulted in fewer collapsed sample holes in the stainless steel gaskets. The pressure calculated for each Raman spectrum was calculated using the ruby fluorescence technique using the λ^5 power law [13]. The Raman measurements of an accuracy of 0.5cm^{-1} were taken using a

Renishaw Raman microscope with either a 514nm line of an Ar^+ laser of the 442nm line of a He-Cd laser. It was discovered that for lower pressures and for the majority of results the 514nm laser was more suitable for detecting the phonon modes while at higher pressures the 442nm laser was more effective.

Measurements were performed at pressures from 1 to 30GPa at room temperature in a (100)-orientation. A x(y',y') backscattering geometry was used and a 40x long working objective lens was used to collect the light. The transmission filters were set at 100% to allow maximum radiation to fall onto the sample while the scanning time varied from scan to scan as the importance factor was to obtain a good spectrum to determine the phonon modes.

The pressure was increased in small steps to ensure small increases in pressure were obtained. This was very important as large turns \ movements of the screw resulted in large jumps or increases in pressure and therefore large gaps in the results. Before taking a scan, the DAC was allowed to settle for 15 minutes as it was observed that there was a pressure delay from turning the screw. The ruby PL was measured before and after each scan allowing an average of the two measurements to be taken as the pressure point for that scan. If the pressure had jumped up rapidly during scanning, the Raman spectrum for that pressure was taken again to help reduce any errors in the results.

4.3 Results and Discussion

4.3.1 Phonon modes

Figure 4.1 shows the Raman Spectrum of bulk GaP at ambient pressure. The spectrum shows two phonon modes LO and TO [11] which are represented by the peaks that dominate the spectrum. For GaP, the LO and TO peaks are given as $401.6cm^{-1}$ and $364.4cm^{-1}$ respectively. The spectrum also shows typical overtones structures in the region from $720cm^{-1}$ to $785cm^{-1}$. These are visible when the sample is out of the cell. At higher pressures, these peaks are obscured by background noise and so are not

discussed in this thesis. The reason for this is that the DAC cuts out a large majority of the weak Raman signal and only the stronger modes \ peaks are visible.

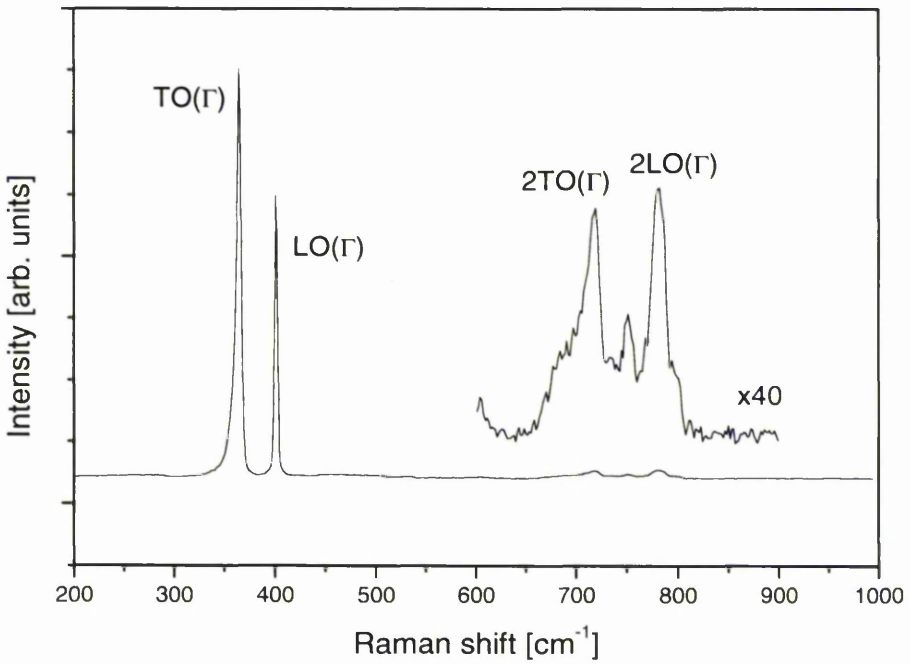

Figure 4.1: Raman scattering spectrum of bulk GaP measured at ambient pressure.

The next stage of the investigation is to increase the pressure within the cell in small steps to scan the change in phonon modes. Figure 4.2 is a collection of Raman spectra of GaP in the spectral range of the first order features taken at different hydrostatic pressures. Figure 4.2 shows the pressure induced shift of the LO and TO phonon modes resulting in the modes increasing in wavenumbers as pressure is increased. Figure 4.2 also demonstrate the weakness of the signal at higher pressures by the magnification used to plot the scans. At around 20GPa (although 514nm was still used at higher pressures), the laser was changed from 514nm to 442nm and this resulted in a sharp increase in the intensity of the phonon peaks.

The behaviour of absolute and relative intensities of the LO and TO modes for GaP are shown to be irregular for several reasons. It is most likely that they are caused by non-constant scattering geometries and resonance effects due to pressure-induced energy shifts of the electronic states. At 30.1GPa, it was obvious that the phonon mode peaks had stopped moving indicating the possible occurrence of a phase transition as indicated by Nelmes et al [4]. The intensities of these peaks are again weak which can be explained by the fact that Raman selection rules tend to break down when approaching the phase transition, as in the case for GaP.

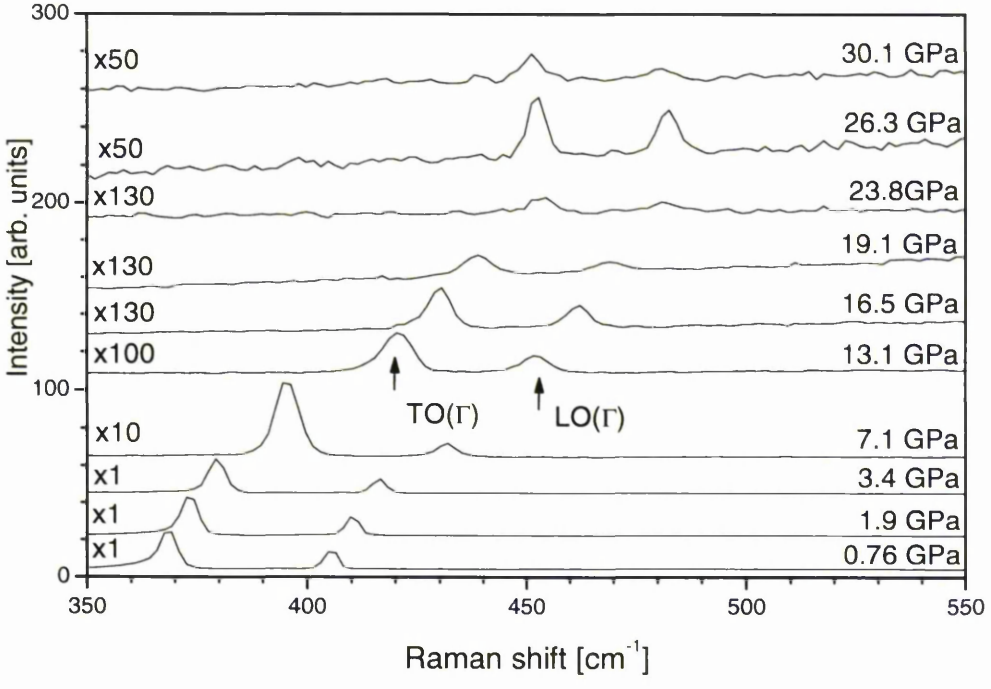

Figure 4.2: Raman spectra of GaP of the TO and LO phonon modes at different hydrostatic pressures.

To observe the effects of pressure on the phonon modes, we need to plot the change in Raman shift of the LO and TO modes with increasing pressure. Figure 4.3 shows the Raman shift of GaP as a function of pressure. It highlights the softening of the GaP

phonons at around 24.5GPa and it agrees well with the Cmcm phase transition observed by Nelmes et al [4].

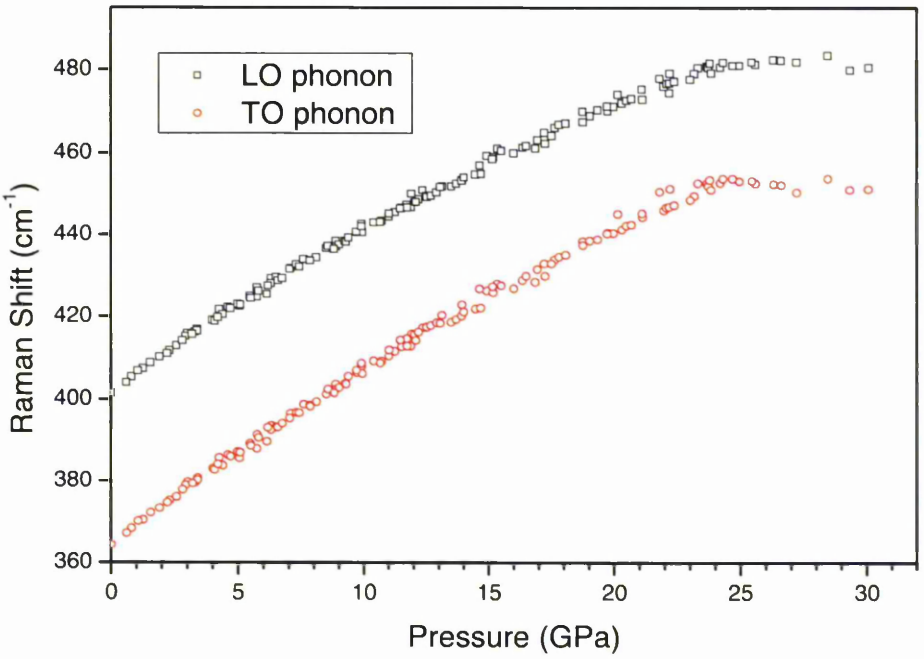

Figure 4.3: Raman shift for the LO and TO phonon modes for GaP as a function of pressure.

Looking closely, it can seen that the plot of the GaP is not linear. This is similar to GaAs results obtained by Güngerich et al [9] where the phonon signals were fitted with a quadratic function in the form of equation 2.28 which uses three fit parameters i.e a constant (σ_0), linear (α) and a quadratic (β)

$$\sigma(P) = \sigma_0 + \alpha P + \beta P^2 \qquad \text{Equation 2.28}$$

For comparison with results (GaP dilute nitrides) in the next chapter (Chapter 5) the fitting of each curve for each mode was done in the pressure range from 0 to 11GPa.

This guarantees comparability of the fit parameter results. Table 4.1 present fit parameters for each mode including the initial Raman peak at ambient pressure σ_0 which is similar to those obtained from figure 4.1. Table 4.1 also includes fit parameters data for other related group III-V materials

Sample	**Mode**	**σ_0 (cm^{-1})**	**α ($cm^{-1}GPa^{-1}$)**	**β ($cm^{-1}GPa^{-2}$)**
Bulk GaP	TO	364.7 ± 0.360	4.66 ± 0.139	-0.041 ± 0.012
Bulk GaP	LO	401.8 ± 0.029	4.52 ± 0.112	-0.055 ± 0.009
GaN [14]	TO	531.7	3.9	----
GaN [14]	LO	736.5	4.4	----
GaAs [9]	TO	268.4	4.22	1.17
GaAs [9]	LO	291.2	4.25	1.09
InN [15]	TO	439.7	5.81	----
InN [15]	LO	591.9	5.96	----

Table 4.1: Data related to the pressure dependence of phonon modes of GaP, GaN, GaAs and InN

The results in table 4.1 show the phonon-like shifts of GaP that can be used to compare with other GaP dilute nitrides. The fit parameters also show a similar comparison to other related samples. The next stage is to take the fit parameters and calculate the mode Grüneisen parameter and anharmonicity.

4.3.2 Mode Grüneisen parameters

The mode Grüneisen parameter is a parameter that shows the relationship between thermodynamics and statistical physics describing the alternation in a crystal lattice vibrational frequency shown by the phonon mode frequency shift based on the lattice volume (in this case) decreasing. It is given by equation 2.31 from chapter 2.

$$\gamma_i = \frac{B_0 \alpha}{\sigma_0} \qquad \text{Equation 2.31}$$

The Grüneisen parameter can be calculated using fit parameters (Table 4.1) and a value for the bulk modulus B_0 taken as 87.4GPa [11] for GaP.

Sample	Mode	Grüneisen parameter
Bulk GaP	TO	1.117 ± 0.033
Bulk GaP	LO	0.983 ± 0.024
GaN [14]	TO	1.47
GaN [14]	LO	1.2
GaAs [9]	TO	1 .17
GaAs [9]	LO	1.09
InN [15]	TO	1.66
InN [15]	LO	1.26

Table 4.2: Grüneisen parameters for bulk GaP, GaN, GaAs and InN.

For GaP, the Grüneisen parameter is calculated as 1.117 ± 0.033 for the TO phonon and 0.983 ± 0.024 for the LO phonon. This again shows a similarity to GaAs (as expected) and not to GaN or InN. The differences in values are large enough to allow us to make good comparisons between bulk III-V compounds and their dilute nitrides. This allows

us to fit the Grüneisen parameters of the studied dilute nitrides against one of the bulk III-V semiconductors in table 4.2.

4.3.3 Anharmonicity

With the knowledge of the pressure-induced shift of the TO and LO modes, we can calculate the anharmonicity of the GaP bond potential. Equation 2.36 gives the anharmonicity of the potential derived by Güngerich et al [9]. With the measured data and literature values taken from Vurgaftman et al [11], the anharmonicity of GaP for the LO phonon mode can be derived.

$$\frac{dD}{db} = \frac{32\pi^2 c^2 m\left(1/\lambda\right)_0}{\sqrt{3}a_0\left(S_{11}+2S_{12}\right)} \cdot \frac{d\left(\lambda^{-1}\right)}{dP} \qquad \text{Equation 2.36}$$

Using the above equation we are able to calculate the anharmonicity for the LO phonon mode of GaP. The anharmonicity is calculated to be $5.414^{x}10^{12}Nm^{-2}$. Comparing this to the anharmonicity calculated by Goni et al [14] for zinc blende GaN which has a value of $14.5^{x}10^{12}Nm^{-2}$ and for $GaAs_{1-x}N_x$ by Güngerich et al [9] ($8.4^{x}10^{12}Nm^{-2}$) this fits in well to what we expect due to the size of the P atom being larger than N atoms in GaN.

4.4 Conclusion

The Raman scattering measurements of the vibrational properties of GaP have been presented. The bulk GaP has been investigated up to 30GPa with a structural phase transition being observed at around 24.5GPa through the softening of the LO and TO phonons. This fits in well with previous x-ray absorption spectroscopy data and work by Nelmes et al but it has not been possible to determine the crystal structure after the phase transition.

The Raman scattering results again fit well with previous high pressure Raman measurements to 11GPa but with the aid of the DAC it has been possible to extend this area of research up to its phase transition. The Grüneisen parameters have been calculated to be 1.117 (TO) and 0.983 (LO). In the next chapter (Chapter 5) it will be possible to compare these Grüneisen parameters and anharmonicity values and explain their meaning more clearly.

4.5 Further work

Further work on GaP could be carried out as there are a number of questions to be answered. For example the determination of the new crystal structure after the phase transition using Raman scattering is unknown. Due to the very similar crystal structure between a Cmcm and a Imm2-type the phases are very close in enthalpy [16] at high pressures. The crystal phase was thought to be a β-tin type structure but work by Nelmes [4] has disproved this due to a number of missed features on the x-ray diffraction pattern [17]. The Imm2 phase has not be reported in experiments however high pressure and temperature studies with a reversible transition from the Cmcm phase might prove valuable.

As this chapter states, the scans were taken using either a 442nm or 514nm laser. It may be useful to examine the sample using the new Raman system stated in this thesis using a 632nm laser as this was found to be useful for measurements in later chapters. This is probably due to the use of lower energy photons which have a deeper penetration depth on the antimonides and could have a similar effect on phosphides.

4.6 References

[1] M. Baublitz Jr, A. L. Ruoff. J. Appl. Phys. **53** 6179 (1982)

[2] J. P. Itie, A. Polian, C. Jauberthie-Carillon, E. Dartyge, A. Fontaine, H. Tolentino and G. Tourillon. Phys. Rev. B. **40** 9709 (1989)

[3] J. Z. Hu, D. R. Black and I. L. Spain. Sol. Stat. Comms. **51** (5) 285 (1984)

[4] R. J. Nelmes, M. I. McMahon and S. A. Belmonte. Phys. Rev. Lett. **79** 3668 (1997)

[5] B. A. Weinstein, J. B. Renucci and M. Cardona. Sol. Stat. Comms. **12** 473 (1973)

[6] K. Aoki and M. Cardona. Phys. Stat. Sol. (b) **121** 441 (1984)

[7] B. A. Weinstein and G. J. Piermarini. Phys. Lett. **48A** (1) 14 (1974)

[8] M. P. Halsall, P. Harmer, P. J. Parbrook and S. J. Henley. Phys. Rev. B. **69** 235207 (2004)

[9] M. Güngerich, P. J. Klar, W. Heimbrodt, J. Koch, M. P. Halsall and P. Harmer. Phys. Rev. B. **71** 075201 (2005)

[10] M. F. Whitaker and D. J. Dunstan. J. Phys. Condens. Matter. **11** 2861 (1999)

[11] I. Vurgaftman, J. R. Meyer, and L. R. Ram-Mohan. J. Appl. Phys. **89** 5815 (2001)

[12] H. V. Hobden and J. P. Russell. Phys. Lett. **13** 39 (1964)

[13] R. A. Forman, G. J. Piermarini, J. D. Barnett and S. Block. Sciences. **176** 284 (1972)

[14] A. R. Goni, H. Siegle, K. Syassen, C. Thomsen and J. M. Wagner. Phys. Rev. B. **64** 035205 (2001)

[15] C. Pinquier, F. Demangeot, J. Frandon, J. C. Chervin, A. Polin, B. Couzinet and O. Briot. Phys. Rev. B. **73** 115211 (2006)

[16] A. Mujica, A. Rubio, A. Munoz and R. J. Needs. Rev. Mod. Phys. **75** (3) 863 (2003)

[17] M. Baublitz and A. L. Ruoff. J. Appl. Phys. **53** 6179 (1983)

Chapter 5: Vibrational properties of $GaP_{1-x}N_x$ under hydrostatic pressure

5.1 Introduction

Much recent attention has been given to the study of nitride related compounds due to their potential application in short wavelength optical devices such as blue LEDs [1-3]. It is known that the incorporation of nitrogen into GaP strongly modifies the band structure and forms isoelectronic electron traps, which persist as localised states up to nitrogen concentration of a few percent [4]. However one obstacle preventing the successful growth of larger percentages of nitrogen in GaP is due to the large mismatch between lattice structures and lattice constants between GaN and GaP. This leads to an extremely large mobility gap [5] however up to a nitrogen content of 3% the $GaP_{1-x}N_x$ can be easily grown directly on a GaP substrate with an acceptable lattice mismatch [6]. Due to this large mobility gap between GaN and GaP, the growth of $GaP_{1-x}N_x$ is only possible under non-equilibrium conditions i.e at low temperatures [7].

Little is known about the phonon properties of $GaP_{1-x}N_x$. Buyanova et al [8] reported on Raman measurements of $GaP_{1-x}N_x$ when the nitrogen content was less that 3%. They observed a two-mode phonon behaviour, a GaP-like mode between 399cm^{-1} to 401cm^{-1} and a GaN-like mode between 495cm^{-1} and 503cm^{-1} for the LO phonon modes. The use of Raman scattering spectroscopy is a useful tool in that much more detailed information about the structural properties of alloy systems can be obtained. This includes lattice perfection, strain and compositional uniformity [8] while the use of a DAC to apply a hydrostatic pressure yields a better understanding of the mechanical properties of the Ga-N bonds in a ternary Ga-N-V alloys.

Gil et al [9] were the first to demonstrate the benefits of applying pressure to a dilute nitride sample by examining the pressure dependence of nitrogen pairs in GaP

beyond a critical composition. Even though the experiment was only done up to 8kbar and a temperature of 2K, it highlighted the benefits.

Moving back to the importance of incorporating nitrogen into GaP and the forming of localised states, the effect of these states on the global electronic properties of the alloy are found to depend sensitively on the local environment of the nitrogen atoms [10]. The vibrational properties of these ternary alloys also reflect the impurity character of the nitrogen atoms in materials such as GaP but also in GaAs [11] as well. When Buyanova et al [8] first reported on the GaN-like mode observed at around $500cm^{-1}$, it was infact a localised vibrational mode (LVM) of nitrogen. Studying the local vibrational mode of nitrogen provides a powerful tool for obtaining information about the influence of nitrogen incorporation on the crystalline structure.

An analysis of the pressure dependence of the mode frequencies, especially the LVM allows us to derive bond strength and anharmonicities. This provides direct information on the nature of the chemical bond. A number of theoretical and experimental studies have taken place about the structural properties including strain and lattice perfection [8,12] however the effect of the epitaxial strain and alloying on the lattice vibrations of $GaP_{1-x}N_x$ due to nitrogen incorporation is less known. This provides an excellent opportunity, with the use of a DAC, to further our knowledge about Ga-N like bonds within GaP but also allow us to observe the local phonon modes as a function of pressure.

5.2 Experimental procedure

The $GaP_{1-x}N_x$ sample studied in this chapter was an epitaxial layer of $GaP_{0.979}N_{0.021}$ grown on a (100) undoped GaP substrate by MOVPE at 700°C at the Renewable Energy Laboratory in Colorado. The epilayer thickness was 1μm and the nitrogen content (2.1%) was derived from x-ray diffraction data. The source materials used to grow the $GaP_{1-x}N_x$ layer were triethylgallium, dimethylhydrazine and phosphine.

As in chapter 4, the sample was thinned to a thickness of about 30μm by polishing most of the GaP substrate away using fine diamond paper. The sample was then cleaved to a size of about 50μm which allowed it to be loaded into the gasket hole. A speck of ruby dust was also added to allow the pressure inside the cell to be calculated.

Raman scattering scans were taken at pressures from 1 to 19GPa at room temperature in a (100)-orientation. A x(y',y') backscattering geometry was used while a 40x long working objective lens collected the light and allowed focusing on the sample surface to be achieved. As the pressure in the DAC only went up to about 20GPa, there was no need for the use of silicon oil. A mixture of methanol and ethanol (4:1) was sufficient for the pressure medium.

For the calculation of pressure, an averaging technique was used again by measuring the ruby PL before and after the Raman scan. A 15 minute time period was again applied after each step increase in pressure to ensure that the pressure, sample and cell movement was stationary within the DAC.

5.3 Results and Discussion

5.3.1 Phonon modes

Figure 5.1 shows a Raman spectrum of $GaP_{0.979}N_{0.021}$ at ambient pressure. Compared to the spectrum obtained for bulk GaP in figure 4.1, the spectrum shows two identical TO and LO phonon modes of the GaP-like bonds but having a slightly different Raman shift to the once seen in GaP. These peaks are at 401.8cm^{-1} for the LO phonon mode and 365.0cm^{-1} for the TO phonon mode. Referring back to the Raman shifts obtained in chapter 4 for bulk GaP (401.6cm^{-1} and 364.4cm^{-1} respectively), they have a slightly higher Raman shift than bulk GaP and a first glance suggests that this is wrong. Buyanova et al [8] showed that in pseudomorphically grown samples the optical phonons frequencies of $GaP_{1-x}N_x$ decreases with increasing nitrogen content. In this sample, both the TO and LO mode frequencies are higher than the peaks measured for

bulk GaP in chapter 4 (the opposite of Buyanova et al). It is believed that this sample is partly relaxed, resulting in an increase in frequency due to tensile strain.

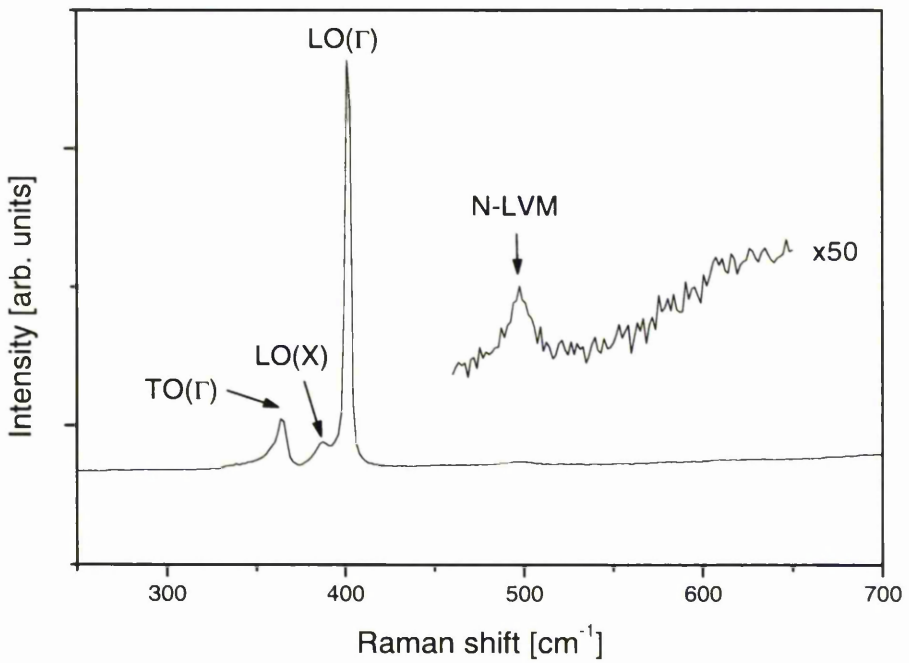

Figure 5.1: Raman spectrum of $GaP_{0.979}N_{0.021}$ at ambient pressure.

A further two peaks can be distinguished in figure 5.1. Both peaks are GaN-like modes and are the phonon frequencies of the GaN bond. These peaks would not be seen as expected in bulk GaP as it contains no nitrogen and thus are only present in this sample and any other sample with nitrogen incorporated into it. Between the two larger GaP-like phonon modes, a weaker signal can be distinguished. This is the LO(X) phonon peak of the GaN measured in this sample to be at $387cm^{-1}$ [13]. This peak is observable because of the breakdown of momentum conservation rules and symmetry lowering due to the incorporation of nitrogen into GaP. However it is a useful indication when polishing and loading the sample into the cell that if this peak is detected by performing

a quick scan, then one will know that the epilayer surface is facing upwards and is clean from any dirt.

Another peak that is not detected in bulk GaP but can be seen in figure 5.1 is at the Raman shift of $497cm^{-1}$. This corresponds to the LVM of the nitrogen atom and again, can only be seen in the $GaP_{1-x}N_x$ sample. This peak is much weaker that the first GaN-like mode, hence the magnification of 50x in figure 5.1. More of this nitrogen LVM is discussed in the next section (5.3.2)

The next figure (Figure 5.2) shows the spectrum of $GaP_{0.979}N_{0.021}$ at various increasing hydrostatic pressures at room temperature using the 514nm excitation laser. Figure 5.2 shows the pressure induced shifts of the GaP-like phonons. For the $GaP_{0.979}N_{0.021}$ sample, the pressure was increased to about 20GPa before the Raman signal became too weak and was swamped by the background noise. For the nitrogen LVM this was at a lower pressure, at approximately 10GPa.

Again we see in figure 5.2 that the absolute and relative intensities of the TO and LO modes show irregular behaviour. Again it can be stated that the most likely cause of this is by non-constant scattering geometries and resonance effects due to pressure induced energy shifts of the electronic states. For $GaP_{0.979}N_{0.021}$ it can be argued that the cause of this is due to the Raman selection rules breaking down near to the phase transition. As the majority of the sample is GaP, it can be assumed that the phase transition is approximately in the same pressure region.

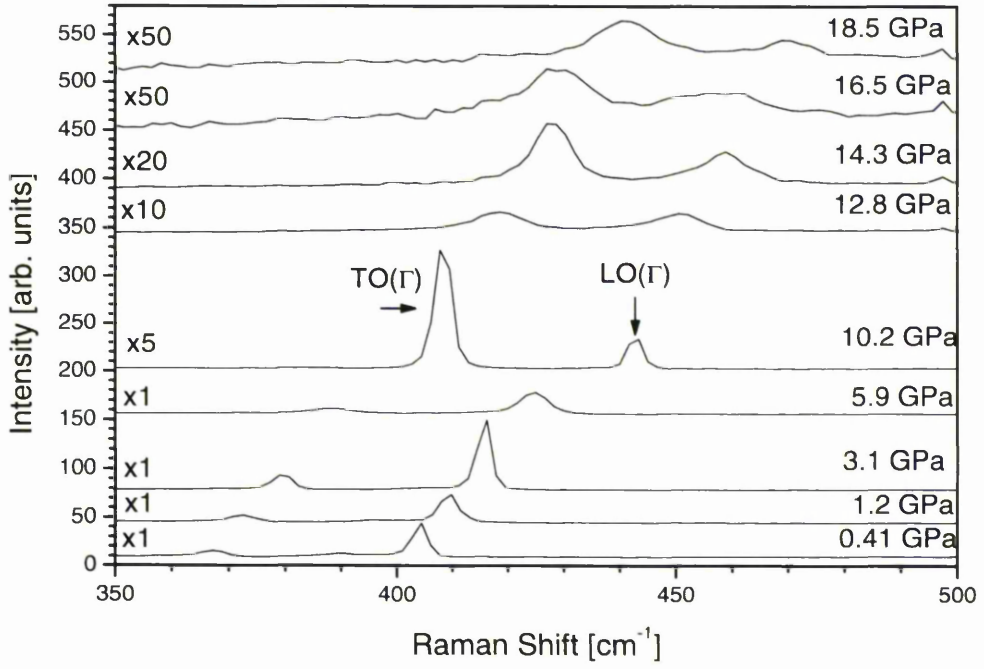

Figure 5.2: Raman spectra of the GaP-like phonons of $GaP_{0.979}N_{0.021}$ at various hydrostatic pressures at room temperature.

The phonon peaks frequencies in figure 5.2 are then plotted against pressure up to a region of 20GPa to show the Raman shift of the GaP-like phonons as a function of pressure. This is shown is figure 5.3.

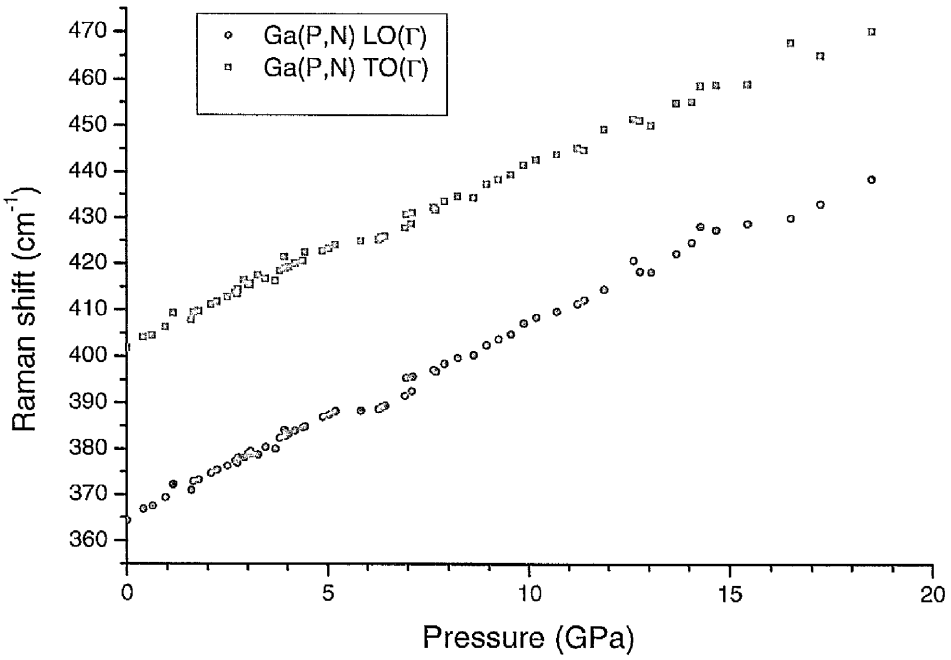

Figure 5.3: Raman shift of the GaP-Like phonons as a function of pressure.

The fit parameter results for figure 5.3 are presented in table 5.1 together with calculations from previous studies of bulk GaP, GaN, GaAs and $GaAs_{0.915}N_{0.085}$.

Sample	Mode	σ_0 (cm^{-1})	α ($cm^{-1}GPa^{-1}$)	β ($cm^{-1}GPa^{-2}$)
$GaP_{0.979}N_{0.021}$	TO	366.0 ± 0.567	4.03 ± 0.245	-0.027 ± 0.021
$GaP_{0.979}N_{0.021}$	LO	403.0 ± 0.525	4.04 ± 0.227	-0.055 ± 0.009
Bulk GaP	TO	364.7 ± 0.360	4.66 ± 0.139	-0.041 ± 0.012
Bulk GaP	LO	401.8 ± 0.029	4.52 ± 0.112	-0.055 ± 0.009
GaN [14]	TO	531.7	3.9	----
GaN [14]	LO	736.5	4.4	----
GaAs [11]	TO	268.4	4.22	1.17
GaAs [11]	LO	291.2	4.25	1.09
$GaAs_{0.915}N_{0.085}$ [11]	TO	266.3	4.33	1.223
$GaAs_{0.915}N_{0.085}$ [11]	LO	287.4	3.97	1.039

Table 5.1: Fit parameters of GaP-like phonon modes of $GaP_{0.979}N_{0.021}$, bulk GaP, GaN, GaAs and $GaAs_{0.915}N_{0.085}$.

The data points from figure 5.3 were fitted with a quadratic function in the form of equation 2.28 which again uses three fit parameters i.e a constant (σ_0), linear (α) and a quadratic (β). As stated in chapter 4, the quadratic fit was fitted up to pressures of 11GPa to allow comparability of results from this thesis and work by Güngerich et al [11].

The calculations for $GaP_{0.979}N_{0.021}$ appear to show a considerable smaller value for the α parameter for the optical phonons TO and LO than in bulk GaP. However, the

total errors in the determination of the fit parameters such as the inaccuracies in pressure determination and the peak frequency determination for each spectrum are larger than the indicated errors given in table 5.1. Due to this, within the experimental accuracy, there is no significant change in the pressure behaviour of the GaP-like phonons due to nitrogen incorporation.

5.3.2 Nitrogen local vibrational mode

The LVM can be seen at 497.3cm^{-1} in figure 5.1 while figure 5.4 highlights the shift in the LVM with pressures up to 10GPa. The LVM signal is very weak and is only clearly detectable at low pressures when the background noise in the DAC is lower however at higher pressures, one can follow or trace the LVM through a series of spectra due to its continuous shift. In figure 5.4 for example, the nitrogen LVM at pressures above 3.1GPa are highlighted with a flat-background fit due to the low signal-to-noise ratio at higher pressures.

The LVM is of great importance to the study of dilute nitrides in general due to the LVM frequency being directly related to the spring constant of the covalent bond between gallium and nitrogen atoms. This allows us to study the mechanical properties that include strain and lattice perfection helping us to a greater understanding of dilute nitrides.

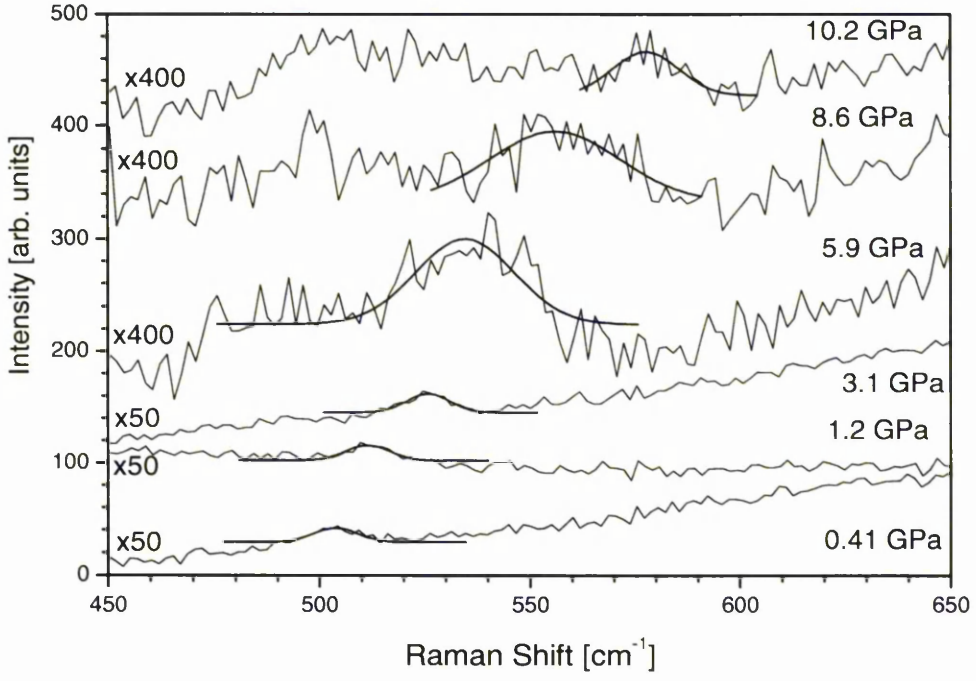

Figure 5.4: Raman spectra of the nitrogen LVM at increasing hydrostatic pressure at room temperature.

The nitrogen LVM frequency and as well as other phonon peaks in this thesis, was derived by fitting a Gaussian line shape to the experimental data. This data was plotted as a function of pressure and is shown in figure 5.5.

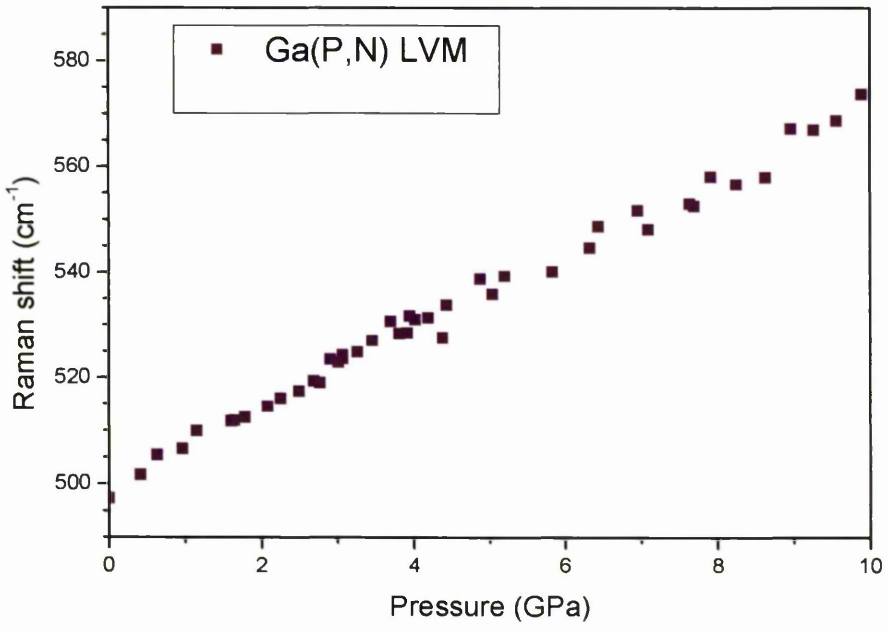

Figure 5.5: Raman shift of the Ga-N-like phonons of the nitrogen LVM.

The calculated fit parameters of the data points in figure 5.5 are presented if table 5.2 with corresponding values for GaN and $GaAs_{0.915}N_{0.085}$.

Sample	Mode	σ_0 (cm^{-1})	α (cm^{-1}GPa^{-1})	β (cm^{-1}GPa^{-2})
$GaP_{0.979}N_{0.021}$	LVM	499.9 ± 0.982	7.48 ± 0.443	-0.027 ± 0.041
GaN [14]	TO	531.7	3.9	----
GaN [14]	LO	736.5	4.4	----
$GaAs_{0.915}N_{0.085}$ [11]	LVM	476.1	10.7	1.692

Table 5.2: Fit parameters for $GaP_{0.979}N_{0.021}$, GaN and $GaAs_{0.915}N_{0.085}$.

Comparing the pressure dependence of the LVM of $GaP_{1-x}N_x$ to previous TO modes studies of $GaAs_{1-x}N_x$ [11] and wurzite GaN [14], the LVM is considerably larger than that of the TO mode of GaN but is weaker than that of $GaAs_{1-x}N_x$. This still indicates that the LVM does not show a GaN- like behaviour.

5.3.3 Mode Grüneisen parameters

Using equation 2.31

$$\gamma_i = \frac{B_0 \alpha}{\sigma_0} \qquad \text{Equation 2.31}$$

It is now possible to calculate the Grüneisen parameters for the TO and LO GaP-like phonon modes and the GaN-like phonon mode of the LVM using the values in tables 5.1 and 5.2. For the $GaP_{1-x}N_x$ sample, the bulk modulus was assumed to be the same for GaP at 87.4GPa [15]. In real life, this is not true as the incorporation of nitrogen into the sample could change the bulk modulus. The following Grüneisen parameters are presented in table 5.3.

Sample	Mode	Grüneisen parameter
$GaP_{0.979}N_{0.021}$	TO	0.962 ± 0.058
$GaP_{0.979}N_{0.021}$	LO	0.876 ± 0.049
$GaP_{0.979}N_{0.021}$	LVM	1.307 ± 0.077
Bulk GaP	TO	1.117 ± 0.033
Bulk GaP	LO	0.983 ± 0.024
GaN [14]	TO	1.47
GaN [14]	LO	1.2
GaAs [11]	TO	1 .17
GaAs [11]	LO	1.09
$GaAs_{0.915}N_{0.085}$ [11]	TO	1.223
$GaAs_{0.915}N_{0.085}$ [11]	LO	1.039
$GaAs_{0.915}N_{0.085}$ [11]	LVM	1.692

Table 5.3: Grüneisen parameters for $GaP_{0.979}N_{0.021}$, bulk GaP, GaN, GaAs and $GaAs_{0.915}N_{0.085}$.

The variation of the bulk modulus with nitrogen concentration is not known and the use of a common value for both the binary and ternary materials may be a rough approximation in the calculation of the Grüneisen parameters. This is one source of error together with the inaccuracies in pressure and peak frequency determination for each spectrum.

Comparing the Grüneisen parameter obtained in chapter 4 for bulk GaP, the parameters for the optical phonons in $GaP_{1-x}N_x$ appear to be considerably smaller in the ternary $GaP_{0.979}N_{0.021}$ than in the binary GaP compound. Due to this and with previous stated errors in mind, there is no significant change in the pressure behaviour of the GaP-like phonons due to nitrogen incorporation.

5.3.4 Anharmonicity

With the knowledge of the pressure induced shift of the LVM, we can calculate the anharmonicity of the GaN bond potential using equation 2.36 from chapter 2.

$$\frac{dD}{db} = \frac{32\pi^2 c^2 m\left(1/\lambda\right)_0}{\sqrt{3}a_0\left(S_{11}+2S_{12}\right)} \cdot \frac{d\left(\lambda^{-1}\right)}{dP} \qquad \text{Equation 2.36}$$

With the corresponding measured data and literature values the anharmonicity value for the LVM is $7.03^{x}10^{12}Nm^{-2}$ while the corresponding values for GaN and $GaAs_{1-x}N_x$ [11,14] are $14.5^{x}10^{12}Nm^{-2}$ and $78.4^{x}10^{12}Nm^{-2}$ respectively. In agreement to previous work [14], the measured anharmonicity supports the overstretched character of the Ga-N bond.

One thing that is surprising, which is not understood, is that the anharmonicity of the Ga-N bonds in the $GaP_{1-x}N_x$ is smaller that in the $GaAs_{1-x}N_x$. The exact opposite would be expected to occur due to the atom size of P being smaller than that of the As atom. The results imply that there is a smaller local tensile strain in the vicinity of the nitrogen atoms in $GaP_{1-x}N_x$ than in $GaAs_{1-x}N_x$.

Another consideration is the electronegativity of P which is also smaller than that of the As atom. Taking this into account, it can be speculated that the reduction in bond anharmonicity is not only governed by the same difference in atomic size but also affected by the difference in electronegativity between the two group-V species in the crystal.

5.4 Conclusion

In this chapter, the pressure dependent Raman scattering measurements of the vibrational properties of $GaP_{0.979}N_{0.021}$ have been presented and compared to the bulk GaP investigated in chapter 4. The $GaP_{1-x}N_x$ sample has been studied up to 20GPa while the nitrogen LVM has been studied up to approximately 10GPa before the signal became too weak.

The Grüneisen parameter obtained from the analysis of the pressure dependent phonon frequency for $GaP_{1-x}N_x$ indicates that nitrogen incorporation of 2.1% has little influence on the pressure behaviour of the host phonon modes of the GaP. The results have also shown that the LVM of the nitrogen atom is qualitatively consistent with that in previous work of $GaAs_{1-x}N_x$ indicating that in both ternary materials the GaN-like modes do not actually show any GaN-like behaviour under pressure.

5.5 Further work

Much further work is possible on dilute nitrides especially looking at the incorporation of nitrogen into GaP. In this study, only one sample was studied which had a percentage of 2.1% while further studies of other different percentages of nitrogen would yield more results and give a better understanding of the behaviour of nitrogen in GaP.

Although the $GaP_{1-x}N_x$ sample was measured up to pressures of 20GPa, it was only possible for the LVM to be studied up to 10GPa before the signal to noise ratio became to large and the background swamped the Raman scattered light. Further work could be achieved by using the new Raman system which could provide clearer spectra at higher pressures due to lower energy photons. This may also provide more information on the anharmonicity of the $GaP_{1-x}N_x$ and would help to explain why there is a smaller value for the anharmonicity than expected. It may turn out to be wrong or could even be proved to be right.

5.6 References

[1] R. F. Davis. Proc. IEEE. **79** 702 (1991)

[2] S. Strite and H. Morkoc. J. Vac. Sci. Technol. B. **10** 1237 (1992)

[3] S. Nakamura, T. Mukai and X. Senoh. Appl. Phys. Lett. **64** 1687 (1992)

[4] K. Aoki and M. Cardona. Phys. Stat. Sol. (b) **122** 441 (1984)

[5] G. B. Stringfellow. J. Cryst. Growth. **27** 21 (1974)

[6] L. Peternai, J. Kovac, J. Jakabovic, V. Gottschalch and B. Rheinlaender. J. Elec. Mat. **35** (4) 654 (2004)

[7] J. N. Baillargeon, K. Y. Cheng, G. E. Holfler and P. J. Pearch. Appl. Phys. Lett. **60** 2540 (1992)

[8] I. A. Buyanova, W. M. Chen, E. M. Goldys, H. P. Xin and C. W. Tu. Appl. Phys. Lett. **78** 3959 (2001)

[9] B. Gil, M. Baj, J. Camassel, H. Mathieu, C. Benoit and J. Pascual. Phys. Rev. B. **29** 3398 (1984)

[10] P. J. Klar. Prog. Sol. Stat. Chem. **31** 301 (2003)

[11] M. Güngerich, P. J. Klar, W. Heimbrodt, J. Koch, M. P. Halsall and P. Harmer. Phys. Rev. B. **71** 075201 (2005)

[12] J. P. Itie, A. Polian and C. Jauberthie-Carillon. Phys. Rev. **40** 9709 (1989)

[13] S. Yoon, M. J. Seong, J. F. Geisz, A. Duda and A. Mascarenhas. Phys. Rev. B. **67** 235209 (2003)

[14] A. R. Goni, H. Siegle, K. Syassen, C. Thomsen and J. M. Wagner. Phys. Rev. B. **64** 035205 (2001)

[15] I. Vurgaftman, J. R. Meyer, and L. R. Ram-Mohan. J. Appl. Phys. **89** 5815 (2001)

Chapter 6: Vibrational properties of $GaSb_{1-x}N_x$ under hydrostatic pressure

6.1 Introduction

Dilute III-V nitrides such as $GaSb_{1-x}N_x$ have emerged as a new kind of material, having the potential for the fabrications of high power laser devices and applications such as LED's that operate in the long wavelength region [1]. Due to the paucity of suitable materials that can operate in the mid-infrared region of 2-4μm [2] $GaSb_{1-x}N_x$ is a promising candidate for such a role however the incorporation of nitrogen in to the $GaSb_{1-x}N_x$ system is the most challenging. GaSb nitrides have been grown either by molecular beam epitaxy (MBE) [3-4] or MOVPE [5] although it has been discovered that with increasing nitrogen content, a major degradation of the material occurs [6]. Despite this, the benefits of dilute nitrides and $GaSb_{1-x}N_x$ outweigh the problems due to a considerable reduction in the energy bandgap.

Theoretical *ab initio* pseudopotential calculations by Belabbes et al [7] predicted a larger bandgap reduction in $GaSb_{1-x}N_x$ than in As-based nitrides systems due to a larger atomic size and electronegativity differences between N and Sb in comparison to N and As. This has been seen in a number of $GaSb_{1-x}N_x$ studies [8-10] which have shown that the replacement of a few percent of nitrogen atoms into GaSb results in a decrease of both the intrinsic bandgap and the lattice parameter of the crystal [11-13]. The reason for this is due to the nitrogen atoms being small in comparison and that they are highly electronegative and isoelectronic. This enables the bandgap of $GaSb_{1-x}N_x$ to be tuned to a particular energy for optoelectronic applications.

Figure 6.1 shows the calculated bandgap variation as a function of nitrogen incorporation for $GaSb_{1-x}N_x$ alloys taken from reference 4. Figure 6.1 clearly shows the variation of bandgaps in this dilute nitride which highlights the benefits of studying this

material and why more research should be performed in understanding the incorporation of nitrogen.

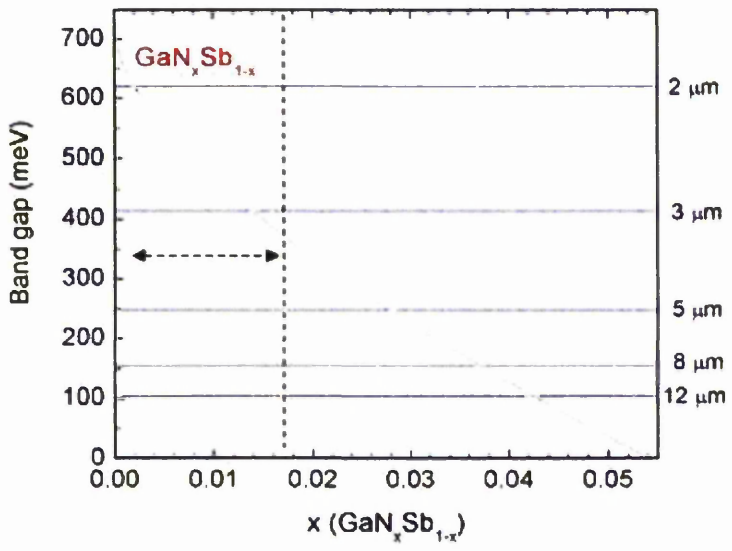

Figure 6.1: Calculated bandgap of $GaSb_{1-x}N_x$ as a function of nitrogen concentration [4]

The group III-antimonide nitrides have received much less attention compared with GaSb as highlighted before but this can change with the use of Raman scattering techniques to help us understand more about the structural properties such as strain and lattice perfection. It appears that no studies exist for the use of the Raman technique on $GaSb_{1-x}N_x$, especially at high pressure. For instance, a recent review by Vurgaftman et al [14] on nitrogen incorporated into semiconductors highlights the lack of experimental results of $GaSb_{1-x}N_x$. This fact has been recently been corrected by work carried out at QinetiQ who have published a number of papers on the band anticrossings in $GaSb_{1-x}N_x$ [15], bandgap reduction in $GaSb_{1-x}N_x$ due to an anion-mismatch [4] and various work on the growth of dilute $GaSb_{1-x}N_x$ by plasma-assisted MBE [3]. These papers contain little optical research, mainly using FTIR and so present a perfect opportunity to conduct Raman studies.

It is stated that in dilute nitrides, the substitution of a highly electronegative nitrogen for a few percent of the host atom results in the formation of a highly localised resonant band close to the conduction band minimum [3]. The result of these unique properties are formed due to the nitrogen large covalent energy and electronegativity which give rise to short III-V bond lengths and significant distortion to the alloys [4]. Even thought Klar [16] talks about the incorporation of nitrogen into GaP, it would be sensible to talk about the same effects happening in $GaSb_{1-x}N_x$.

Previous Raman measurements up to GaSb phase transition at 7.65GPa were measured back in the 1980's by Aoki et al [17]. They have studied the dependence of Raman frequencies and scattering intensities at pressure for GaSb. The results from this paper will be a vital resource to compare the phonon modes observed in $GaSb_{1-x}N_x$ and how these change as a function of pressure.

6.2 Experimental procedure

The $GaSb_{1-x}N_x$ sample studied in this chapter was an epitaxial layer of $GaSb_{0.985}$ $N_{0.015}$ grown on a (100) undoped GaSb substrate by MBE at the QinetiQ Malvern site by Louise Buckle and co-workers. The epilayer thickness was 0.25μm and the nitrogen content was derived from x-ray diffraction data and calculated to be 1.5%. For the GaSb substrate, this had a thickness of 1.50μm.

As in chapter 4 and 5, the sample was thinned to a thickness to about 30μm thick by polishing most of the GaSb substrate away using fine diamond paper. At 30μm thick, the sample still had some of the substrate attached to the back of the epilayer, however it does not cause any problems due to the backscattering geometry of the Raman setup. The sample was then cleaved to a size of about 50μm and loaded together with a speck of ruby into the DAC which contains 150μm diamonds.

Raman scattering scans were taken using the new Raman system and the 632nm laser at pressures from 1 to 8GPa at room temperature in a (100)-orientation. A x(y',y') backscattering geometry was used while a 40x long working objective lens collected the

light and allowed focusing on the sample surface to be achieved. Due to the location of the camera in this setup (refer back to chapter 3.1.2 for more details) the positioning of the sample and ruby was conducted through a back light when the laser light was blocked off.

Once the hole at the centre of the DAC was lined up with the camera, the laser light could again be focused on to the surface of the sample. To ensure that the laser was reflecting off the surface of the sample and that the laser spot was as small as possible, the Grams software was used to measure the intensity of the laser spot. By taking one second static scans, the objective lens could be moved slightly closer or moved away from the DAC. Observing the maximum intensity of the peak ensured the correct position was obtained.

As the pressure in the DAC only went up to about 10GPa, there was no need for the use of silicon oil. A mixture of methanol and ethanol (4:1) was sufficient for the pressure medium. For the calculation of pressure, the same averaging technique used in chapter 4 and 5 was again used by measuring the ruby PL before and after the Raman scan. A 15 minute time period was again applied after each step increase in pressure to ensure that the pressure, sample and cell movement was still within the DAC.

6.3 Results and Discussion

6.3.1 Phonon modes

The first task was to collect Raman scattering measurements of the GaSb (p-type $1.2^{x}10^{17}$) reference sample. The spectrum of this sample is given in figure 6.2 and it shows strong scattering from the LO phonon line as expected in this geometry. The TO phonon is still seen, at a lower energy than the LO phonon while there are also a series of overtones due to the optical phonon modes between $400cm^{-1}$ and $500cm^{-1}$. The TO and LO phonon modes are measured to be $225.35cm^{-1}$ and $235.35cm^{-1}$ respectively. Raman measurements on GaSb provided by Aoki et al [17] provides quadratic expressions on the TO and LO phonon modes under pressures. At ambient pressure

their calculated value for the TO mode is 223.6cm^{-1} while the LO mode is 232.6cm^{-1}. Strangely, the reference sample is showing a higher Raman shift frequency than the GaSb measured in Aoki et al [17]. However this could be accounted for by the fact that the reference sample used in this chapter is a p-type while no information on the type used by Aoki et al is given in the paper.

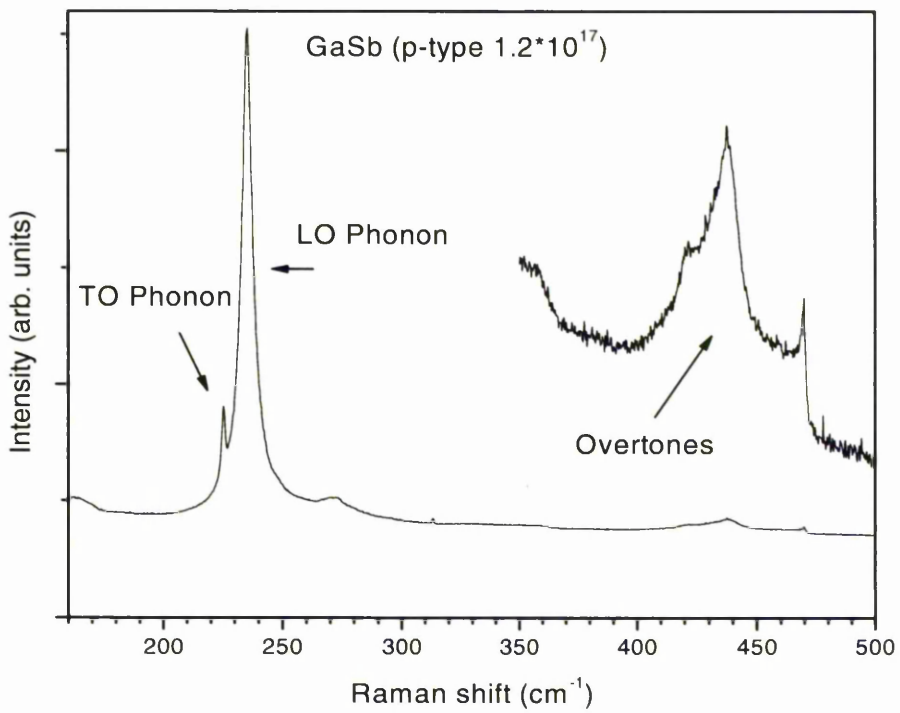

Figure 6.2: Raman spectrum for reference p-type (1.2^x10^{17}) GaSb at ambient pressure.

Figure 6.3 is the Raman scattering spectrum for the $GaSb_{1-x}N_x$ sample $GaSb_{0.985}N_{0.015}$. The nitrogen content in this sample is 1.5% and the spectrum shows the effects of introducing nitrogen in to GaSb by the shift in the TO-LO phonon lines to a lower energy (225.09cm^{-1} and 232.5cm^{-1} respectively). There has been a reduction in the intensity of the peaks, a broadening has been observed while similar effects being noticed in the overtones. Before discussing the overtones, a reduction in the phonon energy is seen in the TO and LO peaks. This is opposite to what is seen in chapter 5

which suggests that there is no reduction in tensile strain and therefore no relaxing of the sample.

The spectrum around the region of the overtones ($400cm^{-1}$ to $500cm^{-1}$) should contain a nitrogen LVM due to similar results obtained in chapter 5 and other previous studies. Unfortunately at ambient pressure, this LVM is not seen but if it is present in the system, it is likely to be hidden beneath the peak seen at $435cm^{-1}$. Hopefully, high pressure measurements will allow the nitrogen LVM to be observed and measured.

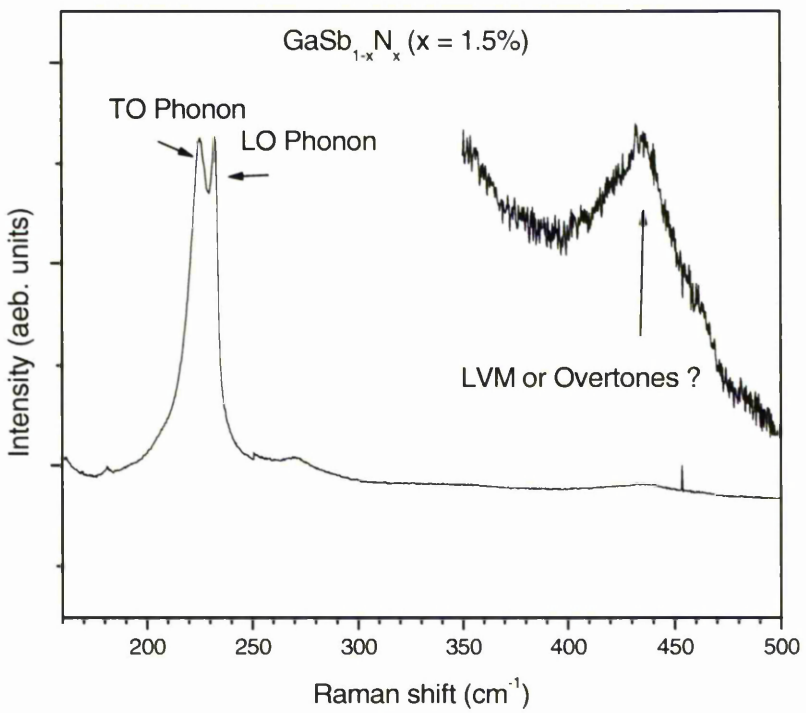

Figure 6.3: Raman spectrum of $GaSb_{0.985}N_{0.015}$ at ambient pressure.

The next step was to place a piece of the $GaSb_{1-x}N_x$ sample into the DAC, increase the pressure and measure the resulting pressure-induced phonon shift. The results of this for the TO and LO phonons are given in figure 6.4 which shows various Raman spectra up to a pressure of 7.48GPa. Aoki et al [17] detected a phase transition at 7.65GPa and the

results confirm this. Due to the errors in measuring the PL of the ruby lines and the equation used to calculate the value, the phase transition observed in this $GaSb_{1-x}N_x$ sample fits well with Aoki work. It should also be pointed out that the incorporation of nitrogen could also slightly change the phase transition value.

Figure 6.4 clearly shows the pressure-induced shift in the TO and LO GaSb-like modes with increasing hydrostatic pressures. At 7.48GPa, the phonon peaks are no longer visible which gives a good indication of a phase transition. The absolute and the relative intensities of the TO and LO modes shows (although not clearly seen in figure 6.3) an irregular behaviour. There are several reasons for this but the main reason is the likely cause of non-constant scattering geometries and the resonance effects due to pressure induced energy shifts of the electronic states.

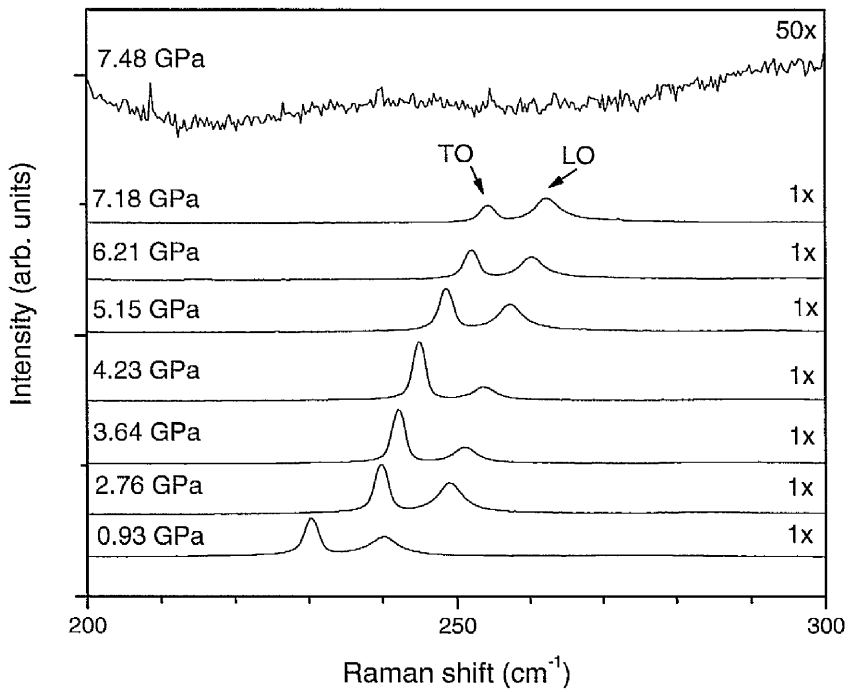

Figure 6.4: Various Raman spectra of the TO and LO GaSb-like phonon modes of $GaSb_{0.985}N_{0.015}$.

The Raman scattering measurements at different hydrostatic pressures are plotted as a function of pressure. These data points are presented in figure 6.5 which shows an almost linear increase in the Raman shift as pressure increases. A closer looks suggests other wise and that a quadratic fit is more suitable to the scattered graphs as the spread of data points are curved at higher pressures. These fit parameters for the TO and LO GaSb-like modes are presented in table 6.1 together with comparison data taken for high pressure Raman studies for GaSb, GaN, GaAs and $GaAs_{0.915}N_{0.085}$.

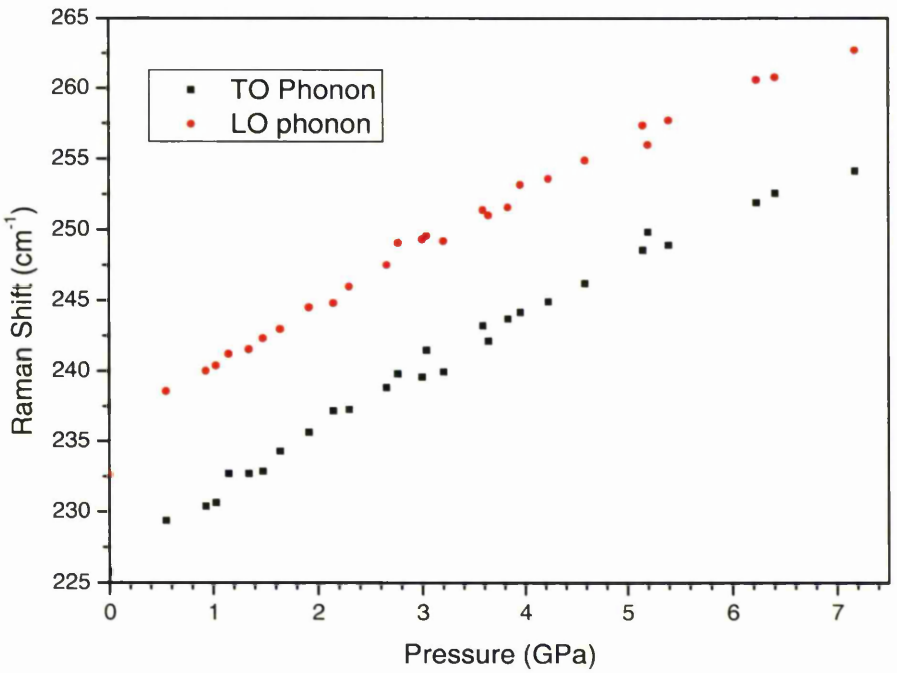

Figure 6.5: Raman shift of the GaSb-like phonons as a function of pressure for the dilute nitride $GaSb_{0.985}N_{0.015}$.

Sample	Mode	σ_0 (cm^{-1})	α ($cm^{-1}GPa^{-1}$)	β ($cm^{-1}GPa^{-2}$)
$GaSb_{0.985}N_{0.015}$	TO	225.90 ± 0.33	5.38 ± 0.21	-0.196 ± 0.029
$GaSb_{0.985}N_{0.015}$	LO	234.58 ± 0.38	5.49 ± 0.24	-0.220 ± 0.033
GaSb [17]	TO	223.6	4.67	-0.11
GaSb [17]	LO	232.6	4.56	-0.12
GaN [18]	TO	531.7	3.9	----
GaN [18]	LO	736.5	4.4	----
GaAs [19]	TO	268.4	4.22	1.17
GaAs [19]	LO	291.2	4.25	1.09
$GaAs_{0.915}N_{0.085}$ [19]	TO	266.3	4.33	1.223
$GaAs_{0.915}N_{0.085}$ [19]	LO	287.4	3.97	1.039
$GaAs_{0.915}N_{0.085}$ [19]	LVM	476.1	10.7	1.692

Table 6.1: Data fit parameters of the pressure-induced phonon modes of $GaSb_{0.985}N_{0.015}$, GaSb, GaN, GaAs and $GaAs_{0.915}N_{0.085}$

The fit parameters of σ_0 and α for the GaSb optical phonons are considerably larger in the ternary $GaSb_{0.985}N_{0.015}$ than in the binary GaSb compound investigated by Aoki et al [17]. The Raman shift at ambient pressure is measured to be at a higher frequency which confirms that there is no reduction in the tensile strain for $GaSb_{0.985}N_{0.015}$. Although the values are considerably higher than GaSb, they are even greater than the

values calculated for GaN [18]. With this in mind, and from studies on $GaAs_{0.915}N_{0.085}$ [19], due to the experimental accuracy there is no significant change in the pressure behaviour of the GaSb-like phonons due to nitrogen incorporation.

The experimental errors that are used for the determination of the fit parameters are greater than the ones indicated in table 6.1. This is due to inaccuracies in the pressure determination and peak frequency for each spectrum. It should also be stated that the Raman shift values obtained for $GaSb_{0.985}N_{0.015}$ at ambient pressure are somewhat lower than the fit parameters suggest. This is more true in the LO phonon mode which explains why 5.49GPa was calculated for the α parameter rather than being closer to 5.56GPa measured for GaSb. This would need investigating.

6.3.2 Nitrogen local vibrational mode

The nitrogen local vibrational mode for $GaSb_{0.985}N_{0.015}$ was studied under increasing hydrostatic pressures and a selection of Raman spectra is presented in figure 6.6. The figure shows a peak, around the $440cm^{-1}$ mark which moves towards higher energies as pressure increases. When a Raman spectrum was taken of the $GaSb_{1-x}N_x$ sample at ambient pressure (Figure 6.3) it was unknown if this peak was the LVM or overtones.

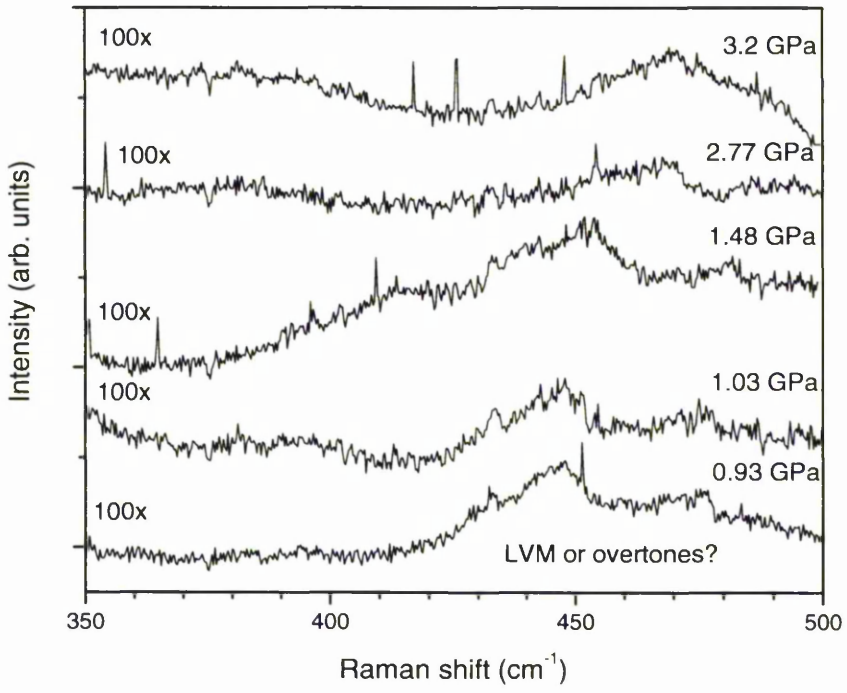

Figure 6.6: Raman spectra for $GaSb_{0.985}N_{0.015}$ at various hydrostatic pressures in the region of the expected nitrogen LVM.

Figure 6.6 clearly shows that the unknown peak is pressure induced but is very weak and so is magnified by 100x. Due to this intensity weakness, only a limited number of Raman scattering spectra was able to provide any clear peaks that could be measured and plotted as a function of pressure. Additional peaks that could possibly be other features were also recorded too but again due to the weak intensity, unfortunately only a handful were measured. Figure 6.7 shows the Raman shift as a function of pressure for the region where the nitrogen LVM might exist.

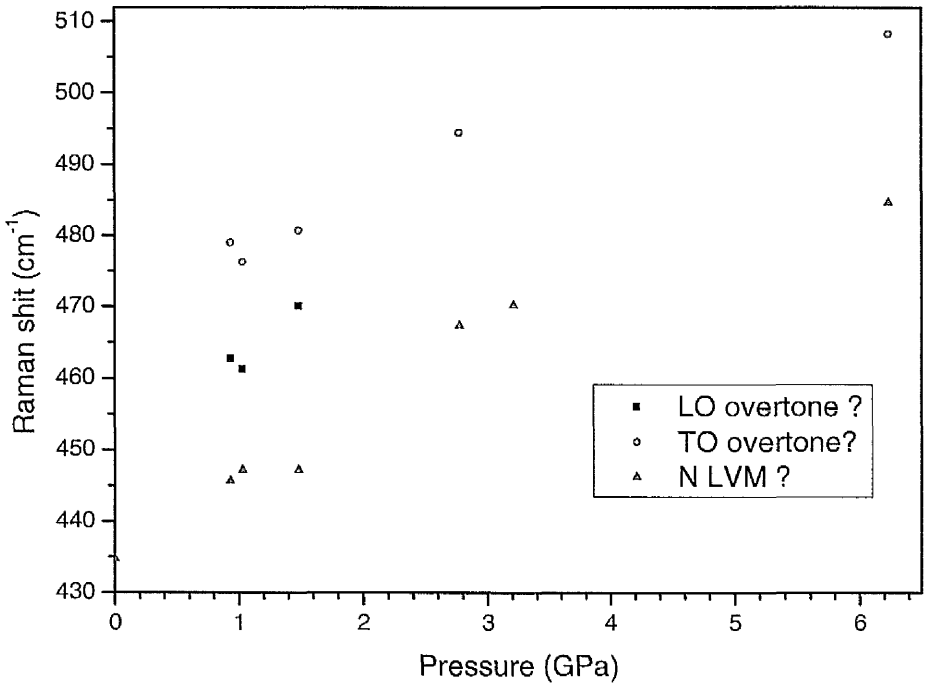

Figure 6.7: Raman shift as a function of pressure for the $GaSb_{0.985}N_{0.015}$ sample in the region of the expected overtones and nitrogen LVM

Figure 6.7 shows the possibility of three peaks which could be the 2TO, 2LO and the nitrogen LVM. However, figure 6.7 does not confirm this as the red and black points are too few to make any conclusion from them. This leaves the blue points which have been measured up to about 6.4GPa. There is a large gap between 3.4GPa and 6.4GPa which is a slight problem however, the fit parameters for the blue points are given in table 6.2 and present some interesting results. It should be noted that the Raman shift for these points is around the location of the nitrogen LVM and there is a high possibility that this peak could be it.

Sample	Mode	σ_0 (cm^{-1})	α ($cm^{-1}GPa^{-1}$)	β ($cm^{-1}GPa^{-2}$)
$GaSb_{0.985}N_{0.015}$	LVM	433.19 ± 2.31	14.17 ± 1.94	-0.936 ± 0.291

Table 6.2: Fit parameters of the possible nitrogen LVM of $GaSb_{0.985}N_{0.015}$.

The results show that the peak, which is assumed to be the nitrogen LVM is considerably larger than that of the TO mode of wurtzite GaN [18] in table 6.1. It is stronger than that both the $GaP_{0.979}N_{0.021}$ sample studied in chapter 5 and previous studies of $GaAs_{0.915}N_{0.085}$ [19] and so indicates that the LVM (assuming that it is) does not show a GaN-like behaviour.

6.3.3 Mode Grüneisen parameters

The bulk modulus used to calculate the mode Grüneisen parameters in $GaSb_{0.985}N_{0.015}$ was 56.3GPa [20] and it's the bulk modulus used for GaSb. As the variation of the bulk modulus with nitrogen concentration is not known, a common value of 56.3GPa is used. It may be in fact that this is a rough approximation in the calculation of the mode Grüneisen parameter using equation 2.31.

$$\gamma_i = \frac{B_0 \alpha}{\sigma_0} \qquad \text{Equation 2.31}$$

The above equations provides the calculated values of the Grüneisen parameters for $GaSb_{0.985}N_{0.015}$ and are presented in table 6.3 with other Grüneisen parameters for GaSb, GaN, GaAs and $GaAs_{0.915}N_{0.085}$.

Sample	Mode	Grüneisen parameter
$GaSb_{0.985}N_{0.015}$	TO	1.341 ± 0.039
$GaSb_{0.985}N_{0.015}$	LO	1.318 ± 0.044
$GaSb_{0.985}N_{0.015}$	LVM	1.841 ± 0.137
GaSb [17]	TO	1.33
GaSb [17]	LO	1.21
GaN [18]	TO	1.47
GaN [18]	LO	1.2
GaAs [19]	TO	1 .17
GaAs [19]	LO	1.09
$GaAs_{0.915}N_{0.085}$ [19]	TO	1.223
$GaAs_{0.915}N_{0.085}$ [19]	LO	1.039
$GaAs_{0.915}N_{0.085}$ [19]	LVM	1.692

Table 6.3: Grüneisen parameters for $GaSb_{0.985}N_{0.015}$, GaSb, GaN, GaAs and $GaAs_{0.915}N_{0.085}$.

The calculated Grüneisen parameters for $GaSb_{0.985}N_{0.015}$ are consistent to what is expected. The parameters for the TO and LO phonon modes are very similar to GaSb and slight differences can be accounted for large errors in the determination of the fit parameters such as errors in measuring the exact pressure. With the experimental accuracy in mind, there is no significant change in the pressure behaviour of the GaSb-like phonons due to nitrogen incorporation. The Grüneisen parameter for the potential LVM, this fits in well with data collected in chapter 5 for $GaP_{0.979}N_{0.021}$ and again in previous studies with $GaAs_{0.915}N_{0.085}$. It is qualitatively consistent with the $GaAs_{1-x}N_x$ and $GaP_{1-x}N_x$ indicating that the GaN mode does not actually show a GaN-like behaviour under pressure.

6.4 Conclusion

The pressure dependent Raman scattering measurements of the vibrational properties of $GaSb_{0.985}N_{0.015}$ have been measured with some success. The $GaSb_{1-x}N_x$ sample has been measured up to its phase transition at around 7.4GPa which agrees with previous high pressure studies. The fit and Grüneisen parameters obtained from the analysis of pressure dependent phonon frequency shift indicates that in $GaSb_{1-x}N_x$ the nitrogen has little influence on the pressure behaviour of the host GaSb lattice. Even though the LVM was not fully measured, the results provide a good argument that the detected peak under hydrostatic pressure is the LVM. The fit and Grüneisen parameter are qualitatively consistent to previous studies on dilute nitrides indicating that the GaN-like modes in $GaSb_{1-x}N_x$ do not show a GaN-like behaviour under pressure.

6.5 Further work

Future work should be concentrated upon detecting the Raman shift of the LVM at more hydrostatic pressures. This will allow a better understanding of the mode and provide more accurate results that can be used to be compared against other dilute nitrides and GaN. Other $GaSb_{1-x}N_x$ samples with a different nitrogen percentage could also be studied, especially with larger nitrogen content as this should provide a stronger nitrogen peak which would then be far easier to observe. Finally, with further measurements on the LVM for the $GaSb_{0.985}N_{0.015}$ sample it would then be possible to calculate the anharmonicity of the GaN bond potential.

6.6 References

[1] J. W. Ager and W. Walukiewicz. Semicond. Sci. Technol. **17** 741 (2002)

[2] S. Lyer, L. Wu, J. Li, S. Potoczy, K. Matney and P. R. C. Kent. J. Appl. Phys. **101** 113508 (2007)

[3] T. D. Veal, L. F. J. Piper, S. Jollands, B. R. Bennett, P. H. Jefferson, P. A. Thomas, and C. F. McConville. Appl. Phys. Lett. **87** 132101 (2005)

[4] L. Buckle, B. R. Bennett, S. Jollands, T. D. Veal, N. R. Wilson, B. N. Murdin, C. F. McConville and T. Ashley. J. Crystal. Growth. **279** 188 (2005)

[5] J. S. Harris Jr, R. Kudrawiec, H. B. Yuen, S. R. Bank, H. P. Bae, M. A. Wistey, D. Jackrel, E. R. Pickett, T. Sarmiento, L. L. Goddard, V. Lordi and T. Gugov. Physica. Status. Solidi. (b) **224** (8) 2707 (2007)

[6] W. Li, J. B. Heroux and W.I.Wang. J. Appl. Phys. **94** (7) 4248 (2003)

[7] A. Belabbes, M. Frehat and A. Zaoui. Appl. Phys. Lett. **88** 152109 (2006)

[8] T. Ashley, T. M. Burke, G. J. Pryce and A. R. Adams. Solid. State. Electron. **47** 387 (2003)

[9] T. D. Veal, I. Mahboob, C. F. McConville. Phys. Rev. Lett. **92** 136801 (2004)

[10] E. P. O'Reilly and A. Lindsay. Phys. Stat. Sol. (b) **216** 13 (1999)

[11] M. Kondow, T. Kitatani, S. Nakatsuka and M. C. Larson. IEEE. J. Quantum. Electron. **3** 719 (1997)

[12] W. Shan, W. Walukiewicz, J. W. Ager and E. E. Haller. Phys. Rev. Lett. **82** 1221 (1999)

[13] K. Kassali and N. Bouarissa. Microelectron. Eng. **54** 277 (2000)

[14] I. Vurgaftman, J. R. Meyer and L. R. Ram-Mohan. J. Appl. Phys. **89** 5815 (2001)

[15] P. H. Jefferson, T. D. Veal, L. F. J. Piper, B. R. Bennett and C. F. McConville. Appl. Phys. Lett. **89** 111921 (2006)

[16] P. J. Klar. Prog. Sol. Stat. Chem. **31** 301 (2003)

[17] K. Aoki, E. Anastassakis and M. Cardona. Phys. Rev. B. **30** (2) 681 (1984)

[18] A. R. Goni, H. Siegle, K. Syassen, C. Thomsen and J. M. Wanger. Phys. Rev. B. **64** 035205 (2001)

[19] M. Grungerich, P. J. Klar, W. Heimbrodt, M. P. Halsall and P. Harmer. Phys. Rev. B. **71** 075201 (2005)

[20] http://www.ioffe.ru/SVA/NSM/Semicond/GaSb/index.html 25/1/07

Chapter 7: Vibrational properties of $InSb_{1-x}N_x$ under hydrostatic pressure

7.1 Introduction

Indium antimonide (InSb) out of all the binary III-V semiconductors has the smallest bandgap with a cut-off wavelength of 7μm at room temperature. This is ideally matched for mid-infrared wavelengths (3-5μm) however to reach these longer wavelengths, nitrogen can be incorporated into the structure. This changes the binary alloy into a dilute nitride that can access the 8 to 12μm transmission band and a small nitrogen percentage of 1% would reach this goal [1]. Many studies have been concentrated on dilute nitride alloys for $GaAs_{1-x}N_x$ and $InAs_{1-x}N_x$ due to their technological importance for fibre communications at wavelengths of 1.3 and 1.55μm [2-4].

Even though there are fewer studies on $InSb_{1-x}N_x$, the first report on the growth and experimental characterisation was made by Johnson et al [5] and has progressed through Burke at al [6]. The main problem for the lack of studies in the $InSb_{1-x}N_x$ field is due to the problems in growing samples. There is a difficulty in controlling the fraction of substitutional nitrogen atoms in the Sb lattice sites [6]. This prevents the $InSb_{1-x}N_x$ samples having a nitrogen content of more than 1% [7-8] while the nitrogen incorporation efficiency is much less compared to GaAs-based dilute nitrides. This and the accurate determination of its composition [8-9] are still the key issues that require further research.

As previously stated throughout the chapters, the incorporation of nitrogen into the crystal structure of InSb modifies the band structure [10], however at this present time there is a persistent difficulty in growing $InSb_{1-x}N_x$. Only a fraction of the nitrogen atoms in the alloy are being substituted onto the Sb lattice sites [5, 11-12] while the positioning of the remaining detected nitrogen by secondary ion mass spectrometry

(SIMS) has yet to be determined. Due to the location of nitrogen atoms at sites other than that of the group-V lattice sites, attempts to use x-ray diffraction to quantify the effective alloy composition are being hindered [9]. While the incorporation of nitrogen into the Sb lattice reduces the lattice constant towards the value obtained for InN, the non-substitutional nitrogen is thought to cause dilation in the lattice [9].

Raman studies of $InSb_{1-x}N_x$ may be of help to this problem as the vibrational properties reflect the impurity character of the nitrogen atoms in InSb. In other dilute nitride Raman studies [9] and in the samples studied in chapters 5 and 6, all have observed a LVM for nitrogen. If the majority of nitrogen is residing of the Sb lattice, then the LVM would be observable at a frequency in-line with those seen from $GaAs_{1-x}N_x$ and $InAs_{1-x}N_x$.

7.2 Experimental procedure

The $InSb_{1-x}N_x$ sample studied for high pressure Raman measurements was an epitaxial layer of $InSb_{0.9932}N_{0.0068}$ (n-type 2.3^x10^{18}) grown on a (100) undoped InSb (n^+) substrate by MBE at the QinetiQ Malvern site by Louise Buckle and co-workers. The epilayer thickness was 0.25μm and the nitrogen content (0.68%) and was derived from x-ray diffraction data.

As in the other three results chapters, the sample was thinned to a thickness to about 30μm thick by polishing most of the InSb substrate away using standard polishing techniques. Although some of the substrate remained on the sample it was not a problem for the measurement of Raman shift due to the geometry of the way the light is collected. The sample was then cleaved into small pieces of about 50μm which allowed it to be loaded onto the surface of the diamond in the presence of a speck of ruby dust. Careful attention was required to ensure that the sample did not touch the sides of the stainless steel gasket.

Raman scattering scans were taken at pressures from 1 to 3.5GPa at room temperature in a (100)-orientation using the 632nm laser and the new Raman setup

(chapter 3.1.2). A x(y',y') backscattering geometry was used while a 40x long working objective lens collected the light and allowed focusing on the sample surface to be achieved. Similar to other low pressure studies in this thesis, the pressure medium used inside the DAC was again the methanol and ethanol (4:1) mixture and so silicon oil was not required.

For the calculation of pressure, the PL of the ruby dust inside the cell was taken before and after Raman measurements was taken. When the screw on the DAC was turned to increase the pressure inside the stainless steel gasket, a period of 15 minutes elapsed before measurements were taken to ensure that the pressure, sample and cell movement was stationary within the DAC. The PL of the ruby was taken again after the Raman scan was finished and an average of the two was taken.

7.3 Results and Discussion

7.3.1 Phonon modes

To see the effects of incorporating nitrogen into the InSb crystal structure, a spectrum is required of the InSb reference sample at ambient pressure. This allows a comparison to be made with the $InSb_{0.9932}N_{0.0068}$ sample allowing the observer to see any shift in Raman peaks of the TO and LO phonons which is a result from the incorporation of nitrogen. Figure 7.1 is the reference spectrum of InSb and it clearly shows two large phonons of the TO and LO modes at around $180cm^{-1}$ and $190cm^{-1}$. Further along the spectrum at around $380cm^{-1}$ are the overtones of the phonon peaks with the 2LO phonon scattering peak being the most dominant.

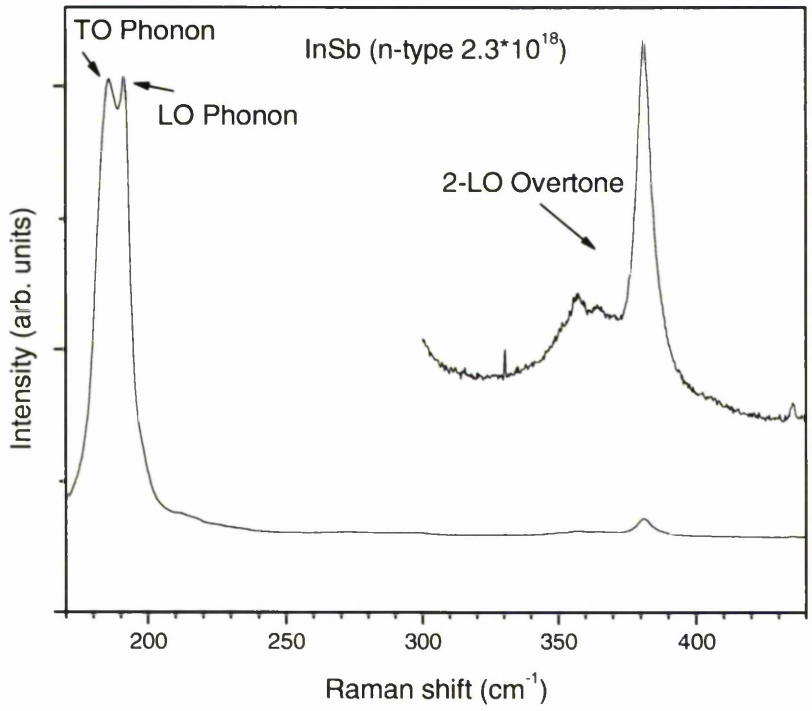

Figure 7.1: Raman scattering spectrum of InSb at ambient pressure.

Figure 7.2 shows the Raman spectrum for $InSb_{0.9932}N_{0.0068}$ at ambient pressure. The same number of features can again be seen on this spectrum such as phonon modes and overtones but there is a new feature at 400cm^{-1}. It is believed that this is the nitrogen LVM as it is close to the frequency expected for this system. As expected, this feature is not seen in figure 7.1 and so one aim of this study is to observe the pressure induced shift of the nitrogen mode (section 7.3.2). This is easier said than done due to the weakness of the mode and the effect of the DAC in cutting out a large majority of the light. The nitrogen LVM is one of a number of differences between the two spectra. Other differences are the reduction in the intensity of the 2LO phonon overtone and a slight decrease in the frequency of the TO and LO phonons.

The first thing to examine is the measured shifts of these peaks from figure 7.1 and 7.2 which surprisingly are different to what is expected. Comparing to values taken from Aoki et al [13], the Raman shift of the TO mode has been measured to be $179.7cm^{-1}$ while for the LO phonon, it is $190.7cm^{-1}$. The phonon TO and LO modes of the reference sample InSb was measured to be $185.63cm^{-1}$ and $191.34cm^{-1}$ respectively. These values are somewhat higher than $InSb_{1-x}N_x$ where the measured TO and LO peaks were $179.27cm^{-1}$ and $186.63cm^{-1}$ respectively. The initial thought was that the wrong spectrum and sample had been used but further Raman measurements have shown that this is not the case.

In section 5, it was reported that the $GaP_{1-x}N_x$ sample was partly relaxed due to a reduction in the tensile strain. This causes an increase in the energy of the phonon modes while for this sample the Raman shifts indicate that this is not the case. Both the TO and LO modes show a reduction which indicates no relaxing of the tensile strain and the sample not being relaxed.

Checks were also made to ensure that the laser shift was calculated in the final peak value. The subtraction (as it turned out) was correct, however the fit parameters may say otherwise and so judgement will be reserved for later.

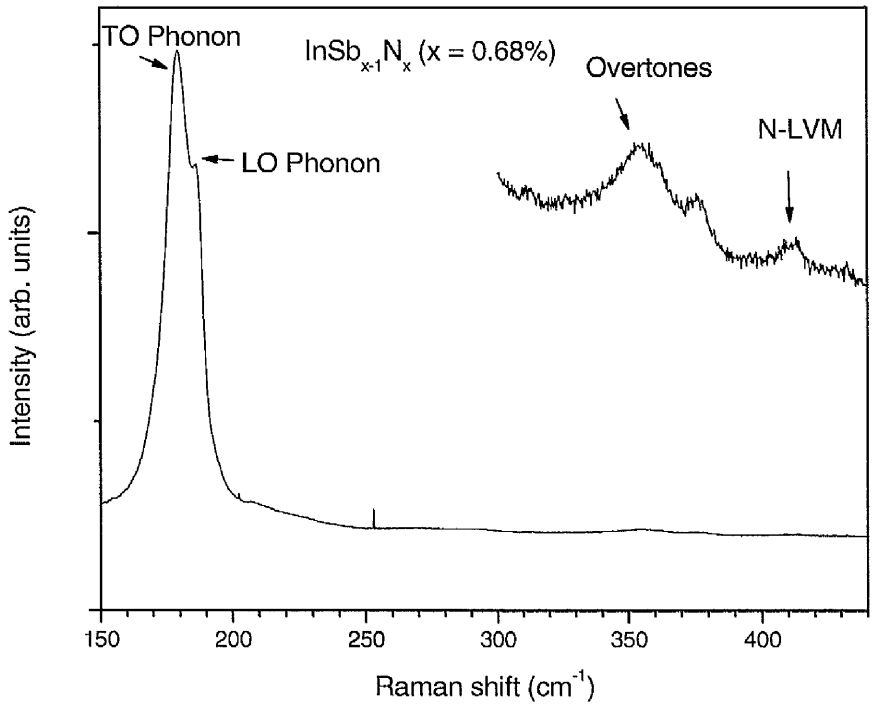

Figure 7.2: A Raman spectrum of $InSb_{0.9932}N_{0.0068}$ at ambient pressure with the nitrogen LVM spectrum being magnified by 50x.

The next stage was to measure the pressure induced shifts of the phonon modes and the LVM. Figure 7.3 shows a selection of spectra at different pressures for the InSb-like TO and LO phonon modes. The phonon modes were measured up to 3.56GPa before the signal disappeared. This is expected as Aoki et al [13] calculated the phase transition to occur at 3.10 +\- 0.1GPa. Figure 7.3 also shows the pressure induced shift of the TO and LO modes and how they merge together as the pressure moves towards the phase transition.

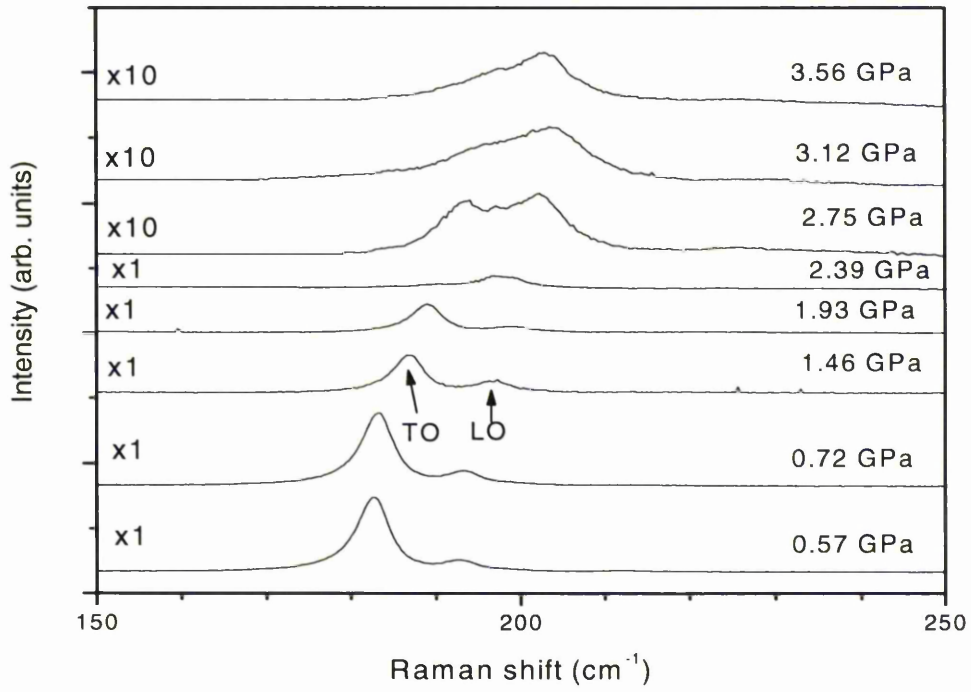

Figure 7.3: Raman spectra of the InSb-like phonons of $InSb_{0.9932}N_{0.0068}$ at various hydrostatic pressures up to its phase transition.

The next step is to plot the TO and LO phonon modes as a function of pressure. Figure 7.4 is a graph of the Raman shift of the InSb-like phonon modes against pressure. Plotting the Raman shift values against their corresponding pressures allows observations to be made on the pressure induced shifts of the modes.

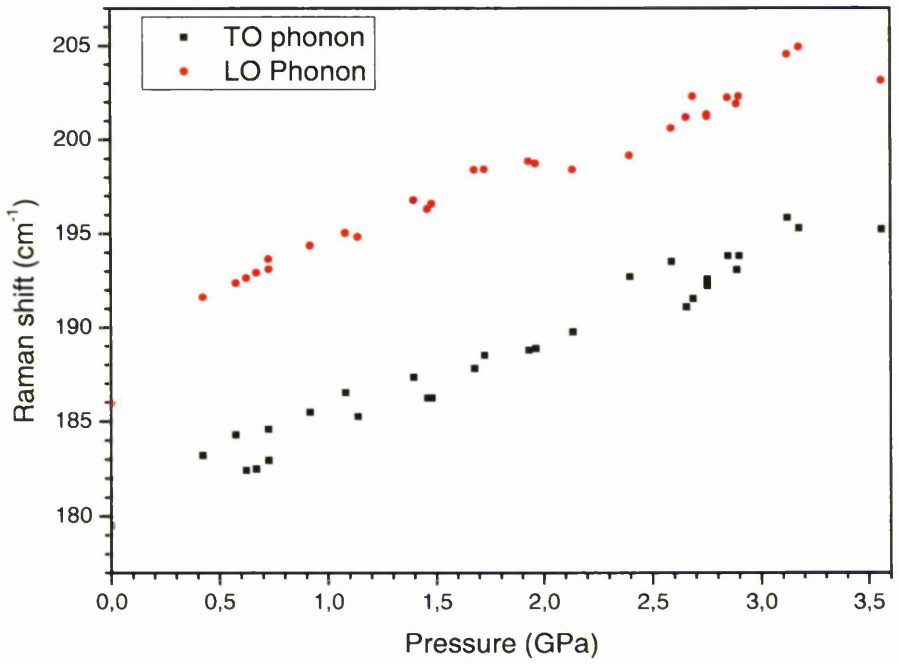

Figure 7.4: Raman shift of the InSb-like phonons of $InSb_{0.9932}N_{0.0068}$ as a function of pressure.

From this graph (Figure 7.4), a quadratic fit can be applied to each set of data that allows the fit parameters to be calculated. Using equation 2.28

$$\sigma(P) = \sigma_0 + \alpha P + \beta P^2 \qquad \text{Equation 2.28}$$

The calculated values for the TO and LO phonons as presented in table 7.1 including reference data for InSb and InN. The α parameter for the optical phonons appear to show a strange variation between the TO and LO phonons. The TO phonon is showing an identical value to the one seen for InSb while the LO phonon appears to be 2cm^{-1}GPa^{-1} greater than the LO phonon for InSb. Serious questions have to be asked about this value and it is believed that the source of discrepancy comes from the Raman shift value measured for $InSb_{1-x}N_x$ at ambient pressure for the LO phonon.

Referring back to Figure 7.2, the value was calculated to be 186.63cm^{-1}. The InSb value for the LO phonon is 190.7cm^{-1} while the fit parameters calculated that at ambient pressure, the value should be 188.11cm^{-1}. This indicates that the measured value could be a source of error and a look at figure 7.4 suggests this too as the data point does not fit in well with the rest of the data.

It should also be noted that the total errors in the determination of the fit parameters in table 7.1 are larger than the indicated errors from the fitting procedure. This is due to inaccuracies in the pressure and peak frequency determination for each spectrum. Therefore with the experimental accuracy, it can definitely be said that for the TO mode there is no significant change in the pressure behavior of the InSb-like phonons due to nitrogen incorporation.

Sample	**Mode**	**σ_0 (cm^{-1})**	**α (cm^{-1}GPa^{-1})**	**β (cm^{-1}GPa^{-2})**
$InSb_{0.9932}N_{0.0068}$	TO	180.25 ± 0.58	4.84 ± 0.74	-0.097 ± 0.201
$InSb_{0.9932}N_{0.0068}$	LO	188.11 ± 0.56	6.95 ± 0.72	-0.709 ± 0.195
InSb [13]	TO	179.7	5.01	-0.10
InSb [13]	LO	190.7	5.11	-0.31
InN [14]	TO	439.7	5.81	----
InN [14]	LO	591.9	5.96	----

Table 7.1: Fit parameters of various phonon modes of $InSb_{0.9932}N_{0.0068}$, InSb and InN.

7.3.2 Nitrogen local vibrational mode

Figure 7.5 shows the Raman spectra at various hydrostatic pressures for the region where the nitrogen LVM is expected. Due to the low intensity of the LVM and that it is even more difficult identifying the LVM when inside the DAC, often it will be swamped by background noise of other features. The result from studying these features with increasing pressure will hopefully separate them as figure 7.2 suggests this will not be a problem. At pressure, figure 7.5 suggests otherwise showing how difficult it is to determine the LVM.

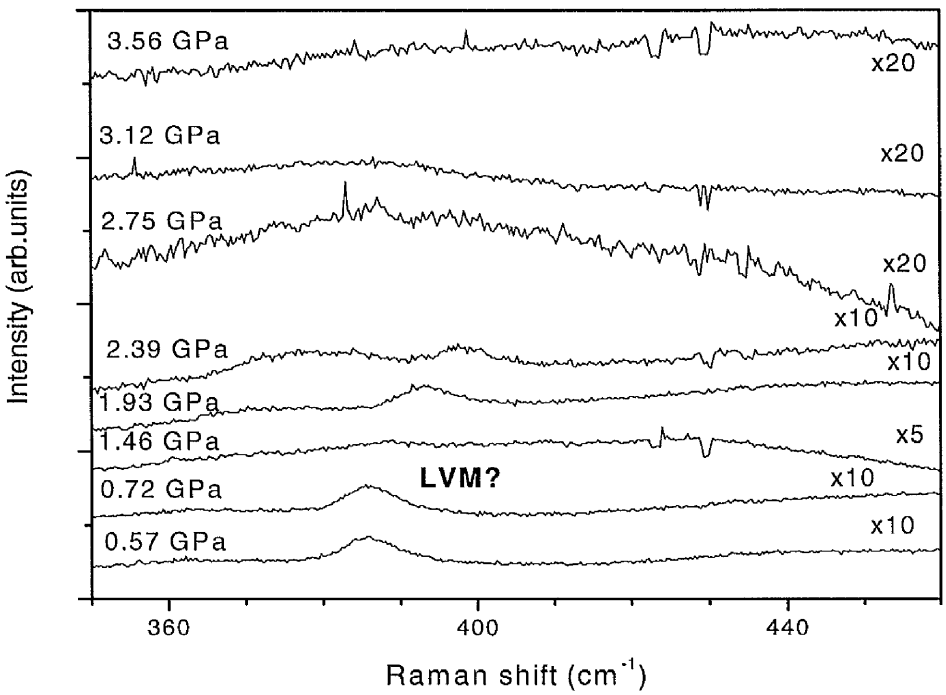

Figure 7.5: Raman spectra of the nitrogen LVM of $InSb_{0.9932}N_{0.0068}$ at various hydrostatic pressures.

By plotting the Raman shift measurements as a function of pressure, figure 7.6 is obtained. A closer inspection to each spectrum gives three different possible peaks. The

black and red data points are consistent with each other with increasing pressure while the third (green) is not. The bad news is that the red and black data points have a Raman shift value that is twice the value of the LO and TO phonons of the InSb-like modes. Therefore in all probability these data points are not the LVM. In addition, at ambient pressure, the peak that was thought to be the LVM, (most likely is) has a value of 411cm^{-1}. Unfortunately there are no conclusive results to indicate whether the LVM shows a InN-like behavior under pressure or not. However, the presence of a single feature of the nitrogen LVM in Figure 7.2 does confirm that most of the N is being incorporated into the crystal structure on a single site. It is almost certainly the In being substituted for nitrogen.

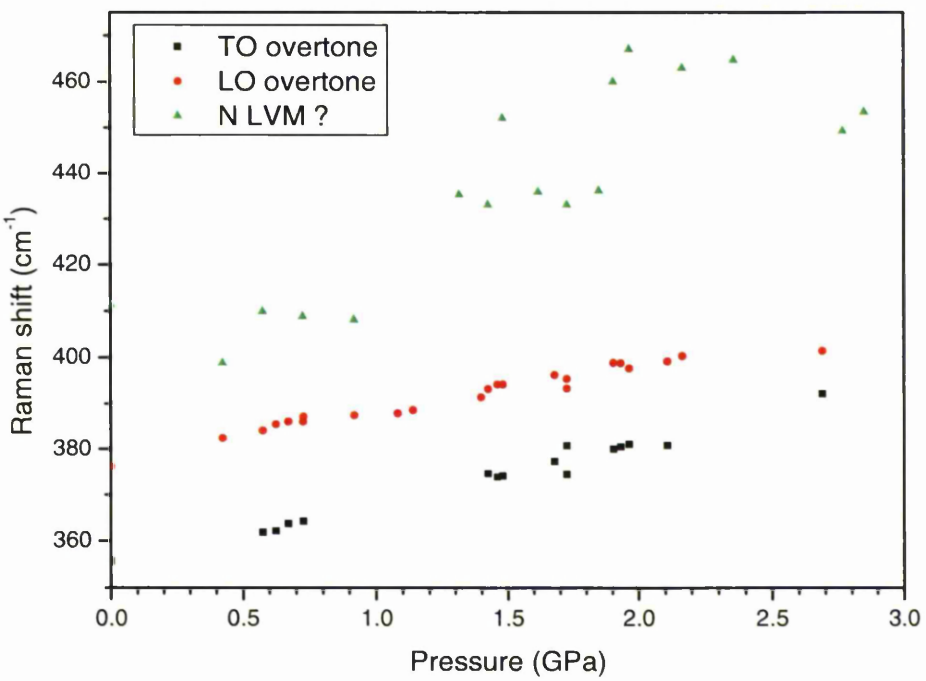

Figure 7.6: Raman shift of the nitrogen LVM of $InSb_{0.9932}N_{0.0068}$ as a function of pressure.

7.3.3 Mode Grüneisen parameters

The mode Grüneisen parameter can be calculated using equation 2.31 and the bulk modulus value of 47.1GPa [15]

$$\gamma_i = \frac{B_0 \alpha}{\sigma_0} \qquad \text{Equation 2.31}$$

These values are presented in table 7.2 for $InSb_{0.9932}N_{0.0068}$, InSb and InN which again shows strange results. At a first glance, the Grüneisen parameter of the TO mode in $InSb_{1-x}N_x$ is less that the InSb while the LO Grüneisen parameter is considerably larger that the LO mode of InSb. However, a closer look at the calculated errors shows no change in the TO Grüneisen parameter and so no significant change in the pressure behaviour of the InSb-like TO phonon. It can be assumed that the LO will follow suit however, due to errors stated previously and that no one knows for sure, the actual value of the bulk modulus in $InSb_{1-x}N_x$ when the nitrogen concentration is 0.68%. As the bulk modulus is taken as a common value for both the binary and ternary materials it may be a rough approximation.

Sample	Mode	Grüneisen parameter
$InSb_{0.9932}N_{0.0068}$	TO	1.265 ± 0.153
$InSb_{0.9932}N_{0.0068}$	LO	1.740 ± 0.103
$InSb_{0.9932}N_{0.0068}$	LVM	-----
InSb [13]	TO	1.41
InSb [13]	LO	1.17
InN [14]	TO	1.66
InN [14]	LO	1.26

Table 7.2: Grüneisen parameters for $InSb_{0.9932}N_{0.0068}$, InSb and InN.

7.4 Conclusion

Pressure dependent Raman scattering measurements of the vibrational properties of $InSb_{0.9932}N_{0.0068}$ have been reported in this chapter. The sample was investigated up to 3.56GPa to its first phase transition confirming previous Raman studies on InSb. The results are promising but can be improved; even so the following conclusions can be made. The TO and LO phonons of the InSb-like modes show similar comparisons, especially in the TO mode and less so in the LO mode. The Grüneisen parameter for the TO mode obtained from the analysis of the pressure dependent phonon frequency shift indicate that the nitrogen incorporation has little influence on the pressure behaviour. The LO Grüneisen parameter is not so convincing although an argument can be made about the source of errors that would possibly affect the calculated values.

At ambient pressure, the spectrum shows the LVM of the nitrogen atom which unfortunately could not be seen during high pressure measurements. The nitrogen LVM does however confirm that most of the nitrogen is being incorporated into the InSb structure. The effect of this is still unknown as nitrogen atoms could be (at a lesser level) being incorporated on other sites. This could be detected by other features or peaks but they could be obscured under the phonon overtones. To a lesser extent, but not conclusively, you could argue that the values are qualitatively consistent with values obtained for $GaP_{1-x}N_x$ and $GaAs_{1-x}N_x$.

7.5 Further work

The work from this chapter can be further improved in a number of ways. Firstly, more Raman measurements should be taken of the LO phonon and a closer look at its peak value at ambient pressure. Once this is done, the calculated values should be more in line with what is expected and what is seen for the TO InSb-like mode. As the LVM was not detected successfully at pressure, efforts should be made in detecting this peak

as it will provide more information on the behaviour of the nitrogen within the crystal lattice of InSb.

Further measurements would automatically reduce the error; however a correct value for the bulk modulus should be investigated as it is still unknown if the incorporation of nitrogen into the structure changes the bulk modulus. Finally, studies on the sample type of dilute nitride but with a different nitrogen content would be advisable, but only with a higher percentage as this would give a stronger LVM. However, a problem at the time of writing this thesis is that with current growth techniques, only a nitrogen content of less than 1% is possible.

7.6 References

[1] T. Ashley, T. M. Burke, G. J. Pryce, A. R. Adams and A. Andreev. Sol. Stat. Electron. **47** 387 (2003)

[2] M. Kondow, K. Uomi, A. Niwa, T. Kitatani and S. Watahike. Jpn. J. Appl. Phys. **35** (2B) 1273 (1996)

[3] G. Steinle, H. Riechert and A. Y. Egorov. Electron Lett. **37** (10) 355 (2001)

[4] A. W. Jackson, R. L. Naone, M. J. Dalberth. J. M. Smith and K. J. Malone. Electron. Lett. **37** (6) 355 (2001)

[5] A. D. Johnson, R. H. Bennett, J. Newey, G. J. Pryce and G. M. Williams. Matter, Res, Soc. Symp. Proc. **607** 23 (2000)

[6] T. M. Burke, M. Kane, A. D. Johnson, G. Pryce and P. Findley. Proc. NGS10 IPAP Conf. Series **2** 296 (2001)

[7] P. H. Jefferson, L. Buckle, B. R. Bennett and T. D. Veal. J. Crystal. Growth. **304** 338 (2007)

[8] W. Li, B. Heroux and W. I. Wang. J. Appl. Phys. **94** (7) 4284 (2003)

[9] T. D. Veal, I. Mahboob, C. F. McConville, T. M. Burke and T. Ashley. App. Phys. Lett. **83** (9) 1176 (2003)

[10] P. J. Klar. Prog. Sol. Stat. Chem. **31** 301 (2003)

[11] B. N. Murdin, M. Kamal-Saadi, A. Lindsay, E. P. O'Reilly and A. R. Adams. Appl. Phys. Lett. **78** 1568 (2001)

[12] B. N. Murdin, A. R. Adams, P. Murzyn, C. R. Pidgeon and I. V. Bradley. Appl. Phys. Lett. **81** 256 (2002)

[13] K. Aoki, E. Anastassakis and M. Cardona. Phys. Rev. B. **30** (2) 681 (1984)

[14] C. Pinquier, F. Demangeot, J. Frandon, J. C. Chervin, A. Polin, B. Couzinet and O. Briot. Phys. Rev. B. **73** 115211 (2006)

[15] http://www.ioffe.ru/SVA/NSM/Semicond/InSb/index.html 31/01/07

Chapter 8: Conclusion

This thesis has reported on the pressure-dependent Raman scattering measurements of the vibrational properties of GaP, $GaP_{0.979}N_{0.021}$, $GaSb_{0.985}N_{0.015}$ and $InSb_{0.9932}N_{0.0068}$. The binary sample of bulk GaP was investigated up to 30GPa observing its structural phase transition (I-II) from cubic zincblende to the Cmcm structure. The phase transition occurred at around 24.5GPa which confirms previous x-ray absorption spectroscopy data. The pressure induced shift of the TO and LO modes of GaP was measured up to this transition allowing the mode Grüneisen parameters of 1.12 and 0.98 to be calculated. These fitted in well with other group III-V semiconductor materials such as GaAs and InSb and differ to pure nitrides of GaN and InN.

The analysis of pressure-dependent phonon frequency shift in $GaP_{1-x}N_x$, $GaSb_{1-x}N_x$ and $InSb_{1-x}N_x$ has indicated that the nitrogen incorporation has little influence on the pressure behaviour of the host phonon mode. In the case of $GaP_{1-x}N_x$ the α and Grüneisen parameters were found to be considerably smaller while for $GaSb_{1-x}N_x$ and $InSb_{1-x}N_x$ it was the opposite. It is believed that these differences are due to $GaP_{1-x}N_x$ which is thought to be partly relaxed causing a reduction in the phonon frequency due to a reduced tensile stress. The values are within the experimental accuracy and so there are no significant changes in the pressure behaviour of the GaP-like, GaSb and InSb phonons due to nitrogen incorporation.

The nitrogen LVM mode for each nitride sample was measured with varying success. In the case of the $GaP_{1-x}N_x$ sample, the LVM was measured up to 10GPa successfully before the signal became too weak. The results showed that the pressure dependence of the LVM in $GaP_{1-x}N_x$ is qualitatively consistent with the LVM measured in $GaAs_{1-x}N_x$. For $GaSb_{1-x}N_x$ a peak in the same region as the expected nitrogen phonon mode was observed up to 7.5GPa. The results fitted well to those calculated for $GaP_{1-x}N_x$ and those seen for $GaAs_{1-x}N_x$. Therefore it can be assumed that this peak is the LVM in the $GaSb_{1-x}N_x$ sample. The remaining LVM was the one observed at ambient

pressure in $InSb_{1-x}N_x$. However, at increasing pressures, the peak could not be detected and so no conclusion could be made.

Overall, this thesis can be summarised by the following sentences. Firstly, the nitrogen has little influence on the pressure behaviour of the host phonon modes. Secondly, the pressure dependence of the LVM in dilute nitrides indicates that in both ternary materials the GaN-like mode does not actually show a GaN-like behaviour under pressure.